

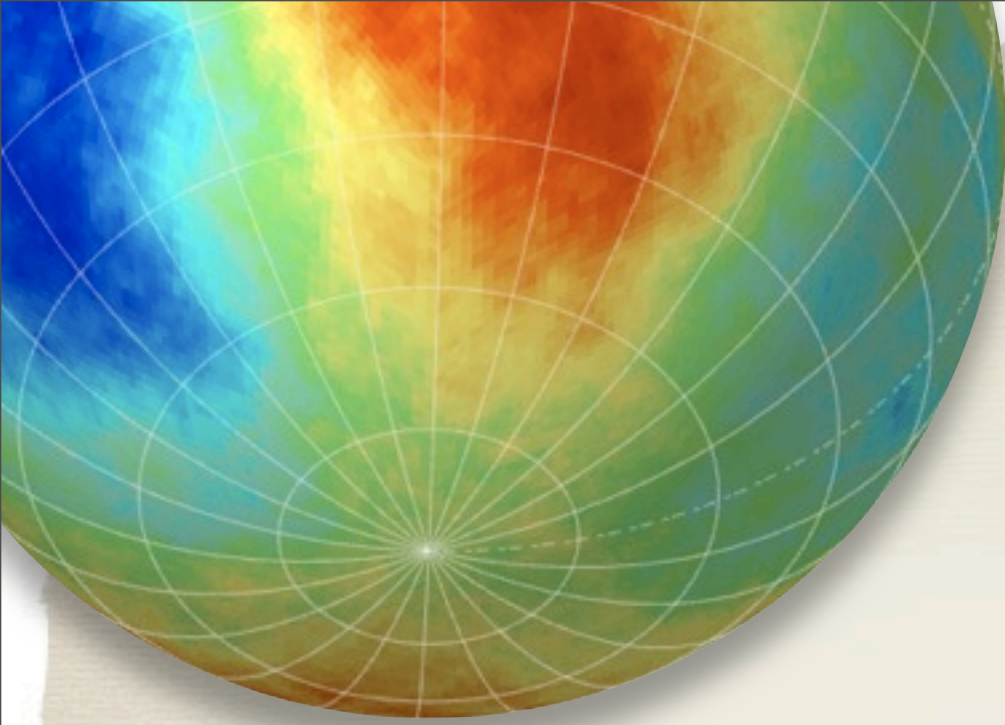
OBSERVATION OF COSMIC RAY ANISOTROPY ABOVE TEV ENERGIES IN ICECUBE

Simona Toscano *on behalf of the* IceCube collaboration



3rd Roma International Conference
on Astro-particle Physics

25-27 May 2011
Roma Italy



Outline

- * The **IceCube** detector
- * Energy dependence of the **large scale anisotropy** (*paper in preparation*):
 - ▶ preliminary results at 20 and 400 TeV.
 - ▶ solar dipole
- * **Medium and small scale** structures (submitted to ApJ, **arXiv:1105.2326**):
 - ▶ analysis
 - ▶ results
- * Conclusions

Bartol Research Inst, Univ of Delaware, USA
University of Alaska Anchorage, USA
Pennsylvania State University, USA
University of Wisconsin-Madison, USA
University of Wisconsin-River Falls, USA
LBNL, Berkeley, USA
UC Berkeley, USA
UC Irvine, USA



Universität Mainz, Germany
DESY Zeuthen, Germany
Universität Wuppertal, Germany
Universität Dortmund, Germany
Humboldt Universität, Germany
TWH Aachen, Germany
Universität Bonn, Germany
Ruhr-Universität, Bochum, Germany
MPI, Heidelberg, Germany



Uppsala Universitet, Sweden
Stockholm Universitet, Sweden



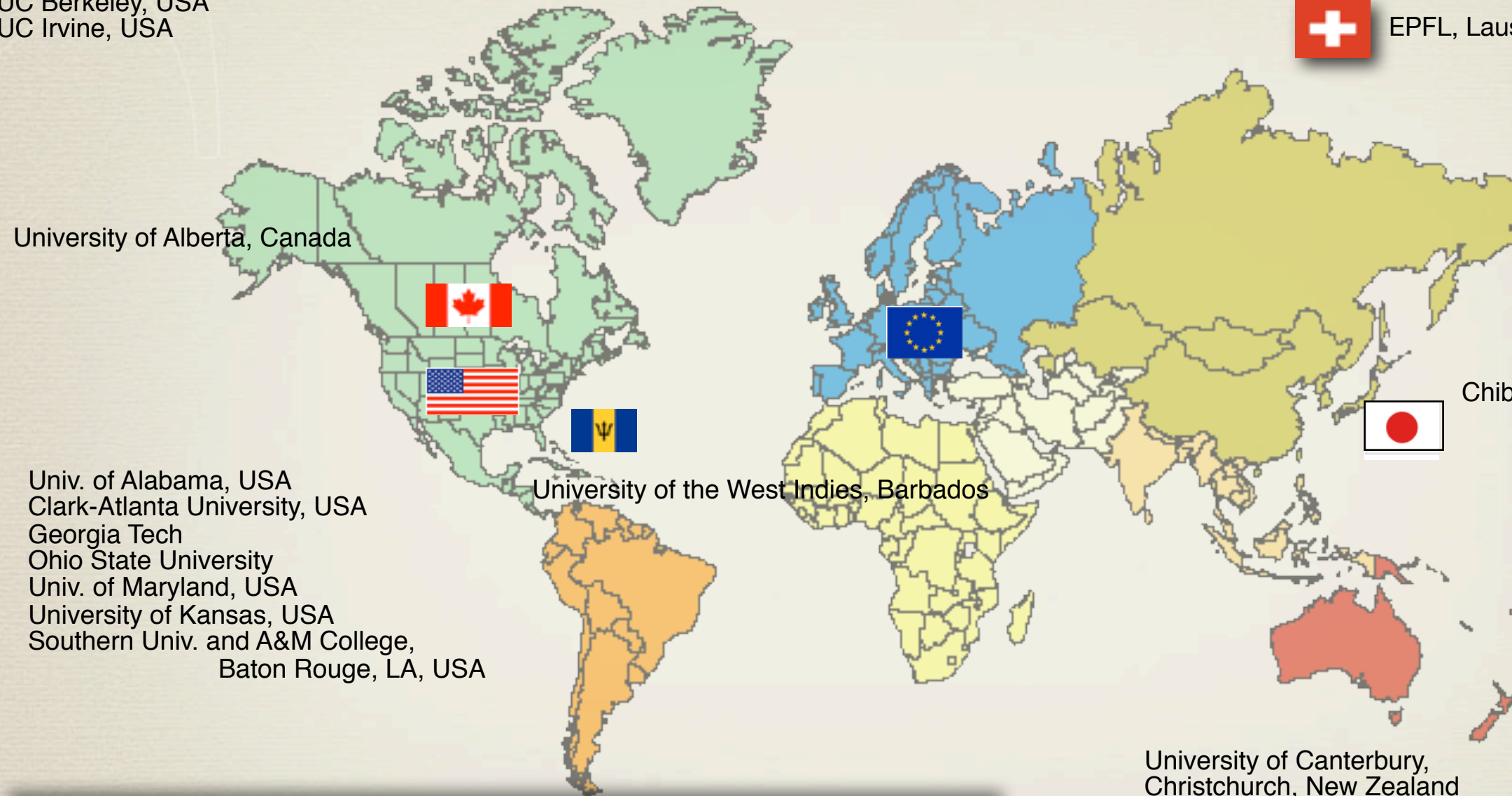
Imperial College, London, UK
University of Oxford, UK



Université Libre de Bruxelles, Belgium
Vrije Universiteit Brussel, Belgium
Université de Mons, Belgium
Universiteit Gent, Belgium



EPFL, Lausanne, Switzerland



IceCube Collaboration

10 countries
36 institutions
~260 collaborators

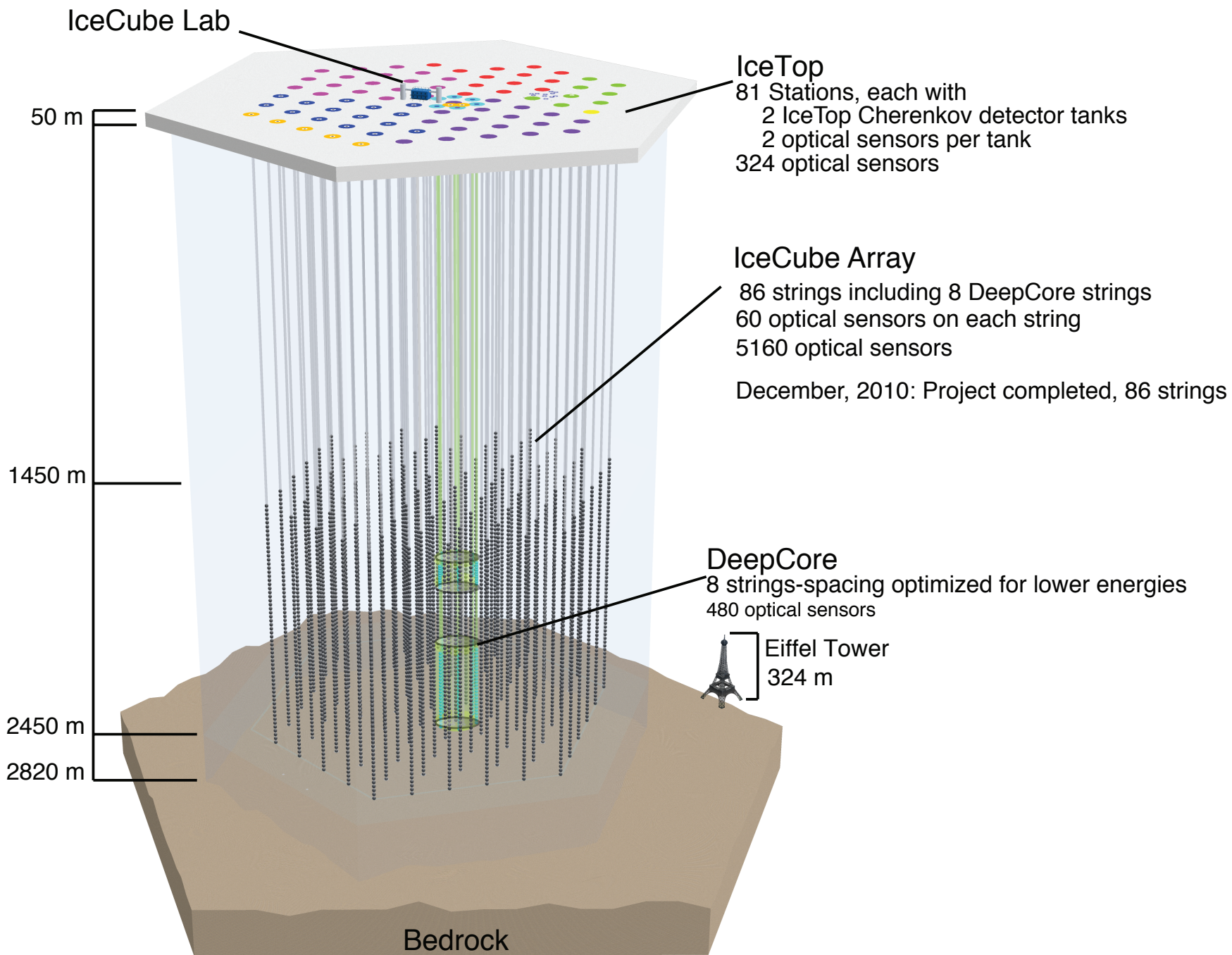
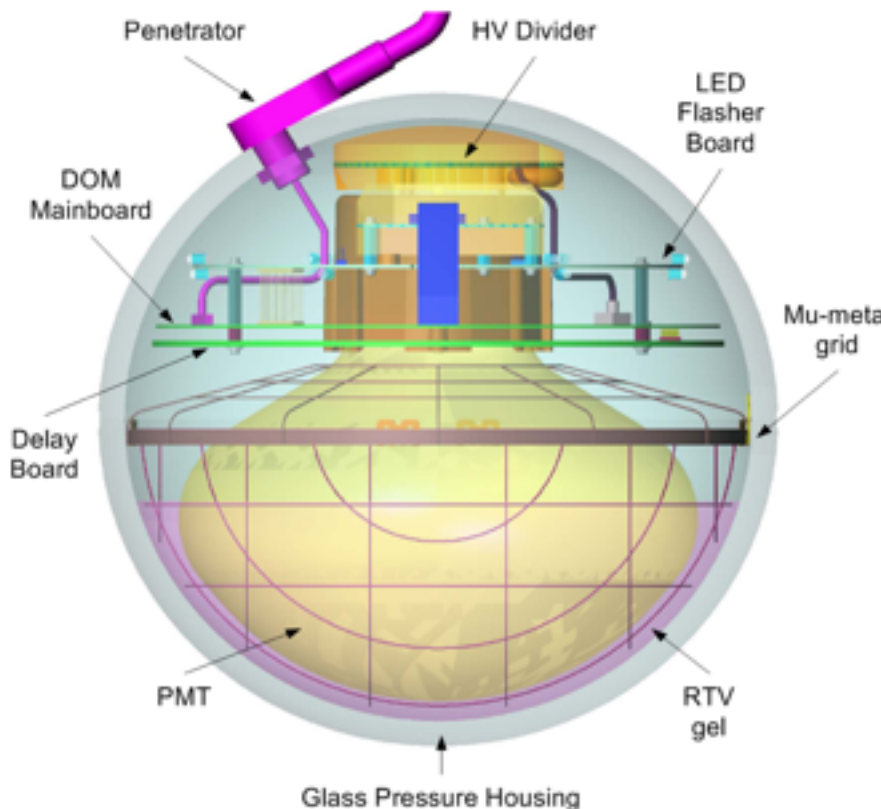


The IceCube detector

- **G. Sullivan** - Status and Recent Results from the IceCube km³ Neutrino Detector (tomorrow Plenary)
- **T. DeYoung** - Particle physics in ice with IceCube DeepCore (today next Parallel session)

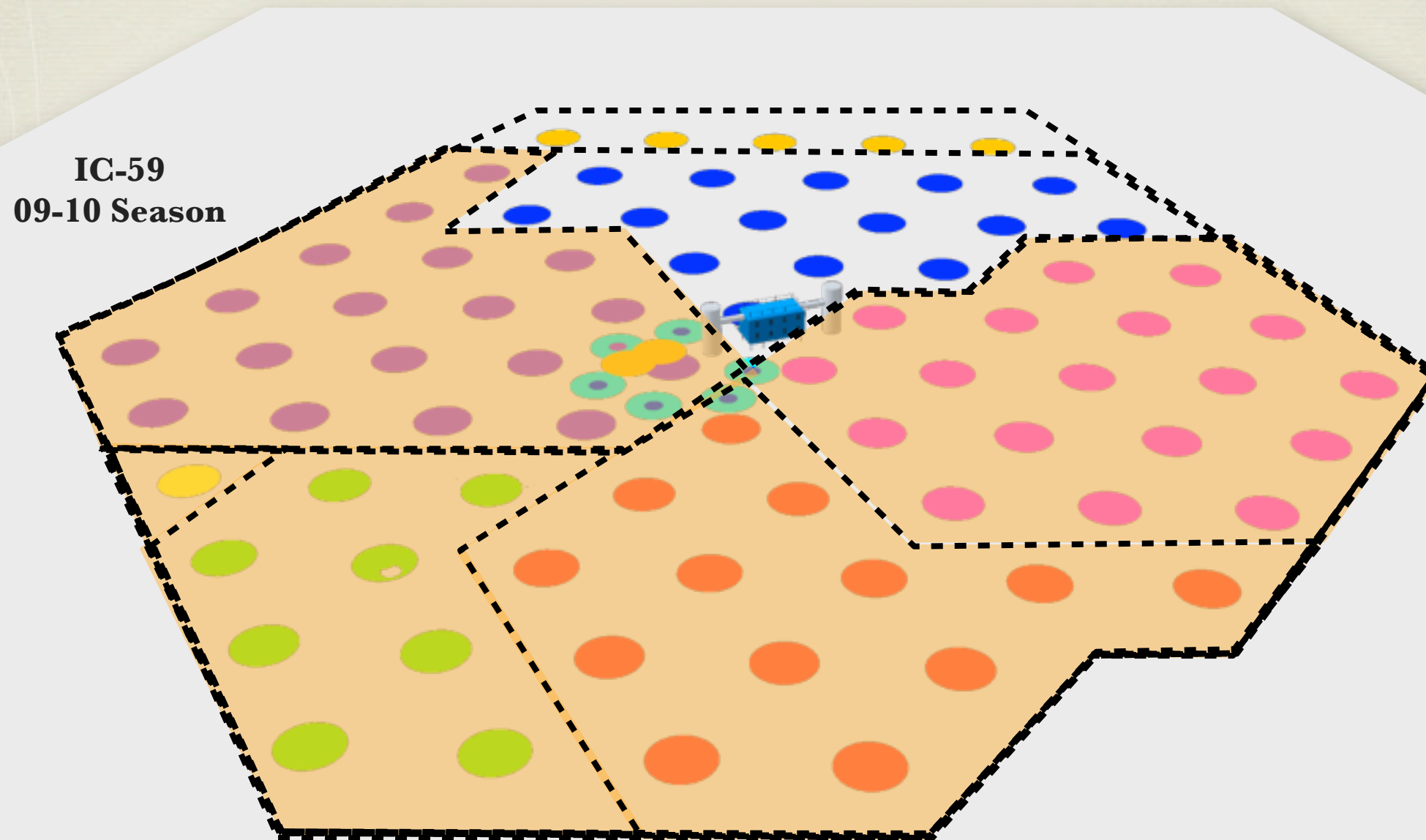
- **86 strings**
- **5160 DOMs**
- **17 m vertical spacing**
- **125 m between strings**

Digital Optical Module



IC59 configuration

Season 2009-2010

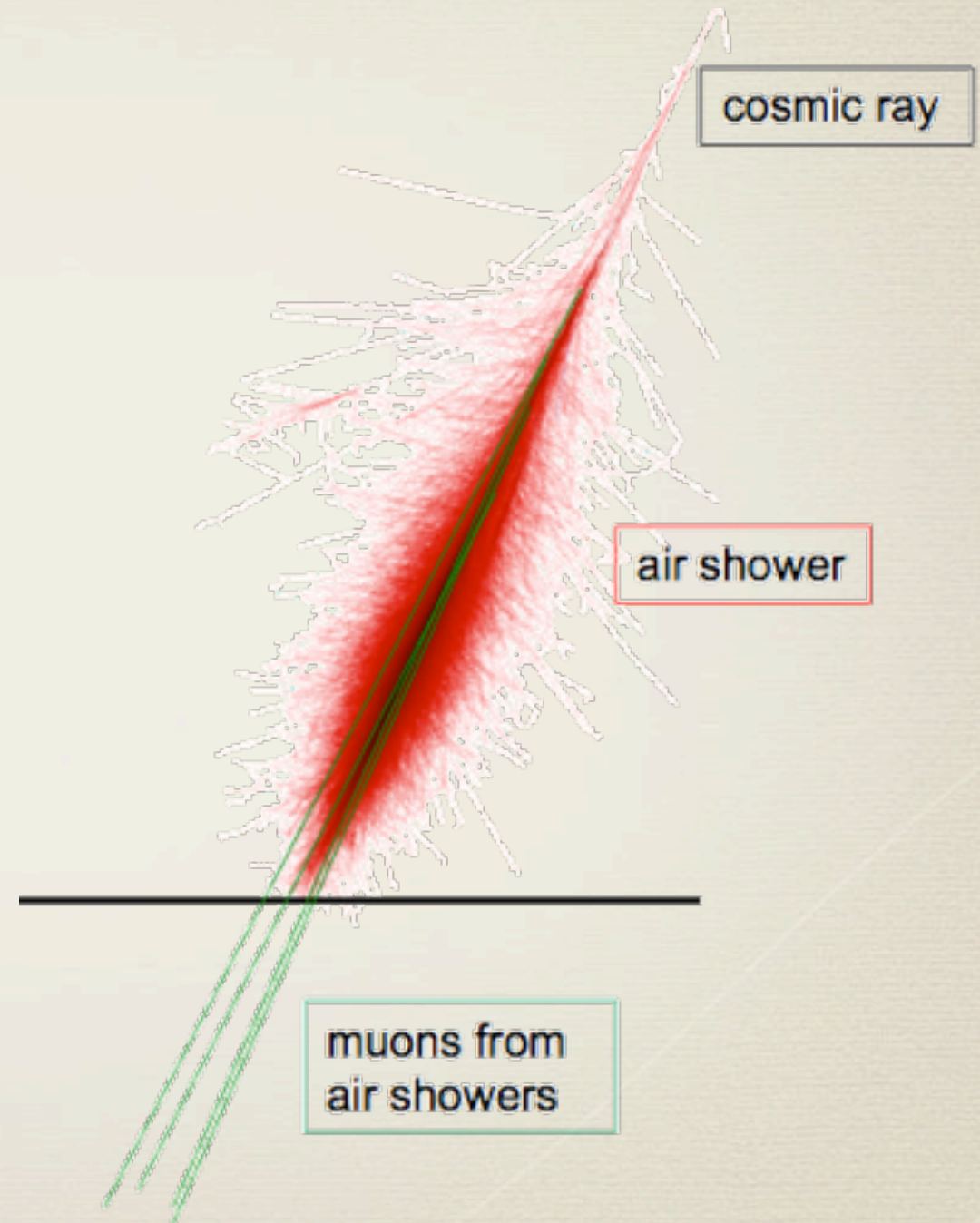


Construction finished on December 2010

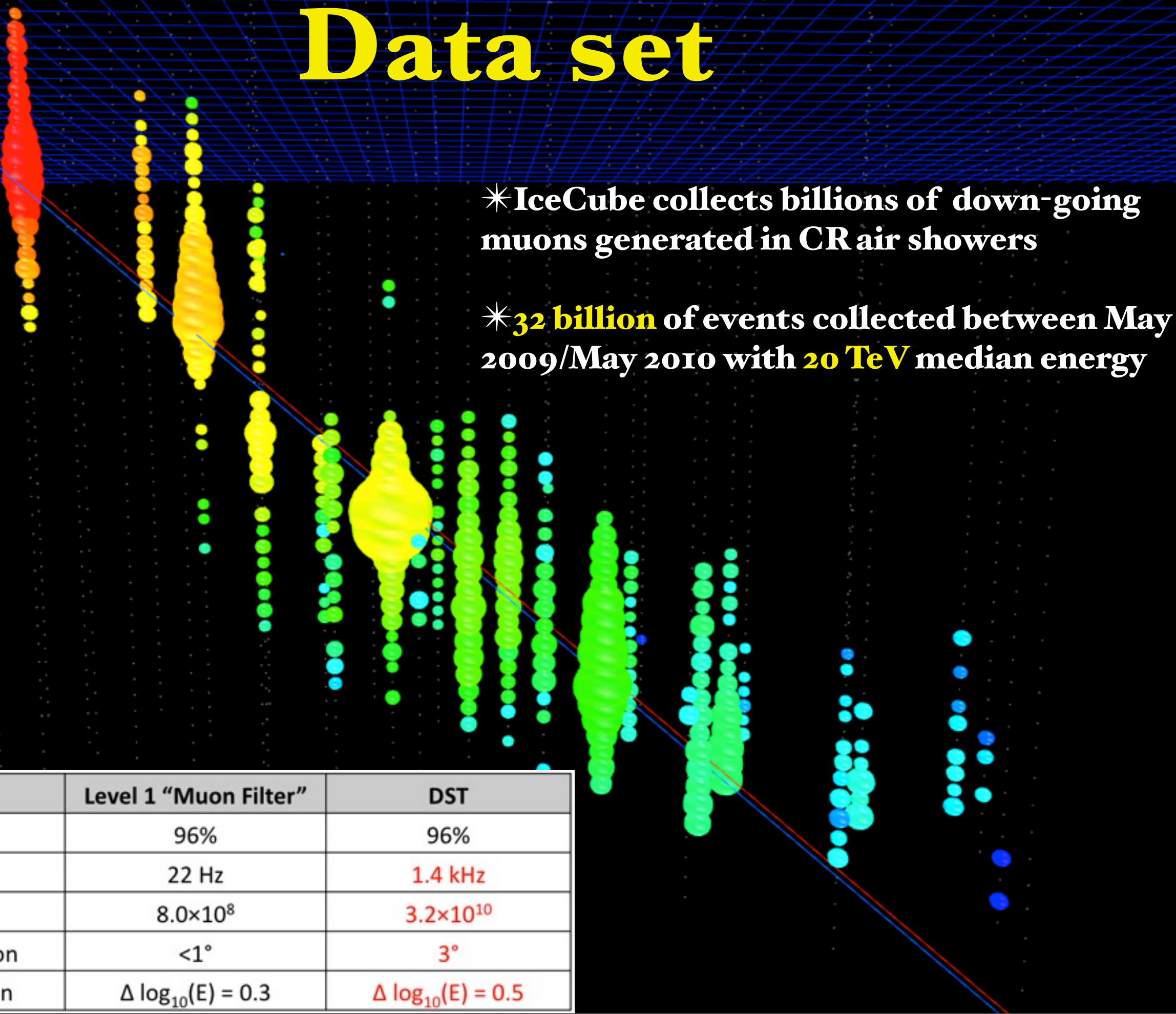
Cosmic rays in IceCube

IceCube tries to identify cosmic ray sources by their neutrino signal, but it also allows for a study of the *cosmic ray flux* itself, as the detector is sensitive to *downward going muons* produced in cosmic ray air showers in the southern hemisphere.

By detecting downgoing muons, IceCube can study the *arrival direction distribution of cosmic rays* in the energy range ~10 TeV to several 100 TeV and produce a cosmic ray sky map of the southern sky.

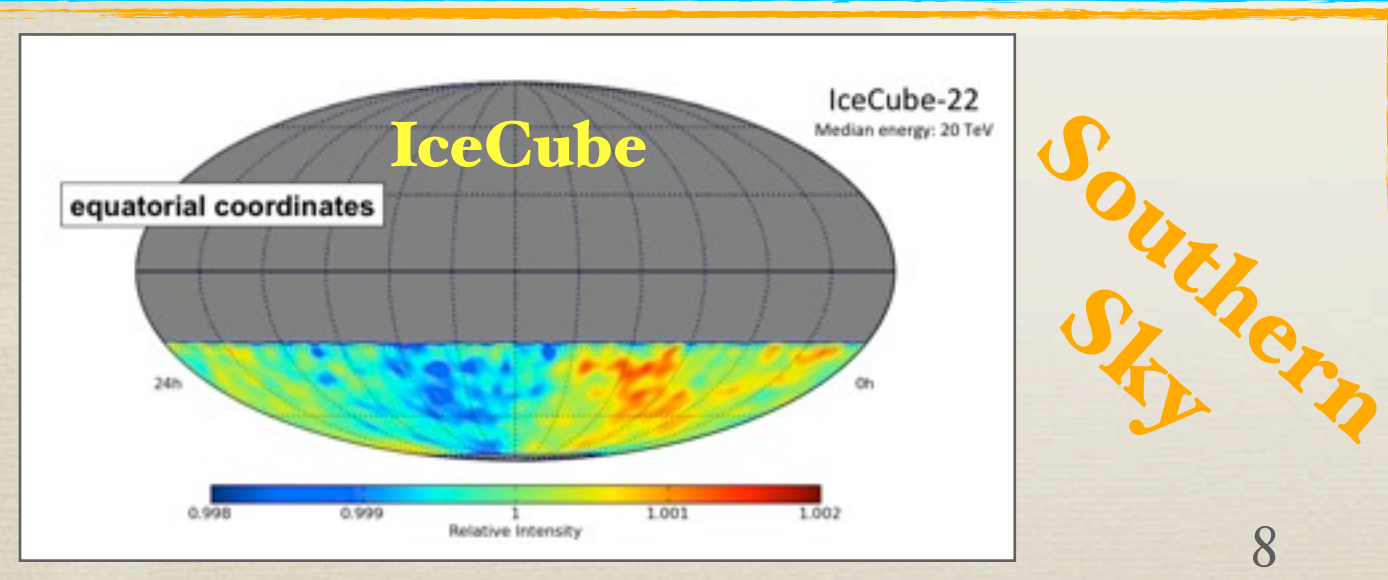
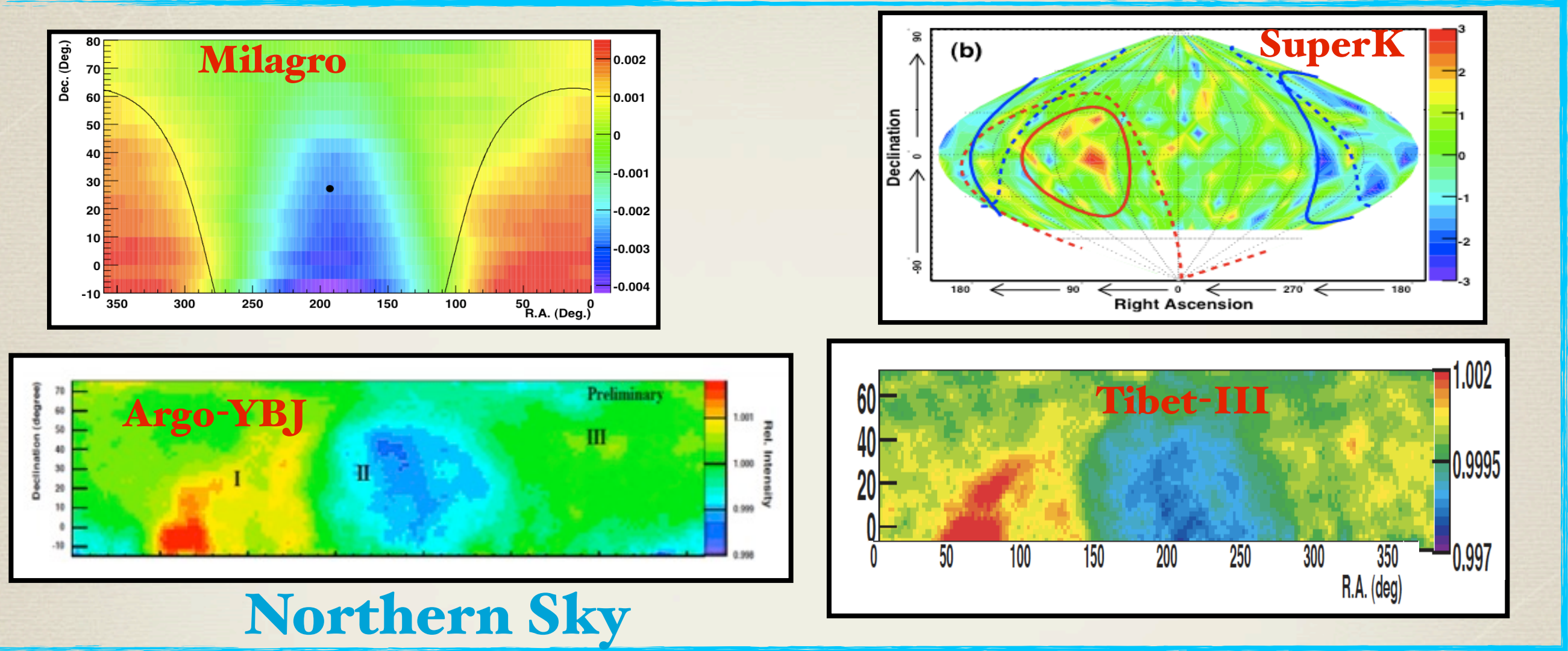


Data set



Observation of the CRs large scale anisotropy

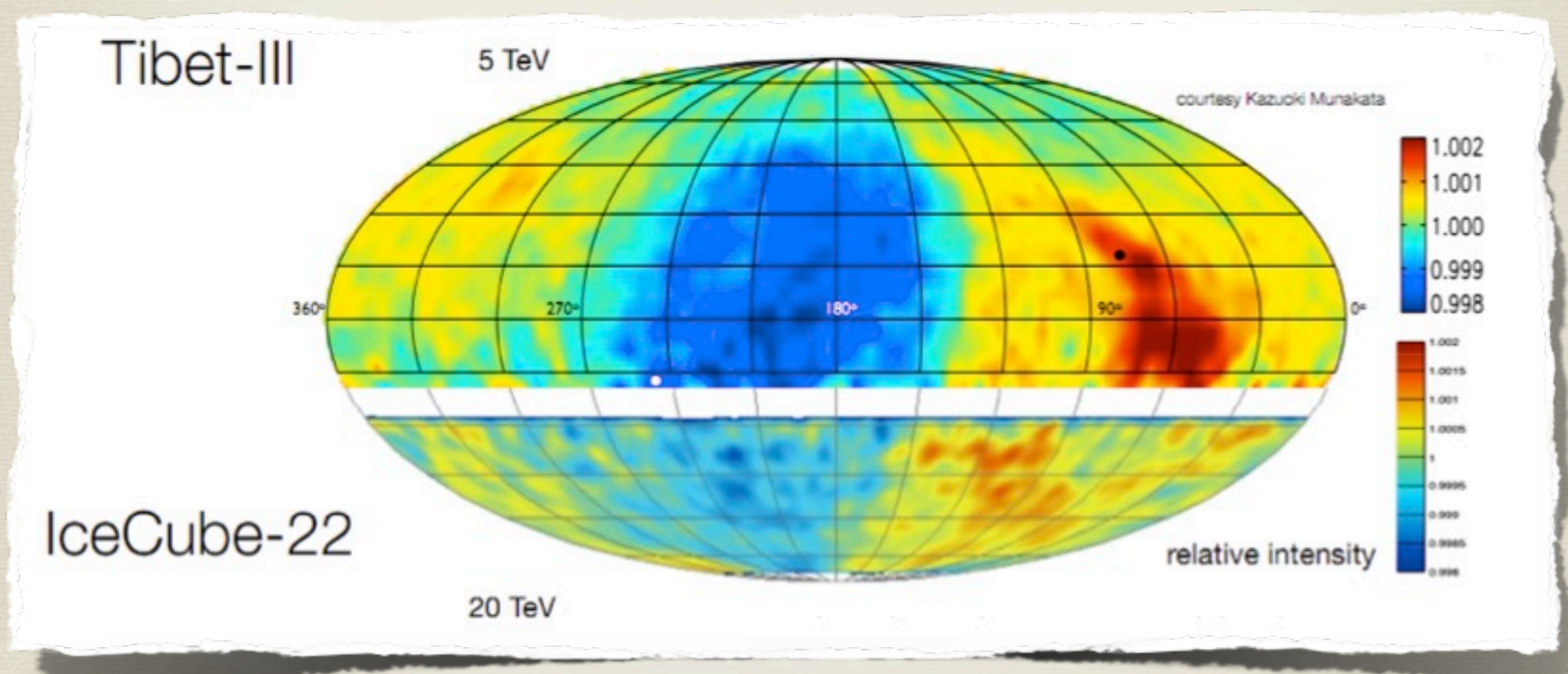
There have been several observations of *large-scale, part-per-mille anisotropy* in cosmic ray arrival directions between 0.1 and 100 TeV.



Tibet AS γ	M. Amenomori et al., <i>Astrophys. J.</i> 626 (2005) L29
SuperK	G. Guillian et al., <i>Phys. Rev. D</i> 75 (2007) 062003
Milagro	A. Abdo et al., <i>Astrophys. J.</i> 698 (2009) 2121
ARGO-YBJ	S. Vernetto, Proc. 31st ICRC, 2009
EAS-Top	M. Aglietta, <i>Astrophys. J.</i> 692 (2009) L130
IceCube	R. Abbasi <i>et al.</i> , <i>Astrophys. J.</i> 718 (2010) L194

Large scale anisotropy

- *IceCube observed a large scale anisotropy at 10^{-3} level for the first time in the Southern Sky.
- *The anisotropy appears to be a continuation of large scale structures observed in the Northern Hemisphere.



Relative intensity of the cosmic ray event rate in equatorial coordinates: for each declination belt of width 3° , the plot shows the number of events relative to the average number of events in the belt.

Energy dependence of the anisotropy

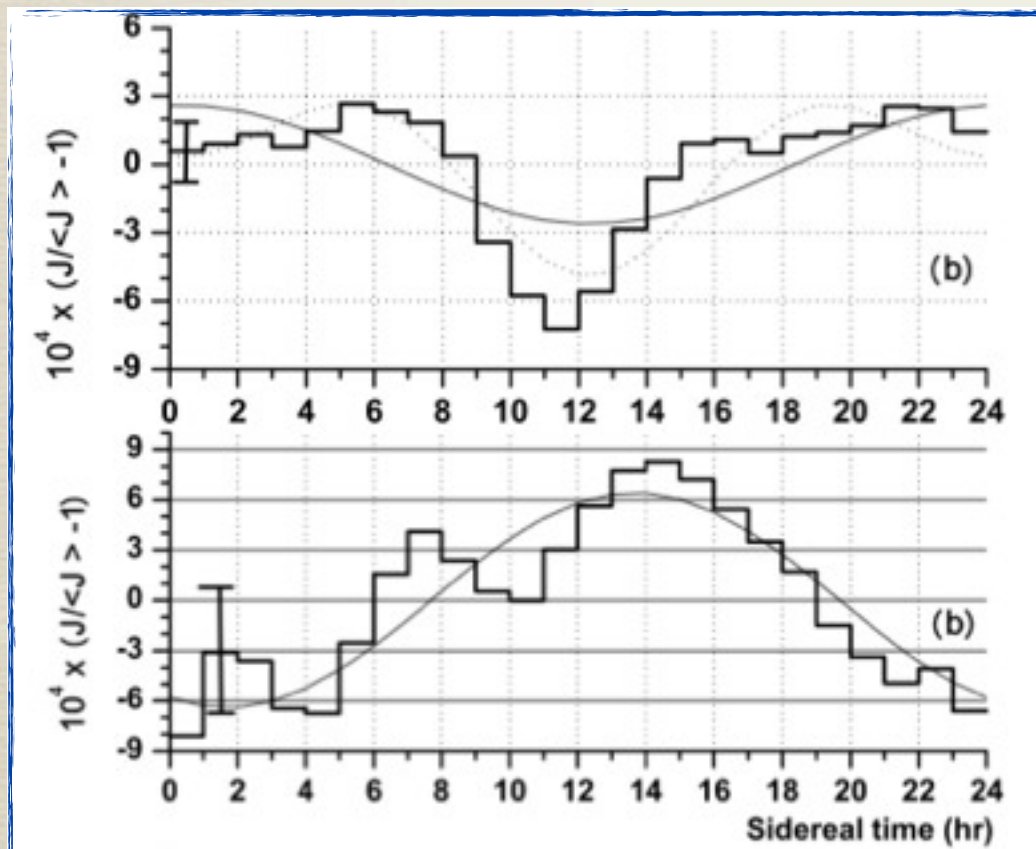
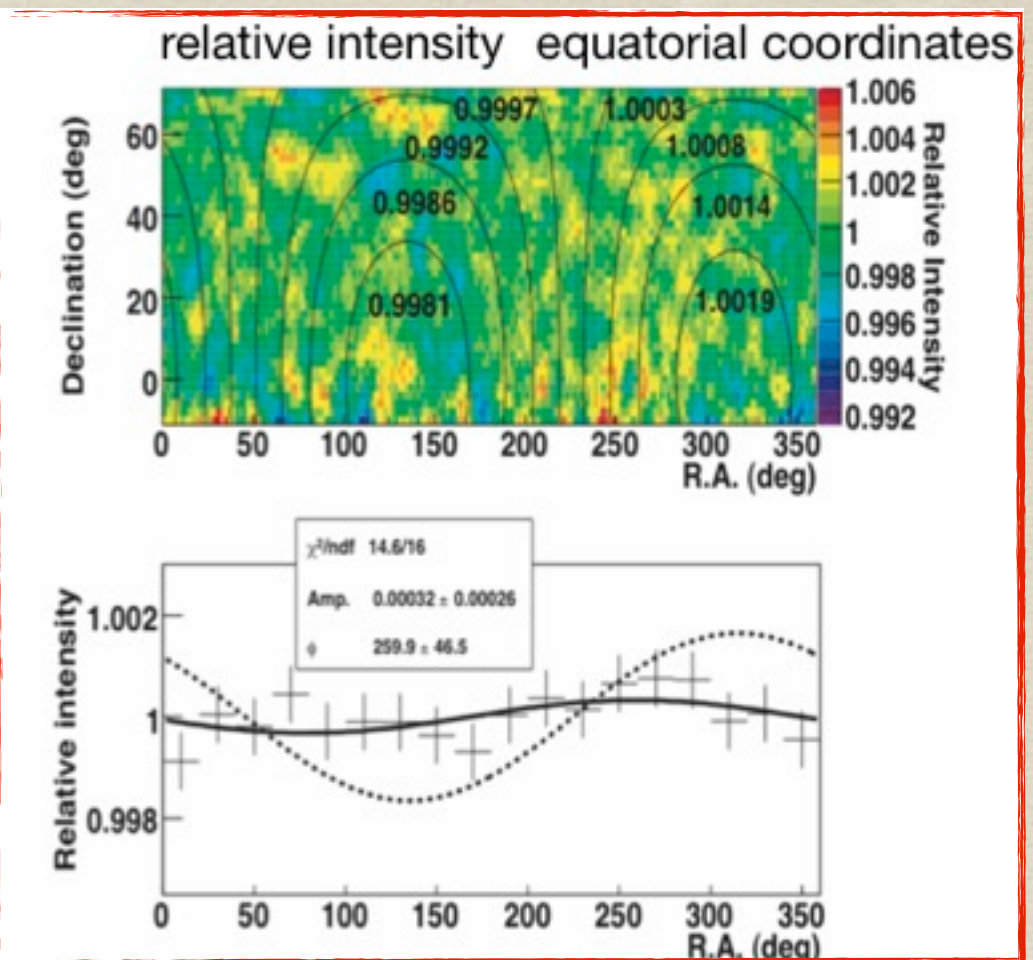
300 TeV

Tibet - III

Amenomori et al., Science Vol. 314, pp. 439, 2006

Amplitude: $(3.2 \pm 2.6) \times 10^{-4}$

consistent with **no anisotropy**



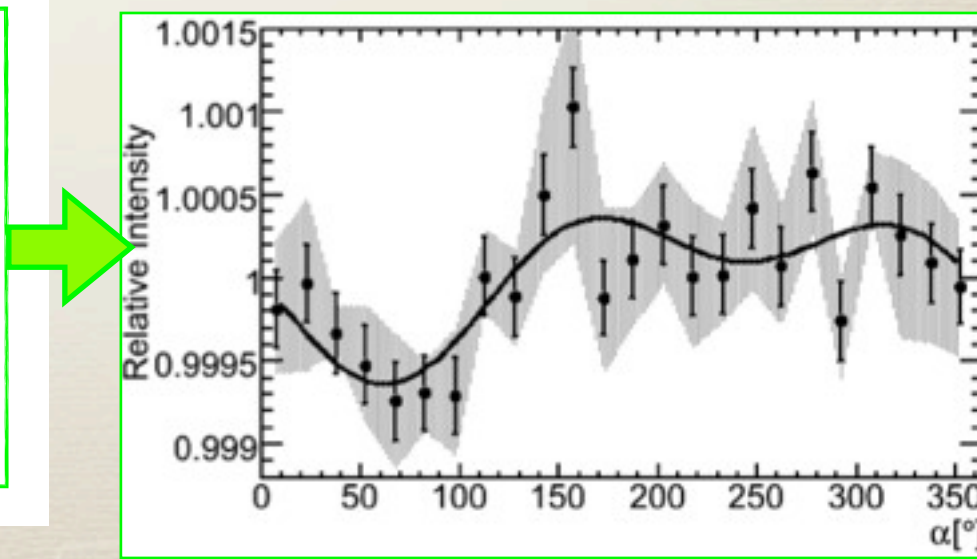
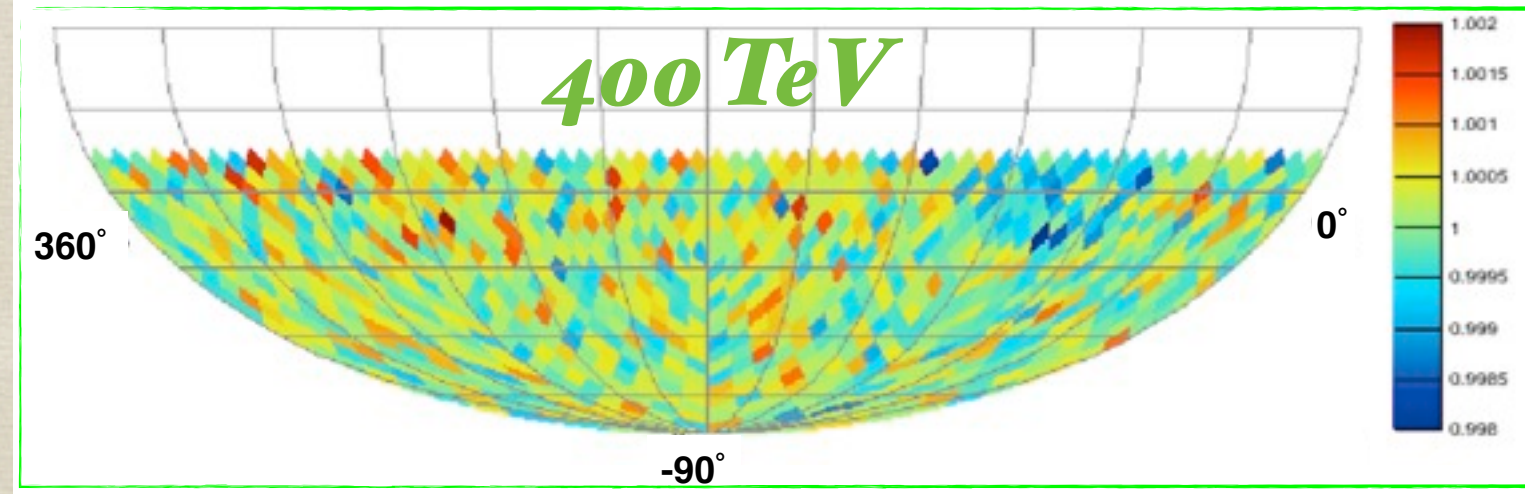
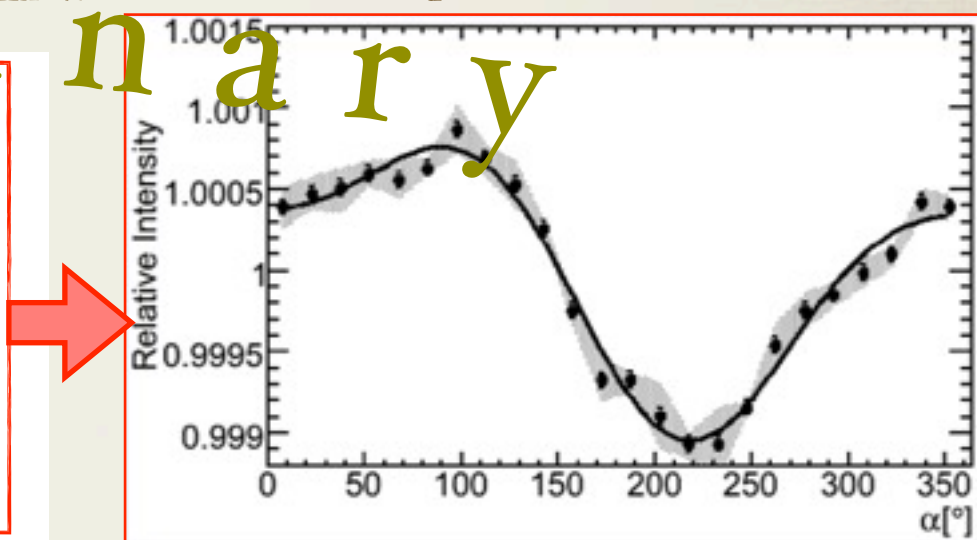
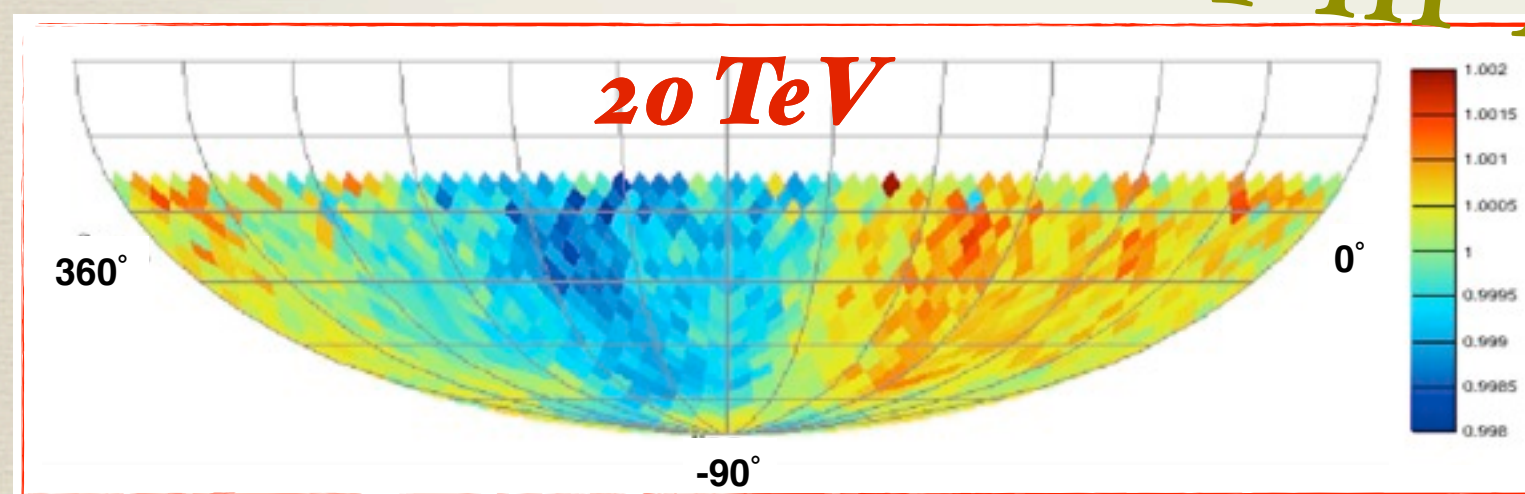
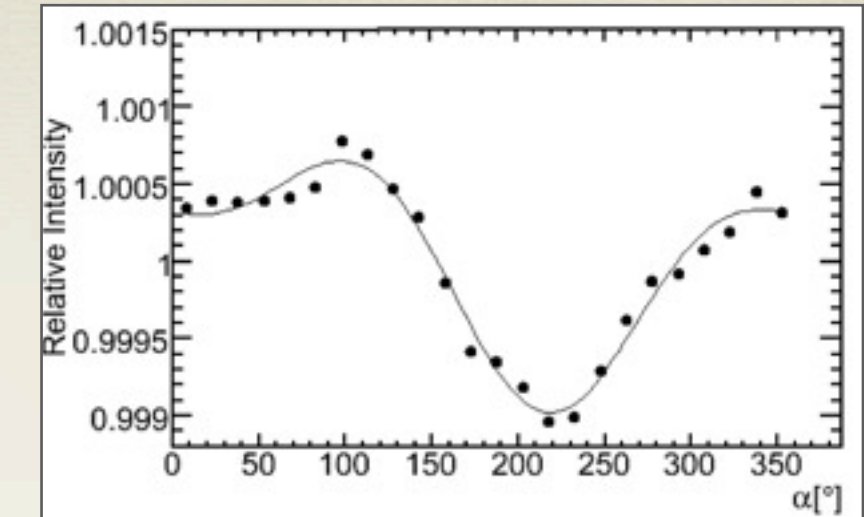
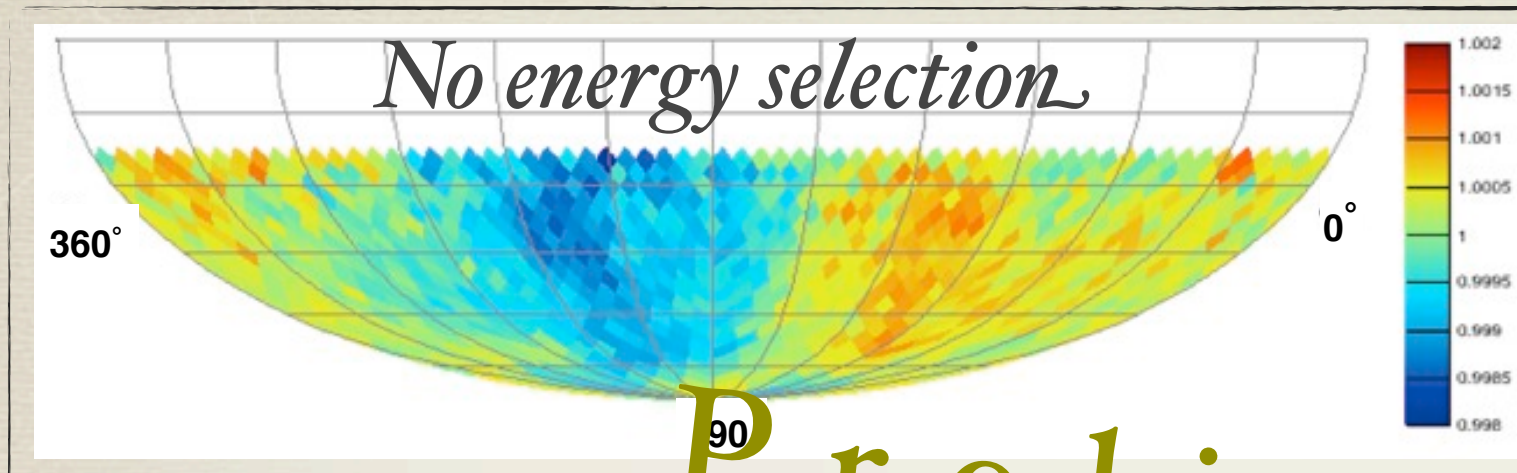
EAS-Top
Aglietta et al., ApJ 692, L130, 2009

Amplitude (370 TeV): $(6.4 \pm 2.5) \times 10^{-4}$

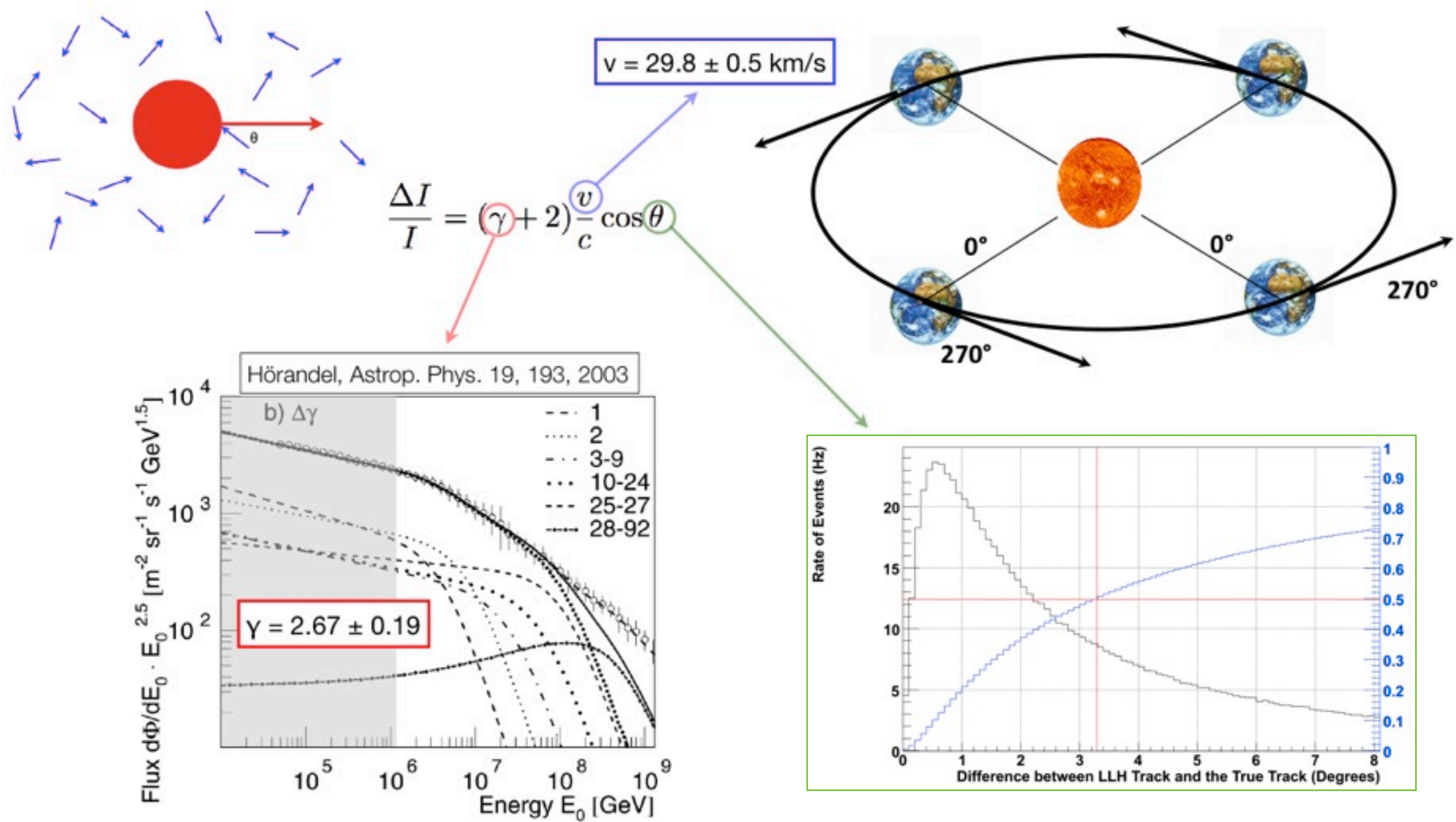
low significance, still not conclusive.

Relative Intensity

Equatorial sky maps in HEALPix with NSide= 16, pix resol ~ 3°



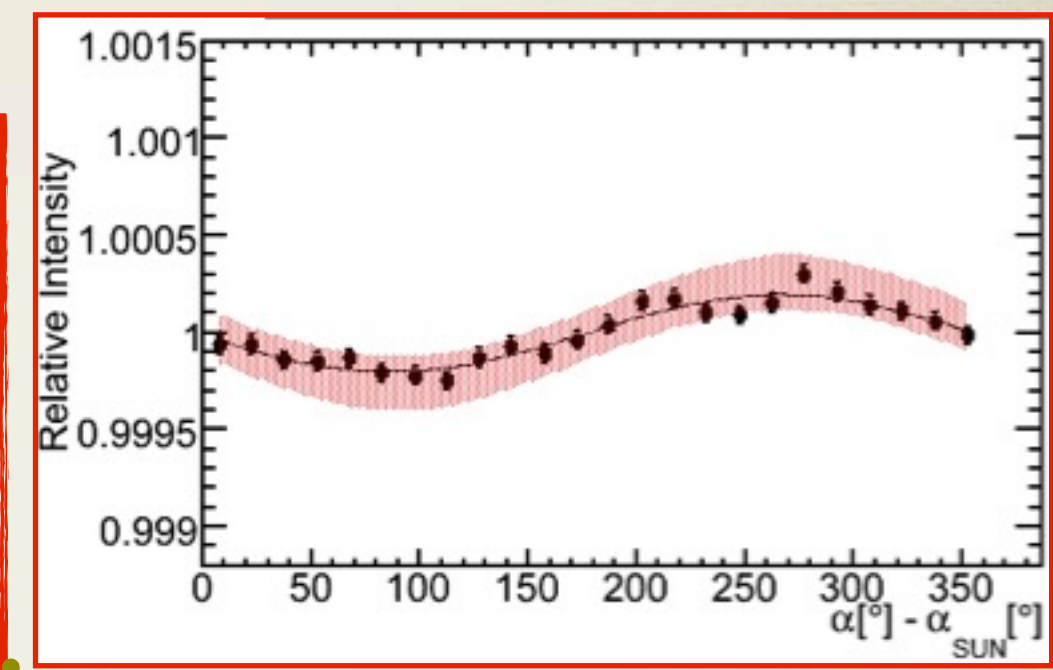
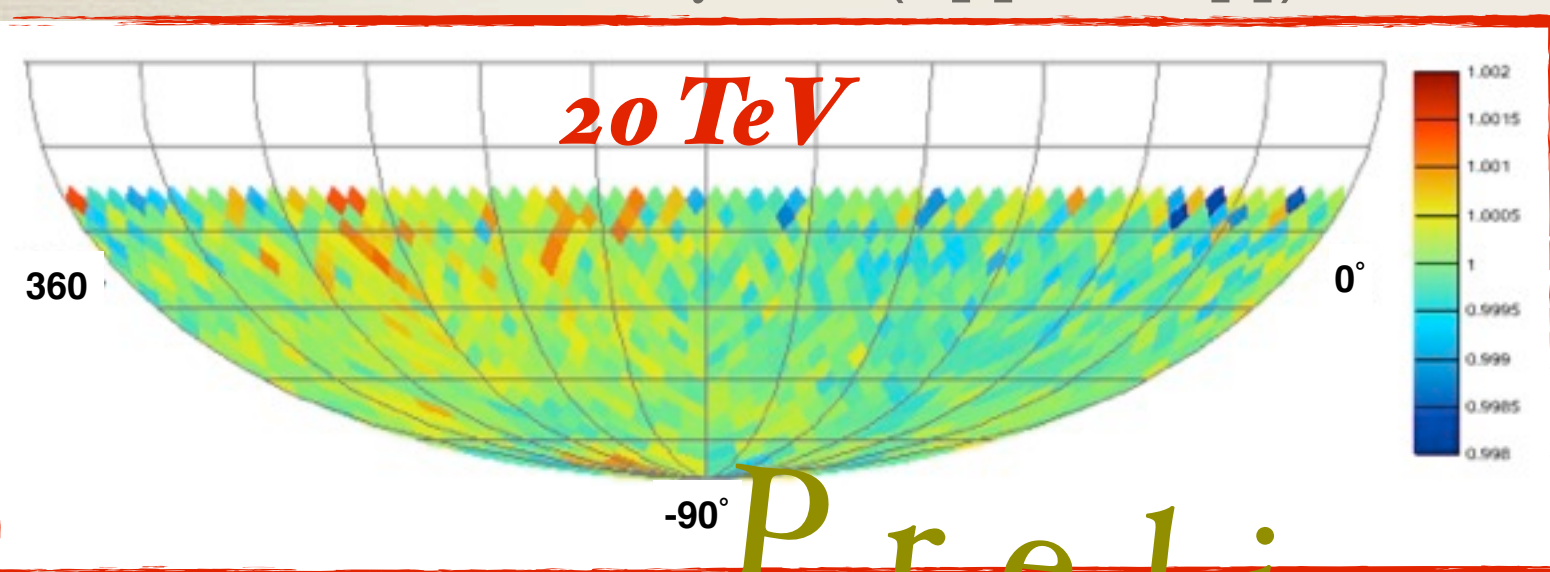
Earth's motion around the Sun: the Solar dipole



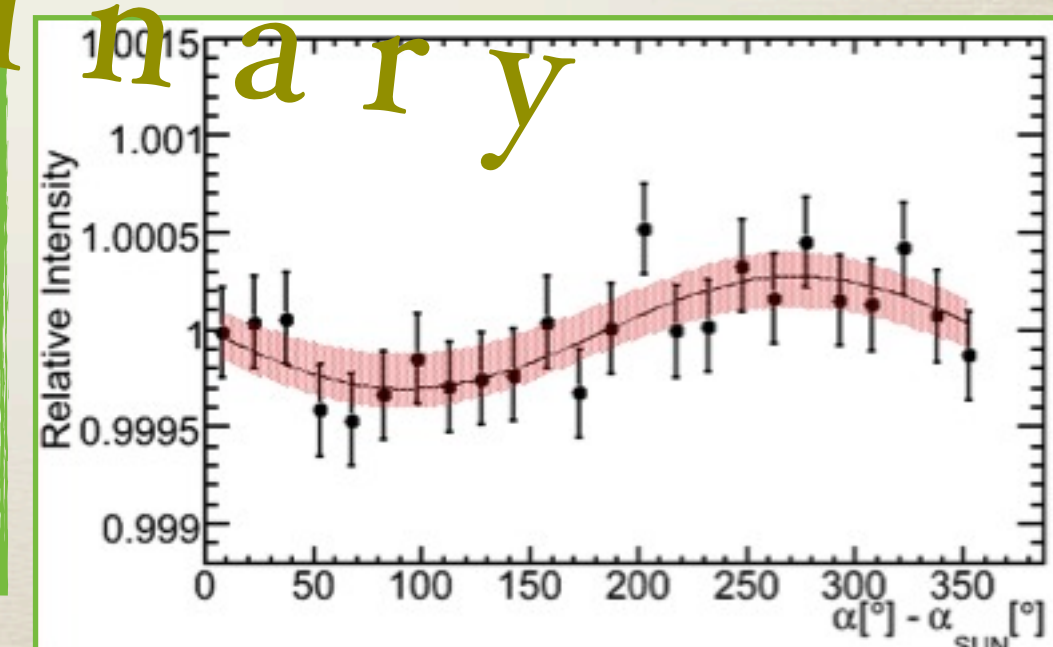
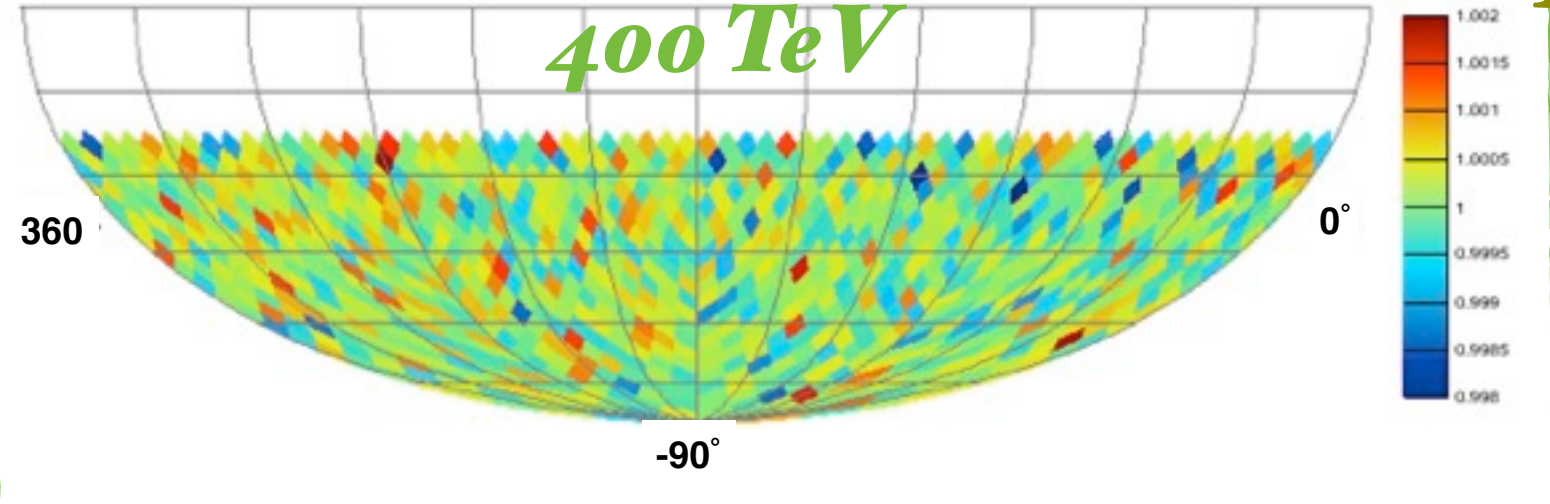
Energy dependence of the Solar dipole

- * IceCube observes the Solar dipole in both energy bins. The observed amplitude is compatible with the expectations within the stat. and sys. uncertainties.
- * The observation of the solar dipole supports the observation of the sidereal anisotropy in cosmic ray arrival direction.

relative intensity Vs. $(\alpha[\circ] - \alpha_{\text{SUN}}[\circ])$



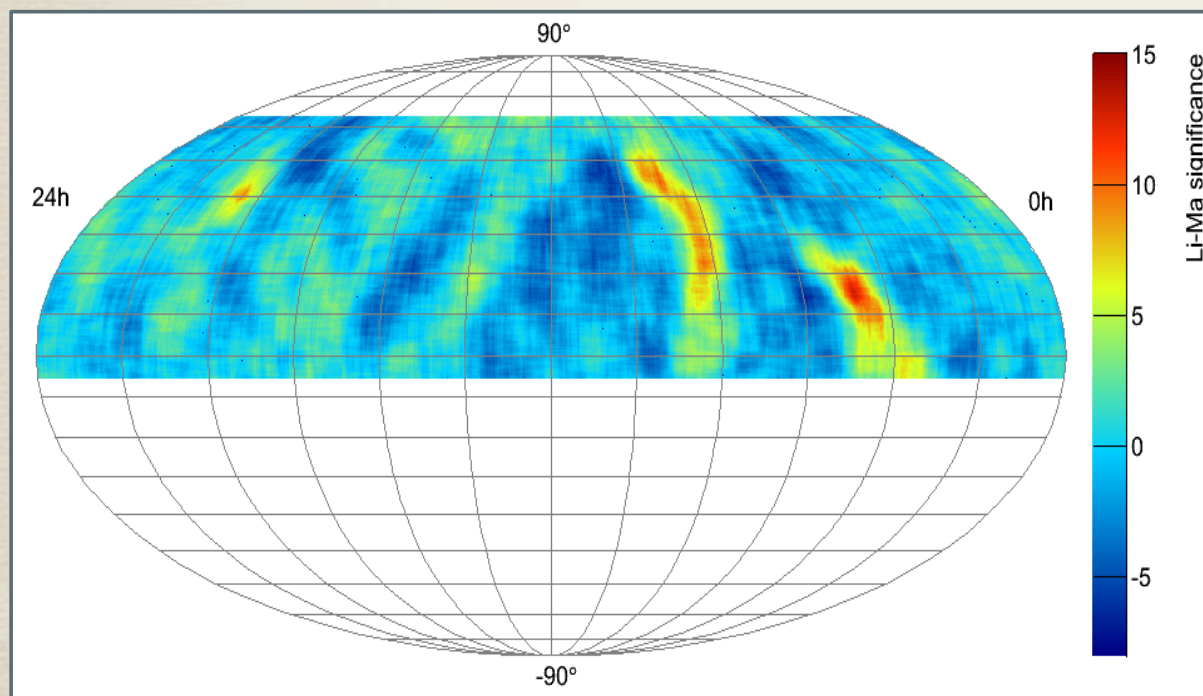
P r e l i m i



Small scale anisotropy

Several experiments have discovered anisotropies on scales of about 10°

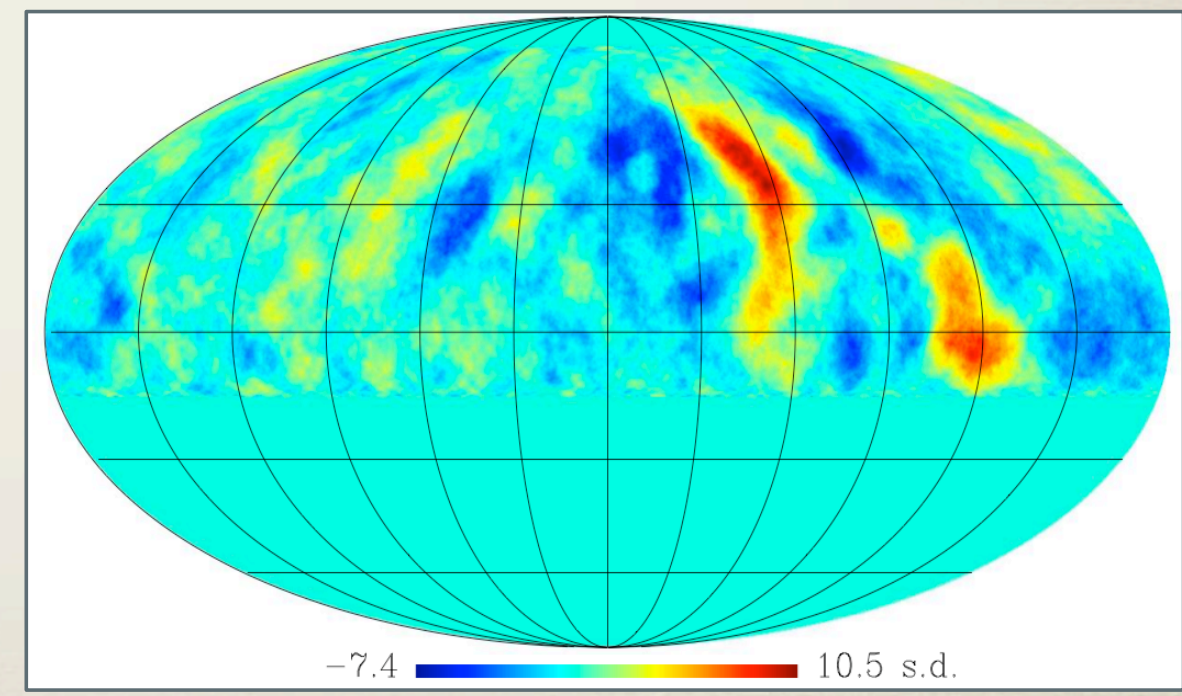
- * Milagro observes two localized regions with **significance $> 10\sigma$** in the total data set of $2.2 \cdot 10^{11}$ events recorded over 7 years. The “hot” regions have fractional excesses of order several times **10^{-4}** relative to the background.
- * Same structures observed by ARGO-YBJ.



Milagro

Median Energy: 1 TeV

A. Abdo et al., PRL 101 (2008) 221101

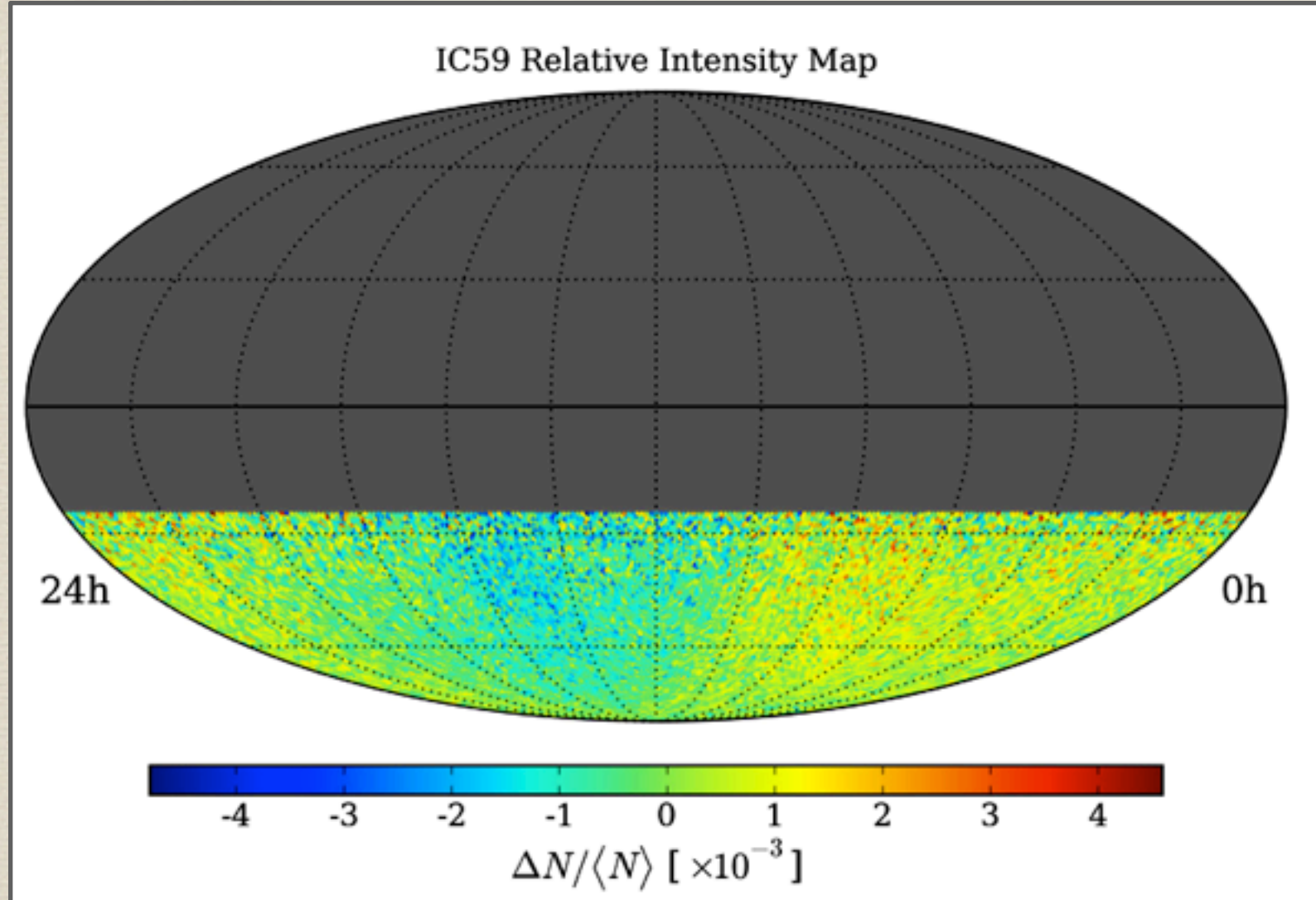


ARGO-YBJ

Median Energy: 2 TeV

Relative Intensity map

Equatorial sky maps in HEALPix: equal area pixel (size ~ 0.9°)



Sky map created using the background estimation technique from real data:

- N_i : number of data events in the i^{th} pixel.
- $\langle N_i \rangle$: expected number of events in an isotropic sky (time scrambling in 24 hr) in the i^{th} pixel.
- Relative Intensity:

$$\frac{\Delta N_i}{\langle N \rangle_i} = \frac{N_i(\alpha, \delta) - \langle N_i(\alpha, \delta) \rangle}{\langle N_i(\alpha, \delta) \rangle}.$$

Relative intensity map is *not isotropic*. In IceCube-59, the *strong large scale structure* already observed in IceCube-22 data is visible in the “raw” data.

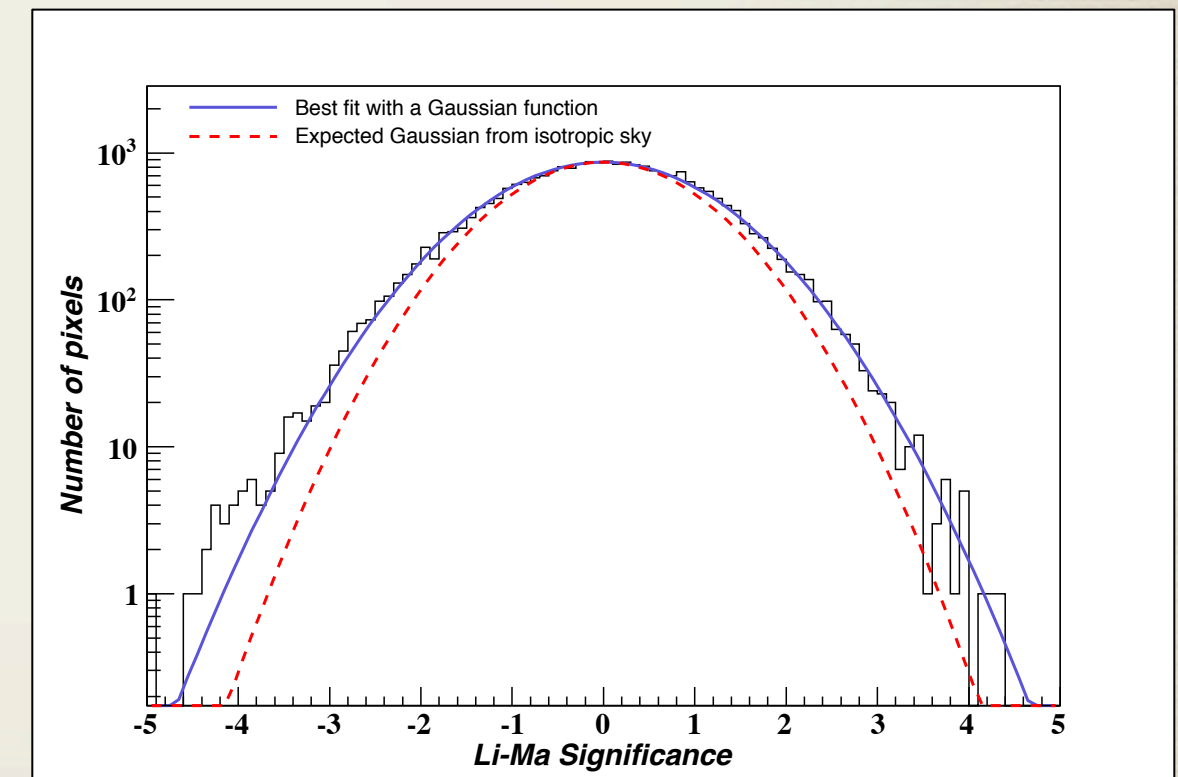
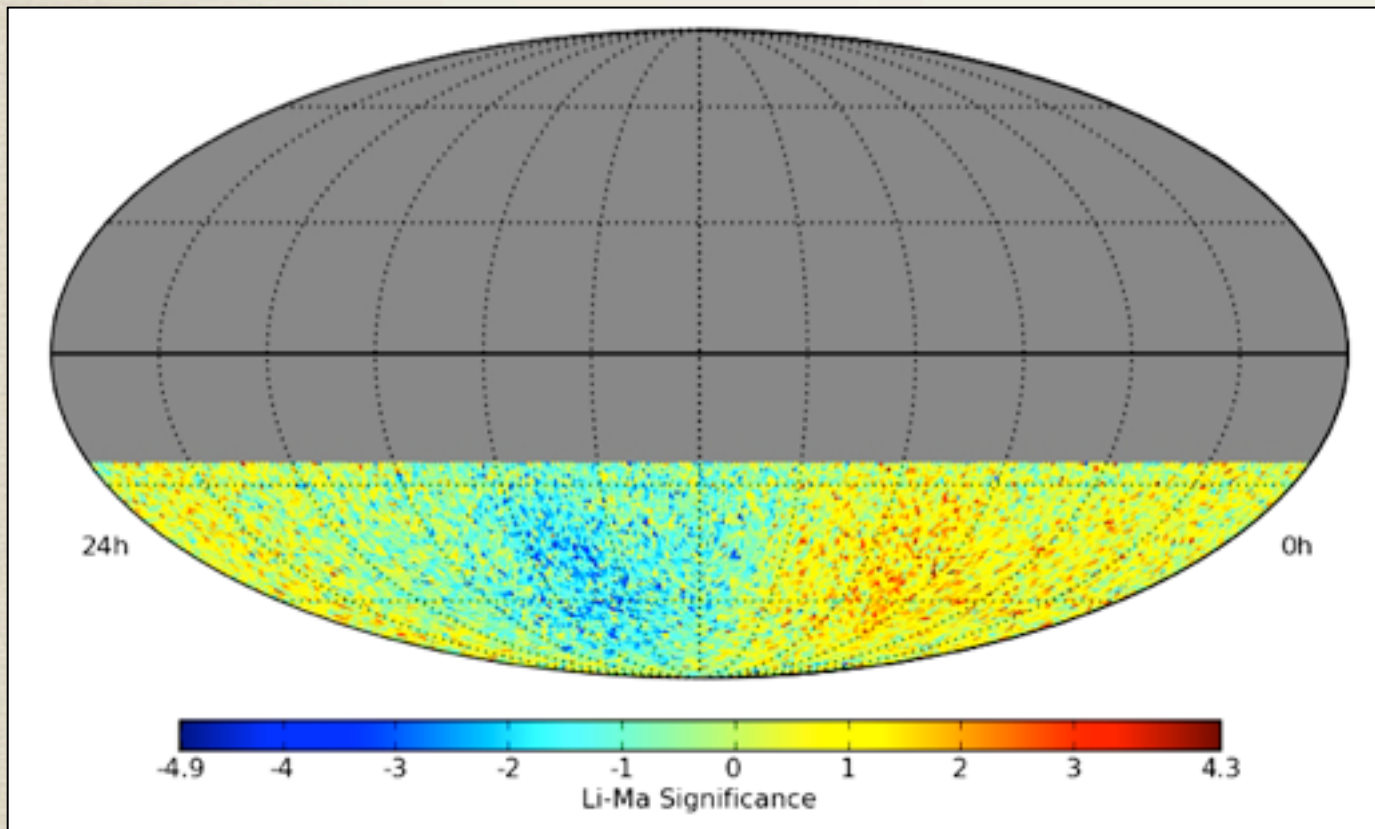
Significance map

Significance calculation:

$$s = \sqrt{2} \left\{ N_{\text{on}} \ln \left[\frac{1 + \alpha}{\alpha} \left(\frac{N_{\text{on}}}{N_{\text{on}} + N_{\text{off}}} \right) \right] + N_{\text{off}} \ln \left[(1 + \alpha) \left(\frac{N_{\text{off}}}{N_{\text{on}} + N_{\text{off}}} \right) \right] \right\}^{1/2}$$

$$\alpha = 1/20$$

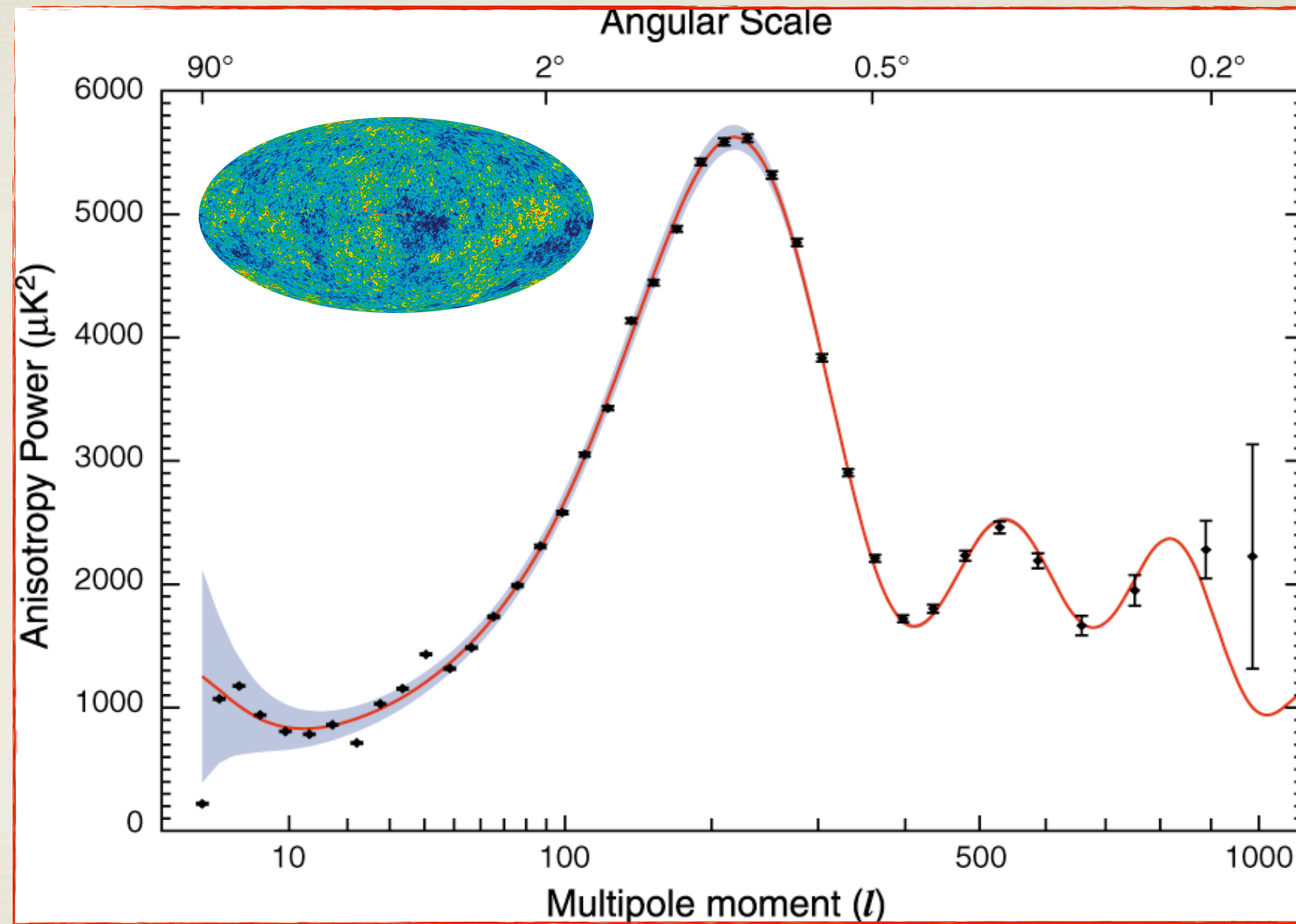
Li, T., & Ma, Y. 1983, ApJ, 272, 317



Power spectrum

Angular size

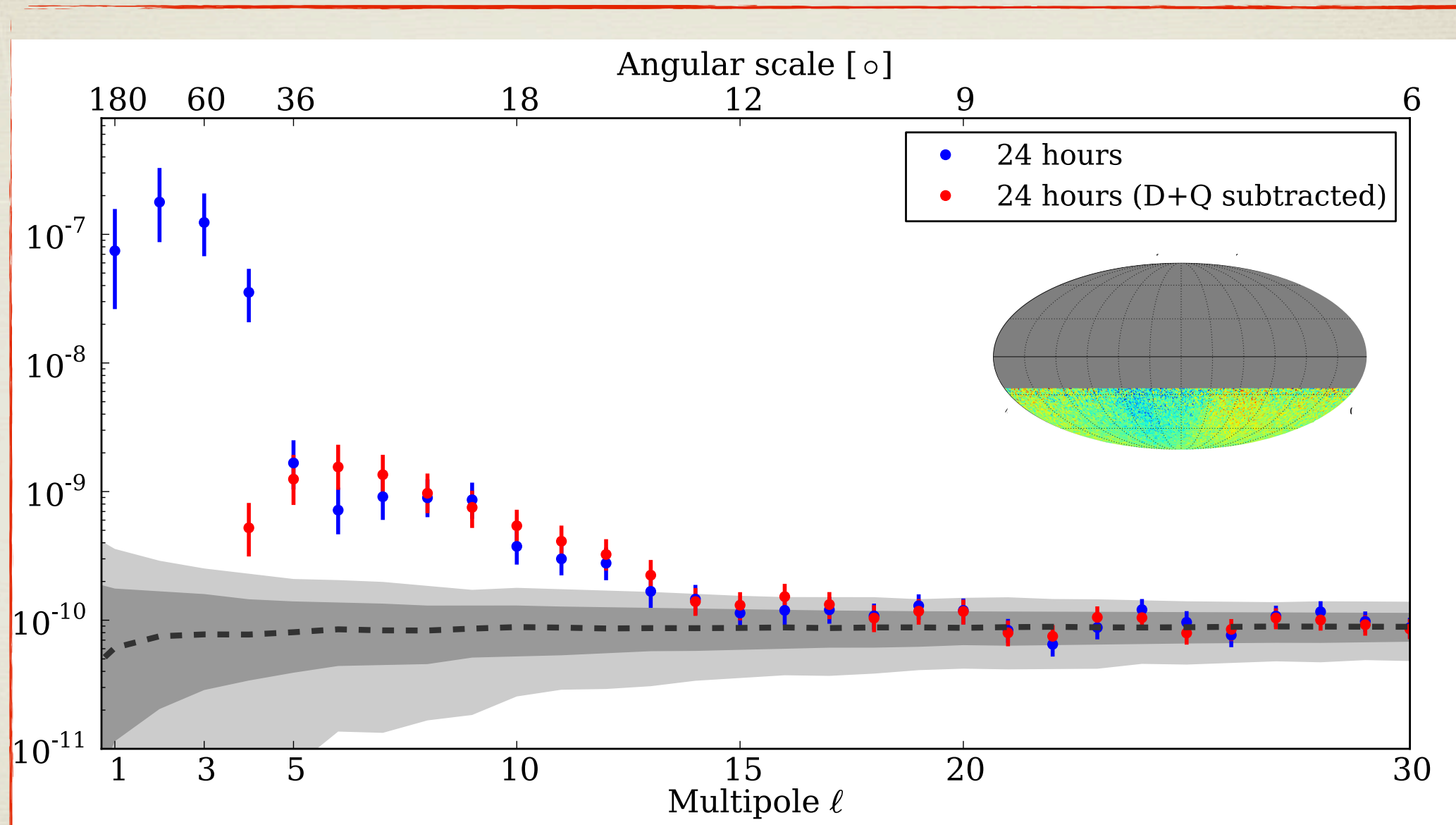
$$\theta \sim \frac{180^\circ}{\ell}$$



Multipole expansion: $\delta I(\mathbf{u}_i) = \sum_{\ell=1}^{\infty} \sum_{m=-\ell}^{\ell} a_{\ell m} Y_{\ell m}(\mathbf{u}_i)$ $\mathcal{C}_{\ell} = \frac{1}{2\ell + 1} \sum_m |a_{\ell m}|^2$

Power spectrum

Angular size $\theta \sim \frac{180^\circ}{\ell}$



Multipole expansion: $\delta I(\mathbf{u}_i) = \sum_{\ell=1}^{\infty} \sum_{m=-\ell}^{\ell} a_{\ell m} Y_{\ell m}(\mathbf{u}_i)$ $\mathcal{C}_{\ell} = \frac{1}{2\ell + 1} \sum_m |a_{\ell m}|^2$

Dipole and quadrupole fit

$$\delta I(\alpha, \delta) = m_0$$

monopole

$$+ p_x \cos \delta \cos \alpha + p_y \cos \delta \sin \alpha + p_z \sin \delta$$

dipole

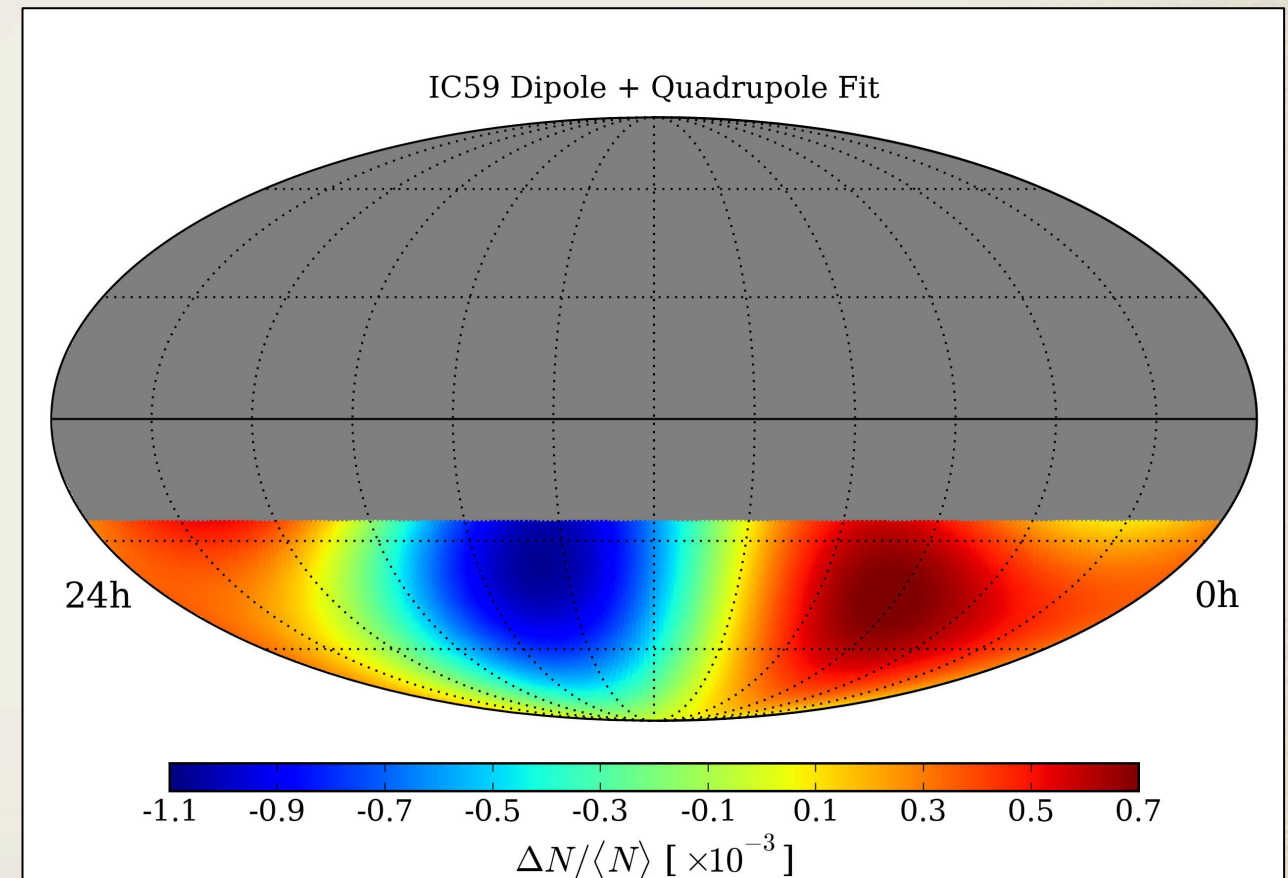
$$+ \frac{1}{2} Q_1 (3 \cos^2 \delta - 1) + Q_2 \sin 2\delta \cos \alpha + Q_3 \sin 2\delta \sin \alpha + Q_4 \cos^2 \delta \cos 2\alpha + Q_5 \cos^2 \delta \sin 2\alpha$$

quadrupole

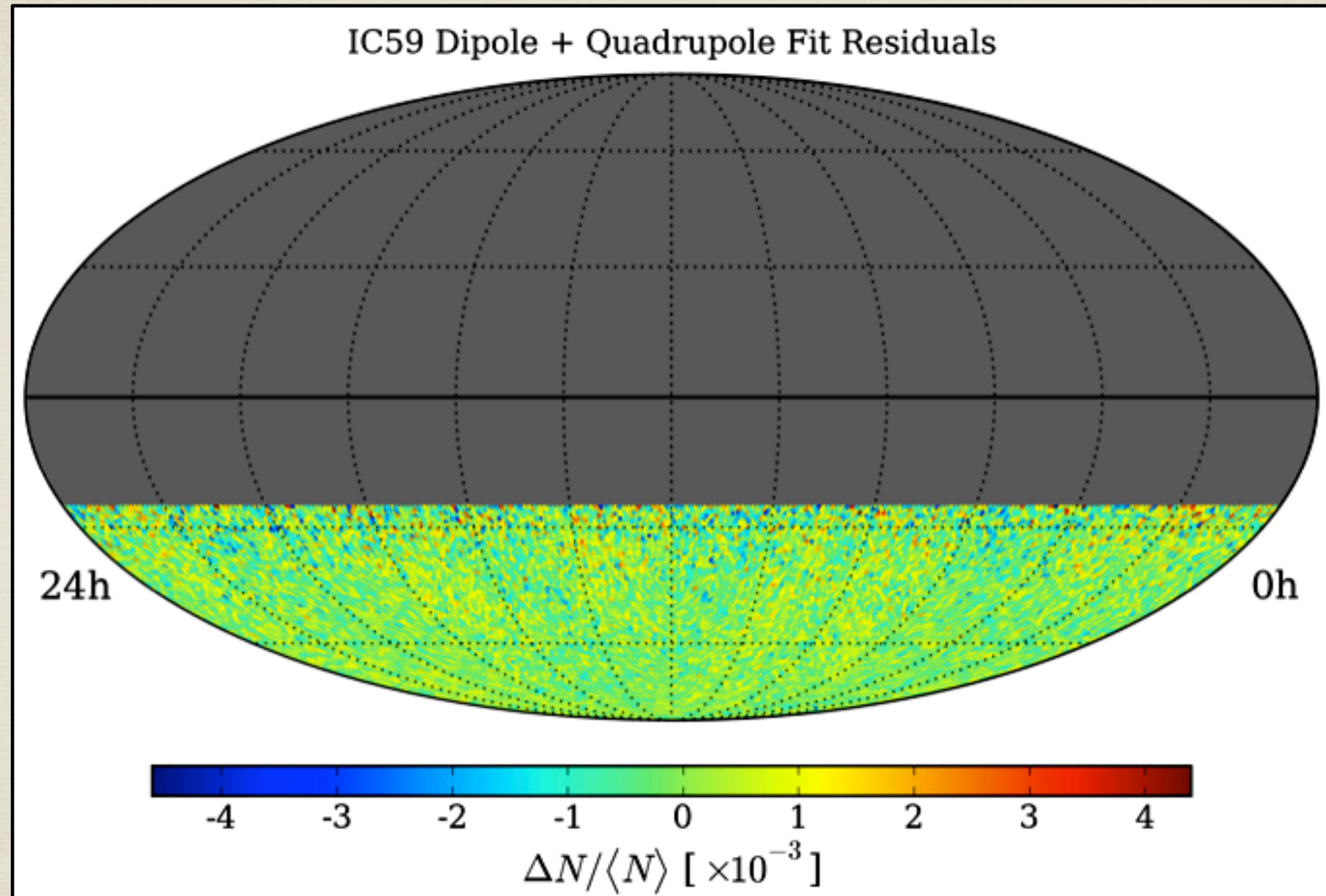
Coefficient	Fit Value
m_0	0.320 ± 2.264
p_x	2.435 ± 0.707
p_y	-3.856 ± 0.707
p_z	0.548 ± 3.872
Q_1	0.233 ± 1.702
Q_2	-2.949 ± 0.494
Q_3	-8.797 ± 0.494
Q_4	-2.148 ± 0.200
Q_5	-5.268 ± 0.200

$$\chi^2/\text{ndf} = 14743.4/14187$$

$$\Pr(\chi^2 | \text{ndf}) = 5.5 \times 10^{-4}$$



Residual map



No structures seem to be present: we need to smooth the map.



MAP SMOOTHING SCAN

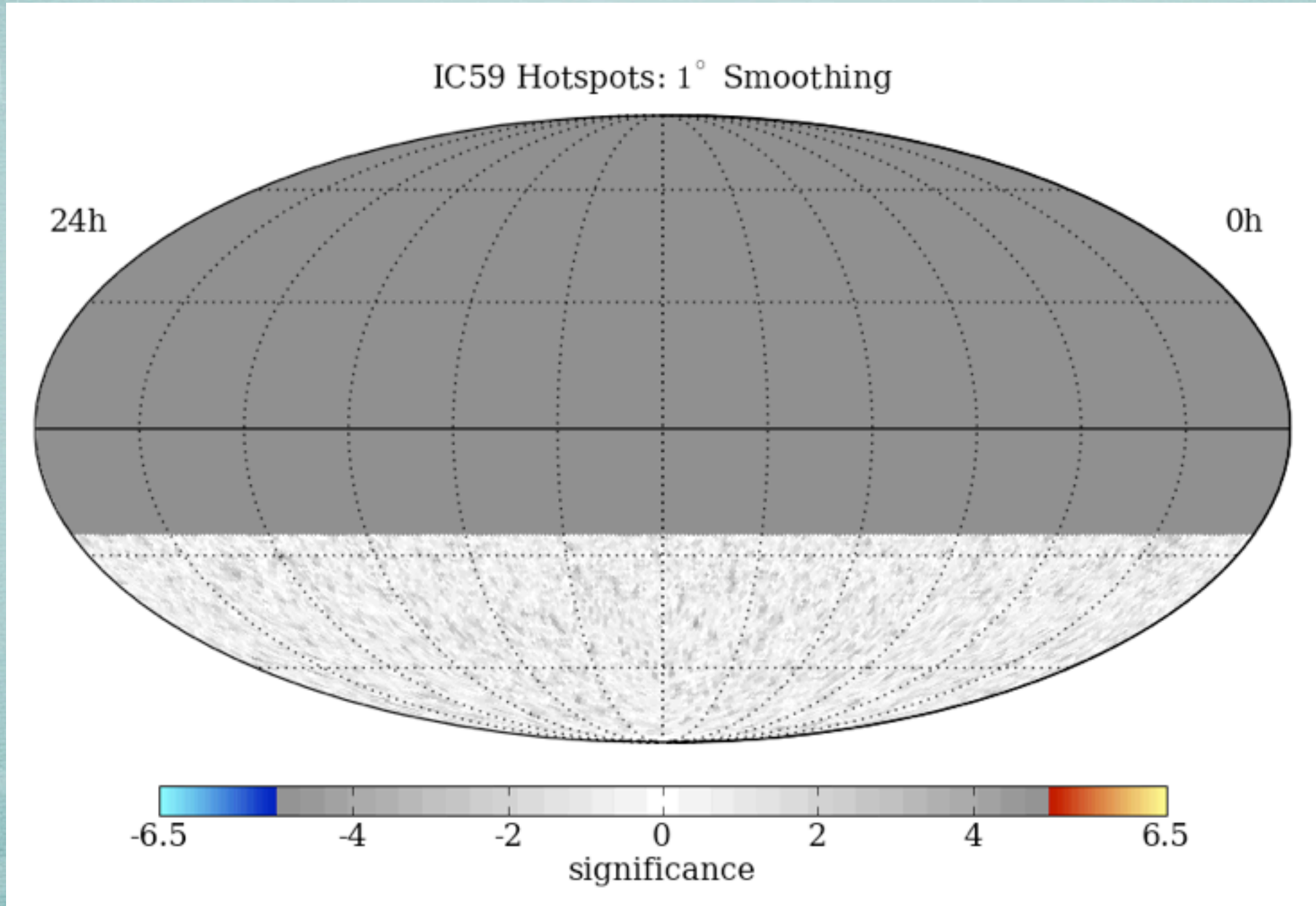
Scan from 1 - 30° in smoothing

Different regions have different optimal angular smoothing

Significances are pre-trial

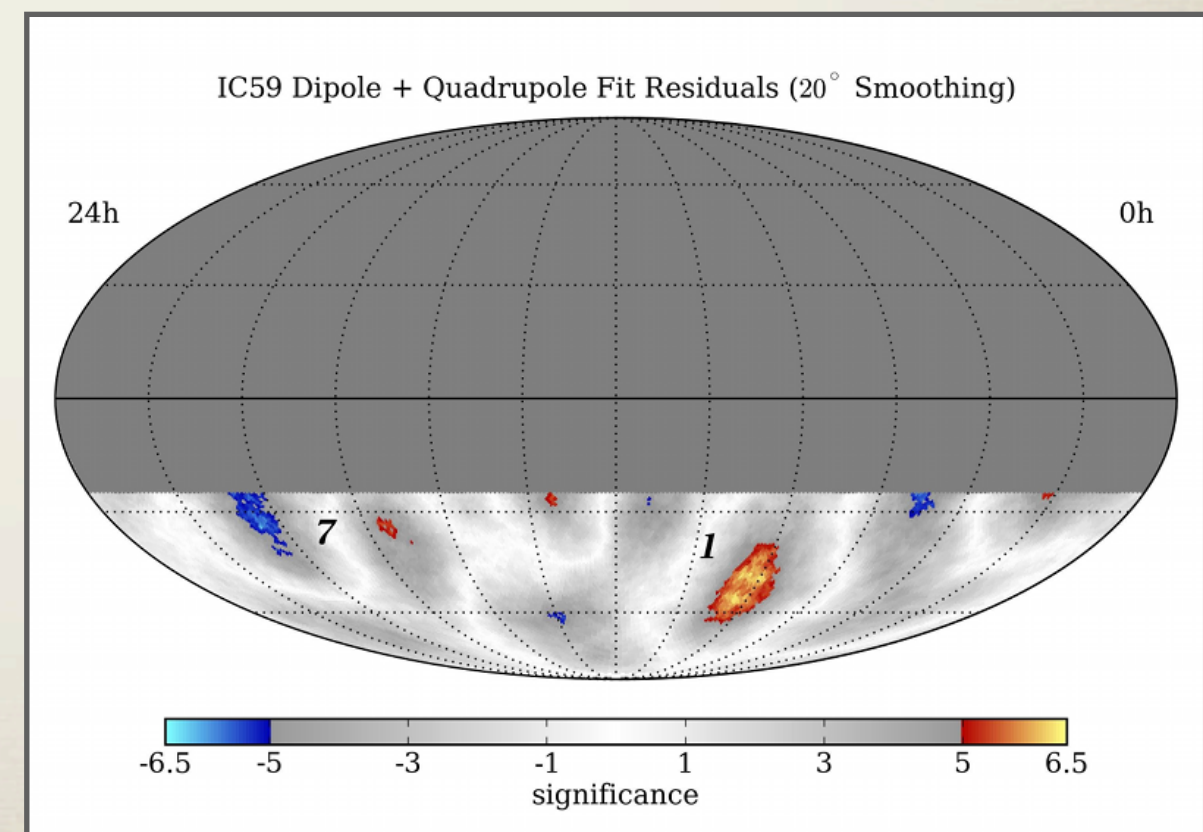
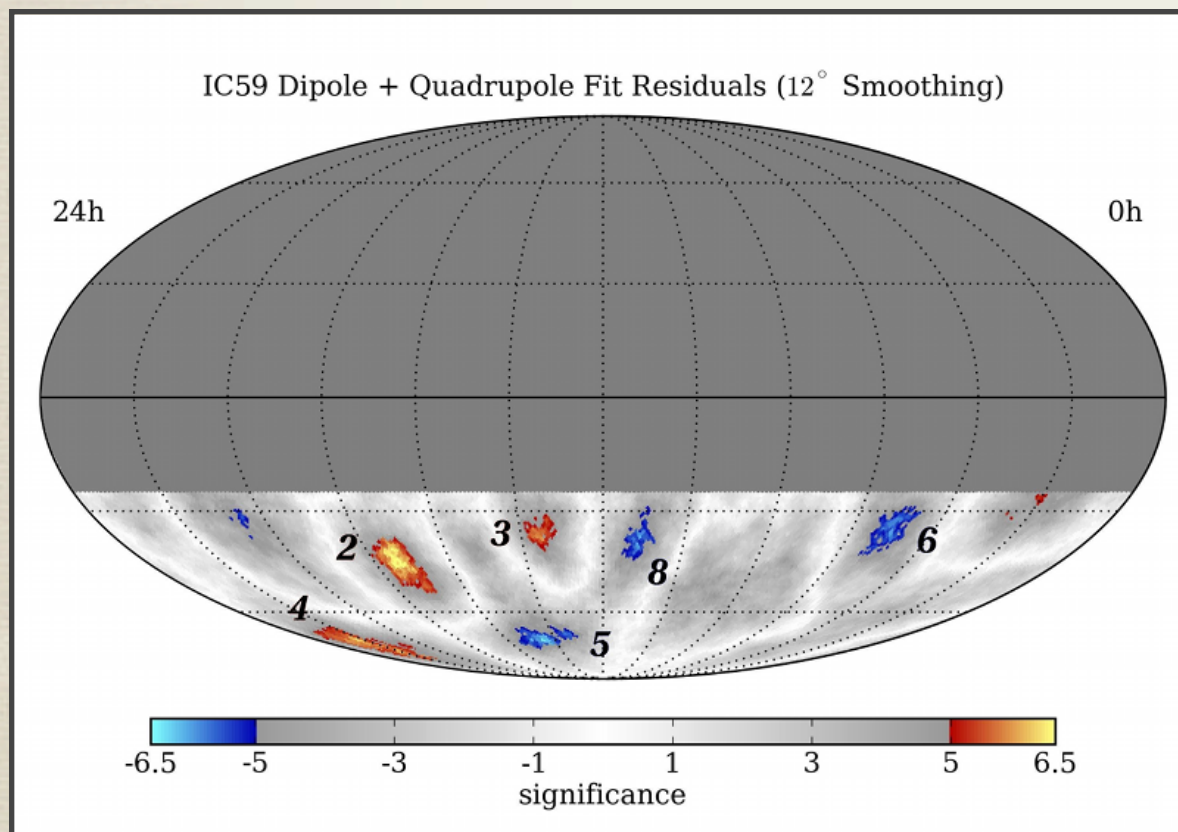
MAP SMOOTHING SCAN

Scan from 1 - 30° in smoothing
Different regions have different optimal angular smoothing
Significances are pre-trial



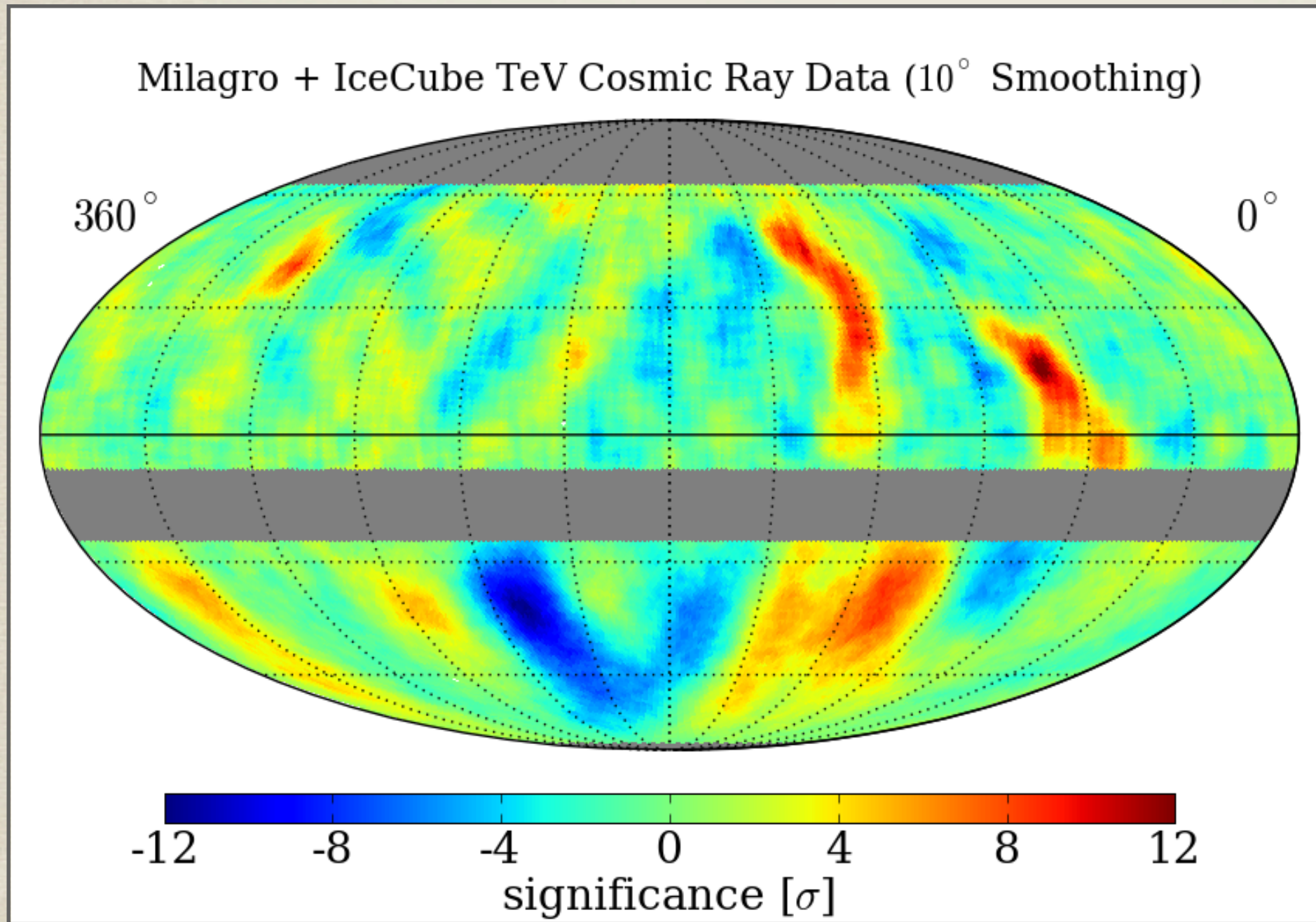
Identification of significant structures

region	right ascension	declination	optimal scale	peak significance	post-trials
1	$(122.4^{+4.1}_{-4.7})^\circ$	$(-47.4^{+7.5}_{-3.2})^\circ$	22°	7.0σ	5.3σ
2	$(263.0^{+3.7}_{-3.8})^\circ$	$(-44.1^{+5.3}_{-5.1})^\circ$	13°	6.7σ	4.9σ
3	$(201.6^{+6.0}_{-1.1})^\circ$	$(-37.0^{+2.2}_{-1.9})^\circ$	11°	6.3σ	4.4σ
4	$(332.4^{+9.5}_{-7.1})^\circ$	$(-70.0^{+4.2}_{-7.6})^\circ$	12°	6.2σ	4.2σ
5	$(217.7^{+10.2}_{-7.8})^\circ$	$(-70.0^{+3.6}_{-2.3})^\circ$	12°	-6.4σ	-4.5σ
6	$(77.6^{+3.9}_{-8.4})^\circ$	$(-31.9^{+3.2}_{-8.6})^\circ$	13°	-6.1σ	-4.1σ
7	$(308.2^{+4.8}_{-7.7})^\circ$	$(-34.5^{+9.6}_{-6.9})^\circ$	20°	-6.1σ	-4.1σ
8	$(166.5^{+4.5}_{-5.7})^\circ$	$(-37.2^{+5.0}_{-5.7})^\circ$	12°	-6.0σ	-4.0σ



Milagro + IceCube combined map

IceCube map contains all data from IC22, IC40 and IC59 data sets



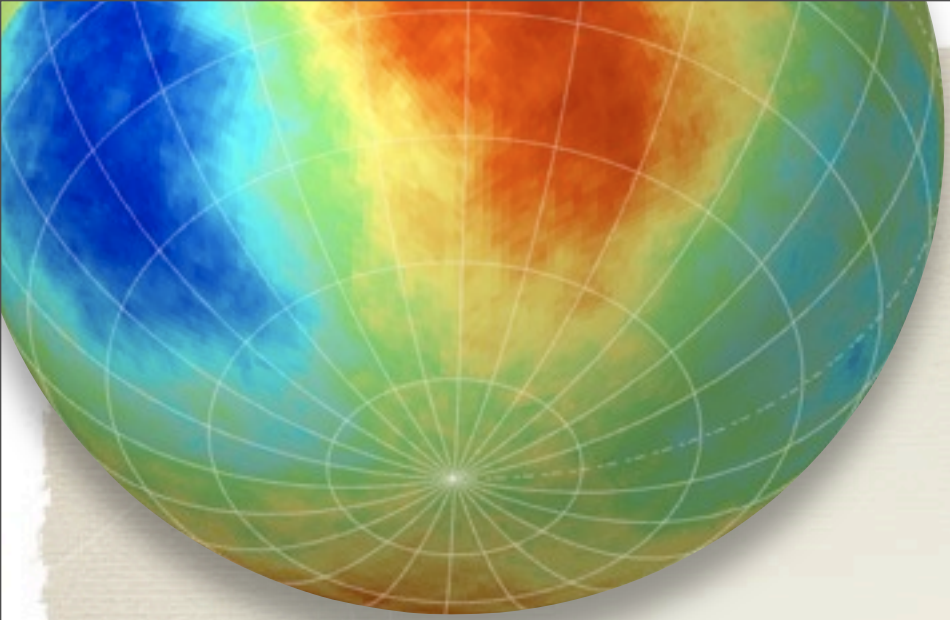
Milagro map:

[Abdo, A. A., et al. 2008, Phys. Rev. Lett., 101, 221101]

- 2.2×10^{11} events
- direct integration (2 hr)
- 10° smoothing
- median energy **1 TeV**

IceCube map:

- 5.6×10^{10} events
- time scrambling (4 hr)
- 10° smoothing
- median energy **20 TeV**

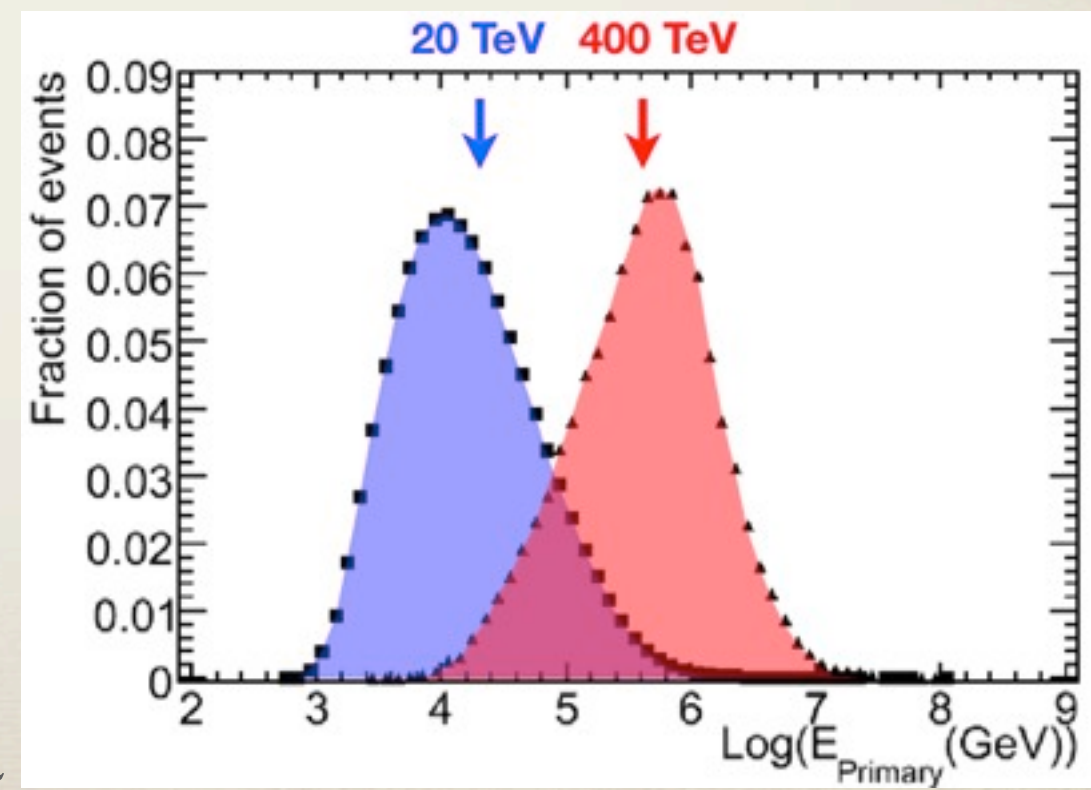
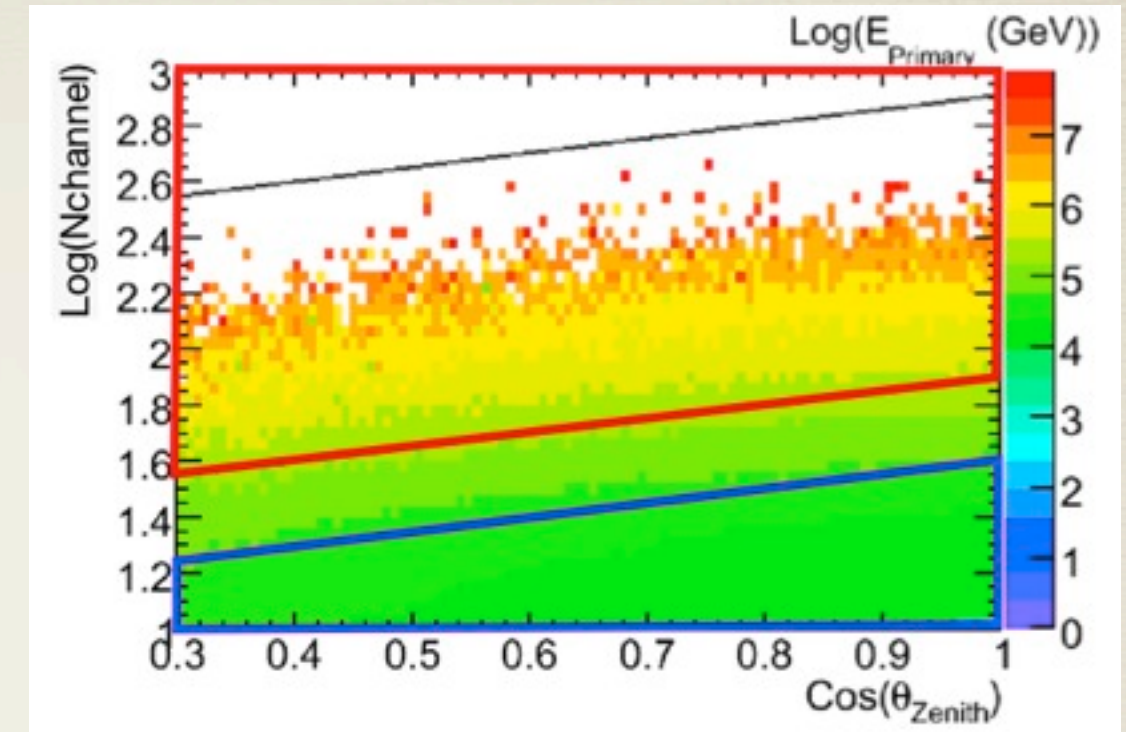
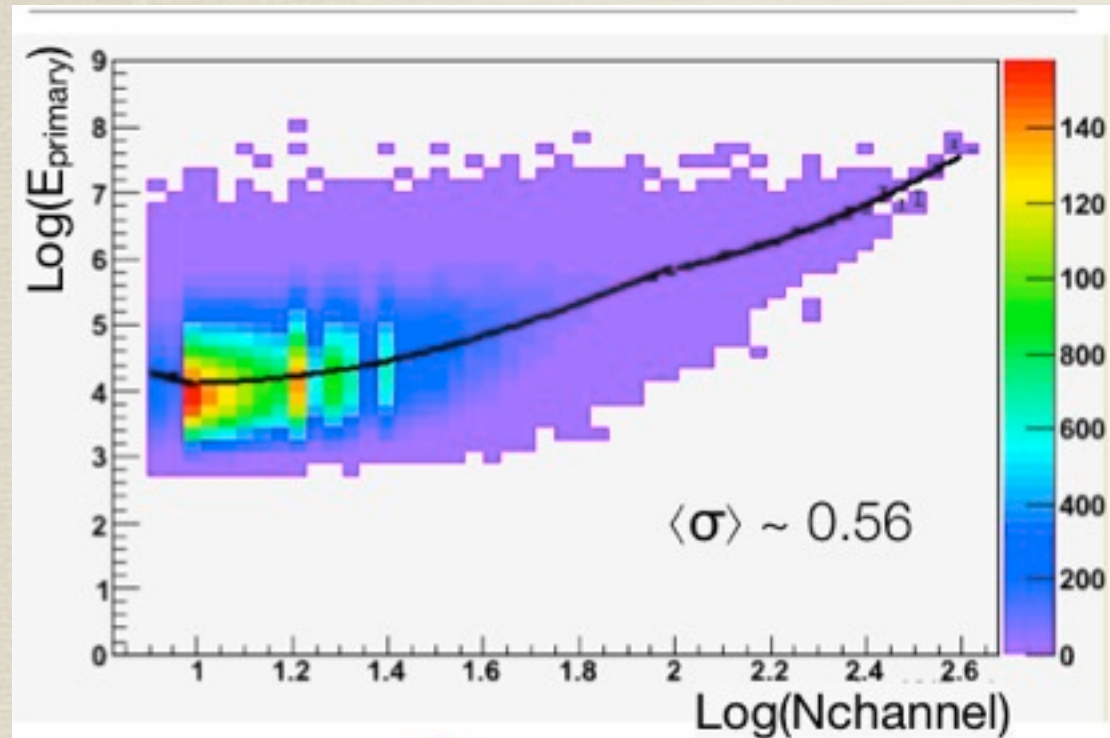


Conclusions

- * **IceCube** detector was **completed in December 2010** and is now taking data in its final configuration (86 strings).
- * **Large scale anisotropy:**
 - ▶ Sidereal anisotropy at 20 TeV confirms previous observation.
 - ▶ First observation of sidereal anisotropy @ 400 TeV in southern hemisphere.
 - ▶ Indication of a persistence of anisotropy @ 400 TeV: evidence of a “dip”.
- * **Small and medium scale** structures:
 - ▶ Southern sky in TeV cosmic rays shows significant anisotropy across a wide range of angular scales (10-180 degrees).
- * **The origin of the anisotropy is still unknown.**

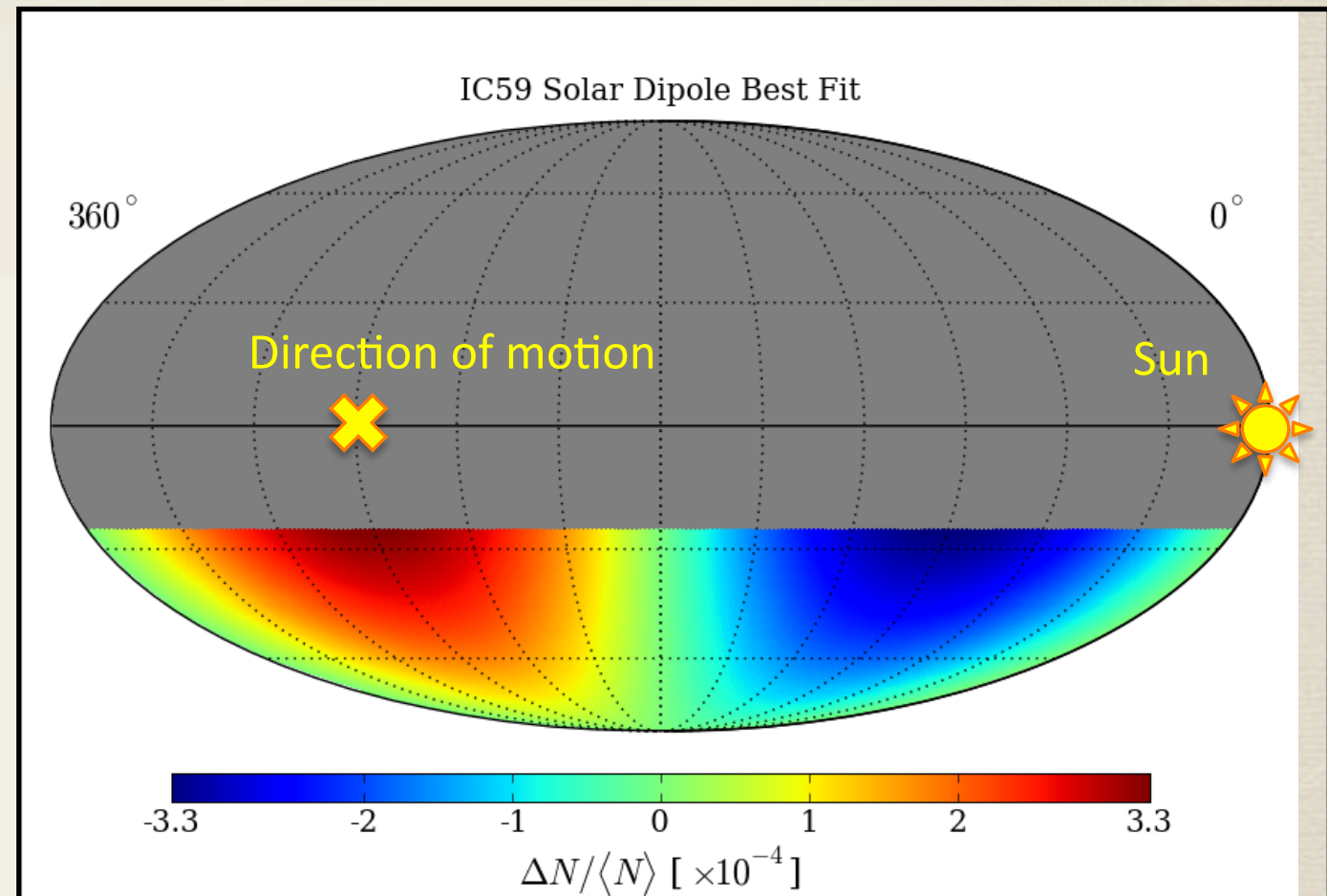
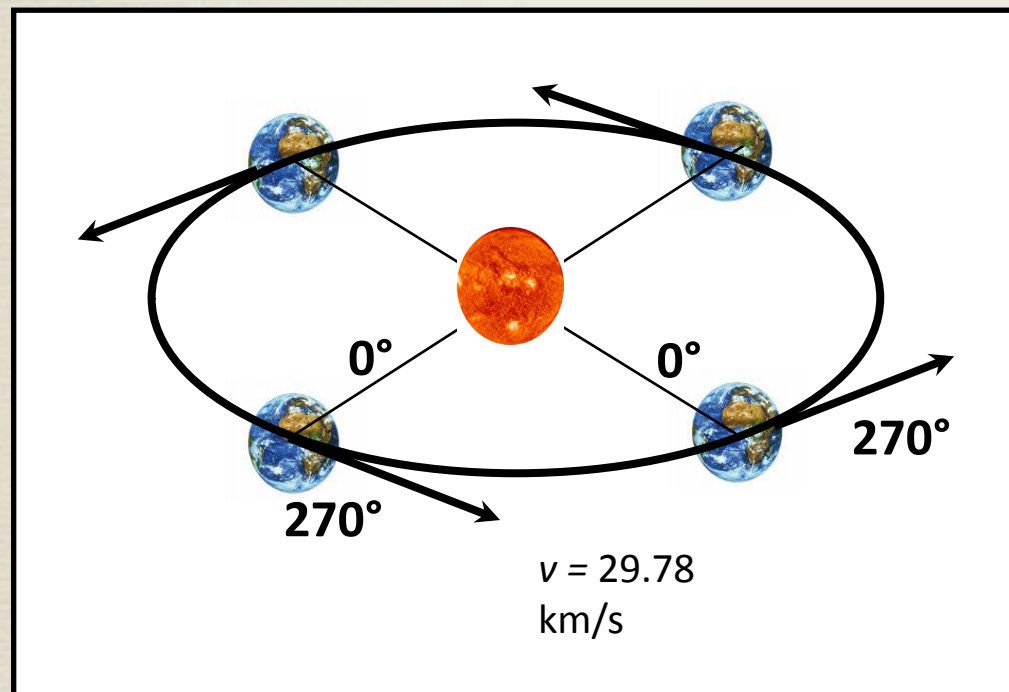
BACKUP SLIDES

Energy estimation



Systematics: Solar Dipole

We are sensitive to the motion of the Earth around the Sun (10^{-4} effect is expected): visible when UT is used in local-celestial coord. transformation.

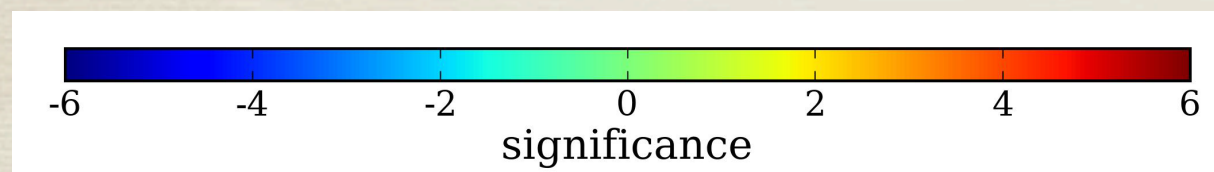


Coefficient	Fit Value ($\times 10^{-4}$)
m_0	-0.029 ± 0.058
p_x	0.017 ± 0.142
p_y	-3.661 ± 0.142
p_z	-0.027 ± 0.072

$$\chi^2/\text{ndf} = 14206.8/14192$$

$$\text{Pr}(\chi^2|\text{ndf}) = 0.416$$

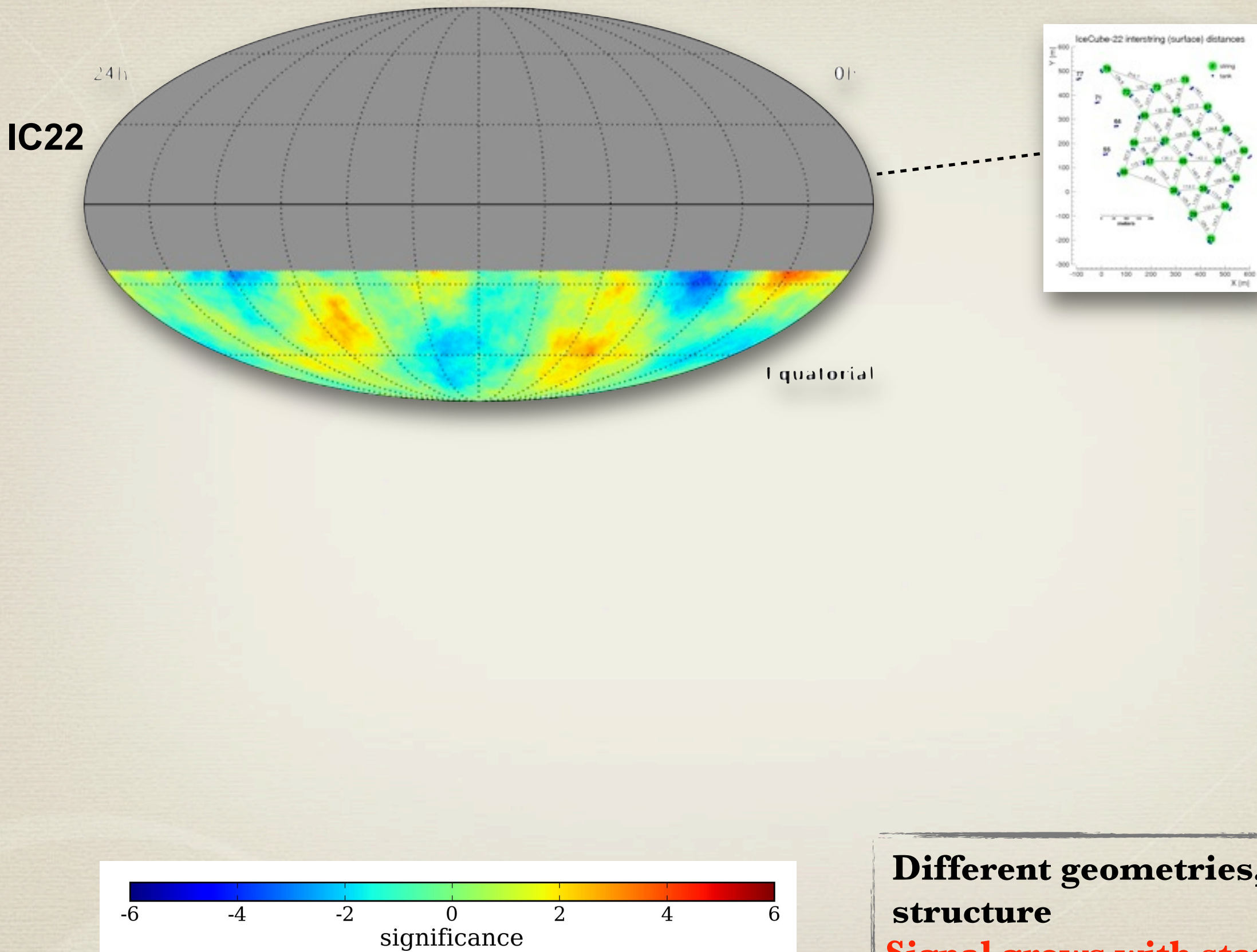
Systematics: previous data sets



27

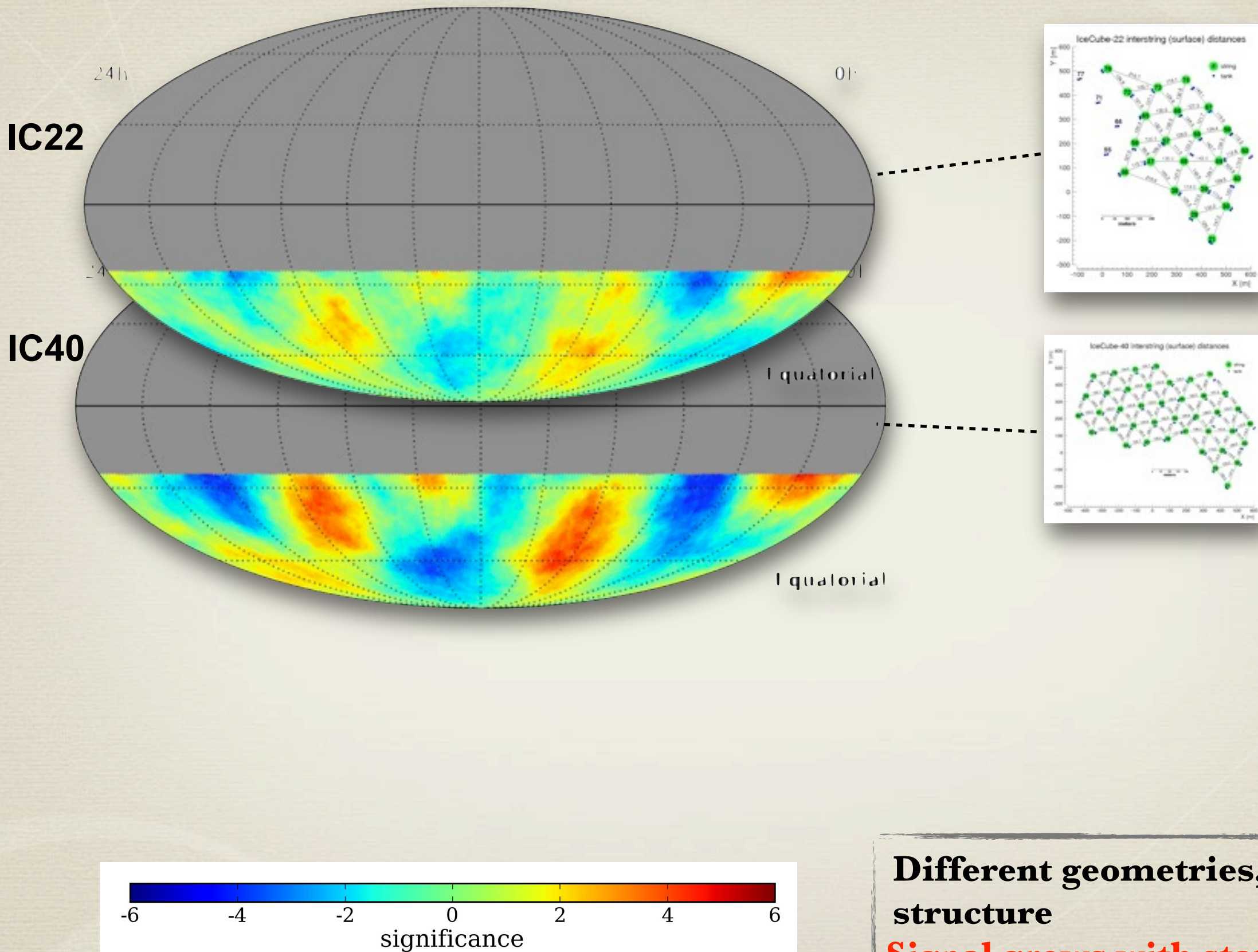
Different geometries, same structure
Signal grows with statistics

Systematics: previous data sets

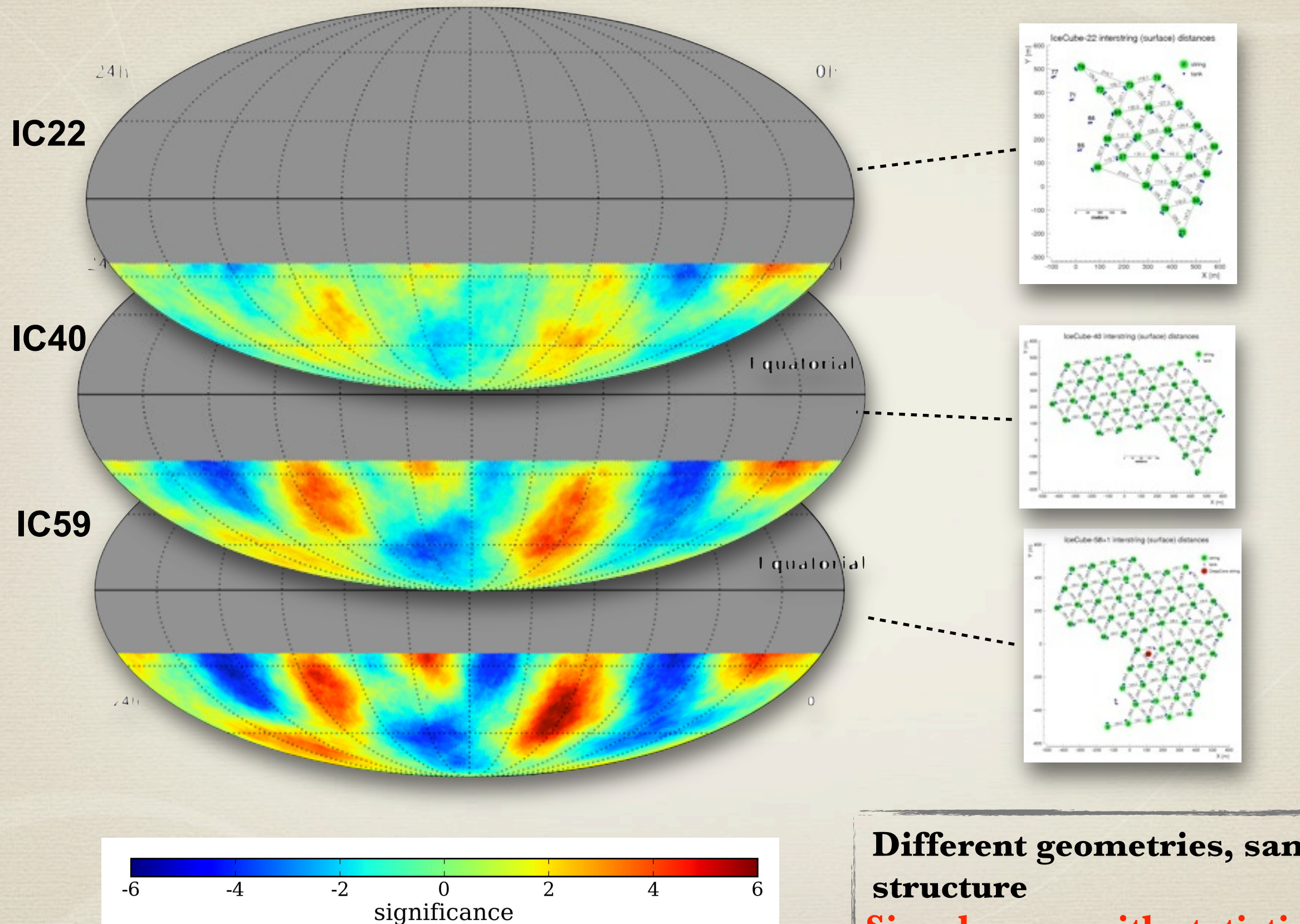


Different geometries, same structure
Signal grows with statistics

Systematics: previous data sets



Systematics: previous data sets

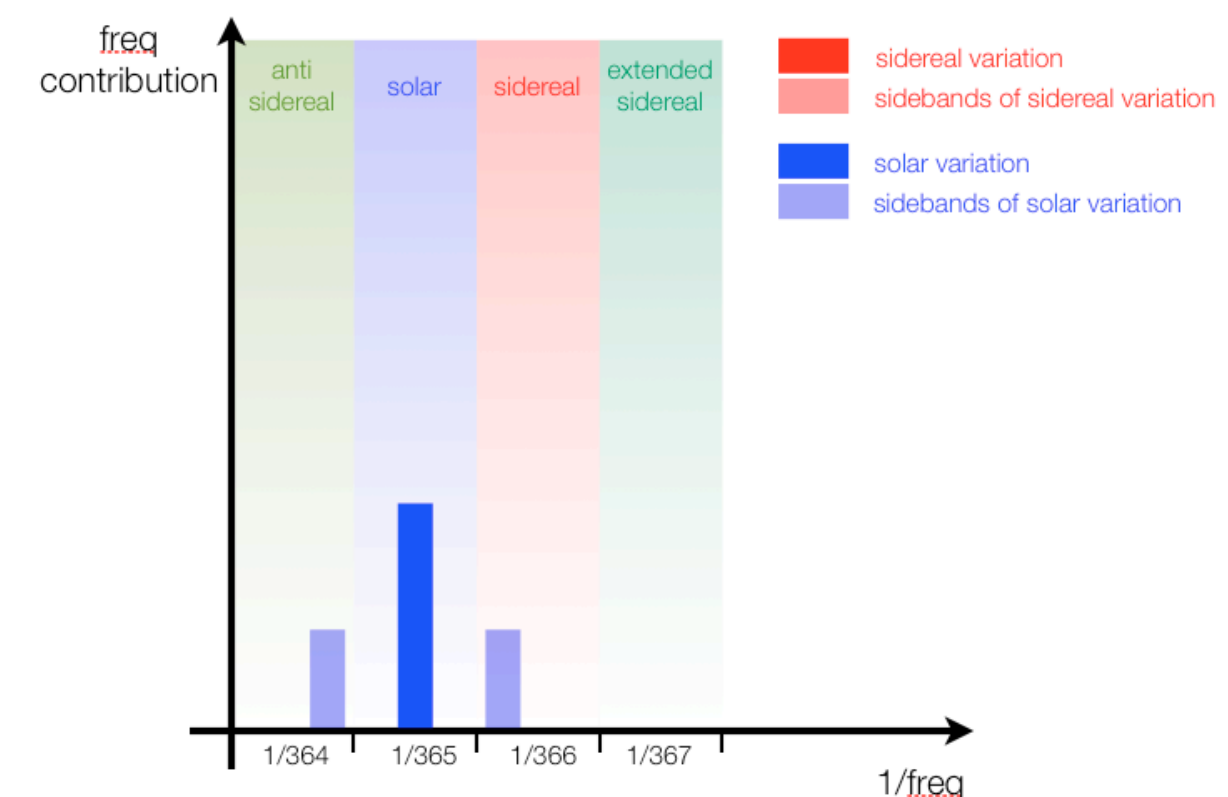
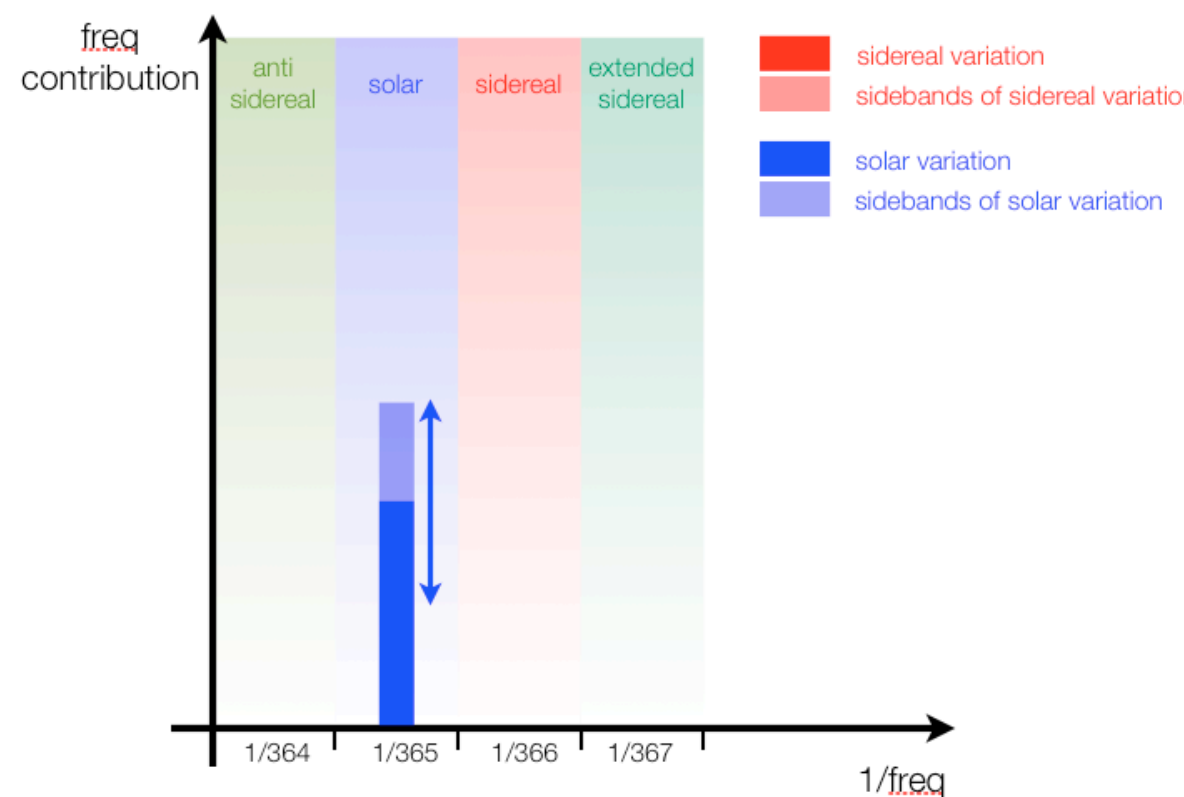


Different geometries, same structure
Signal grows with statistics

anti- / extended-sidereal reference frames

A static distribution in **solar** (sidereal) reference frame averages to zero in **sidereal** (solar) frame after one year

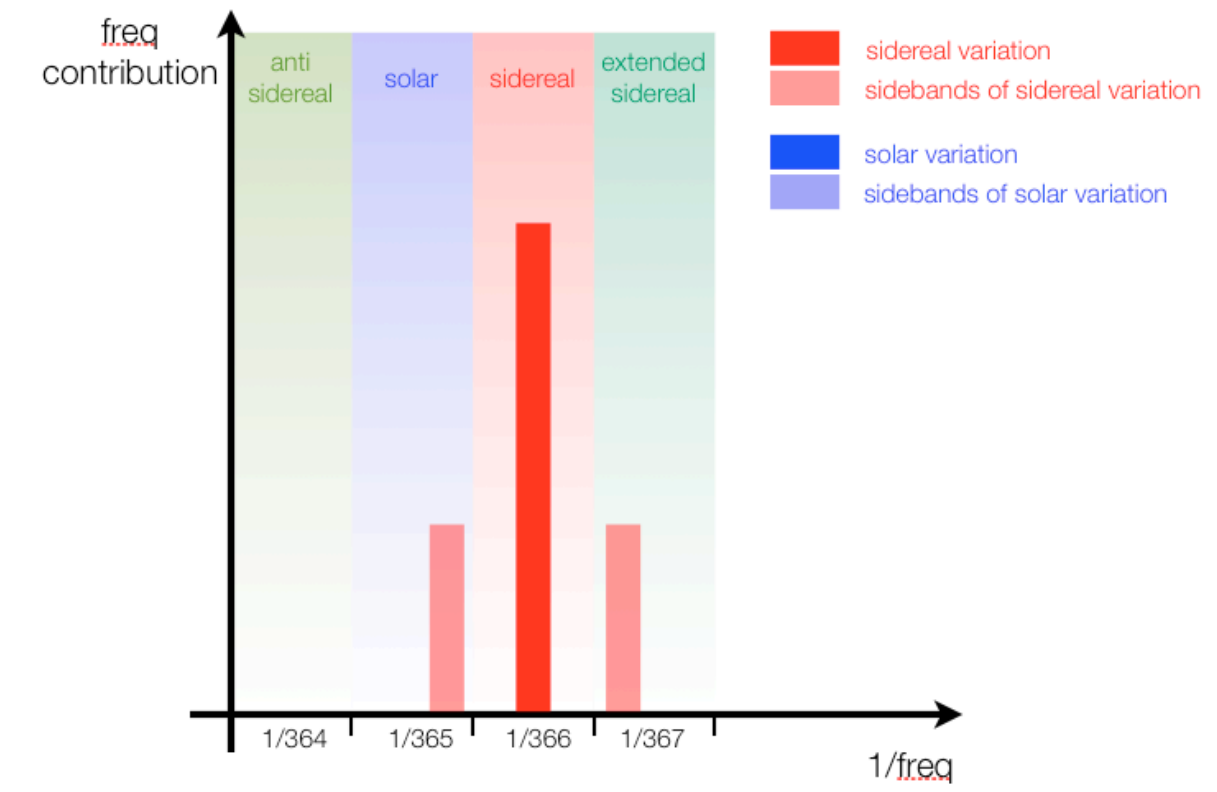
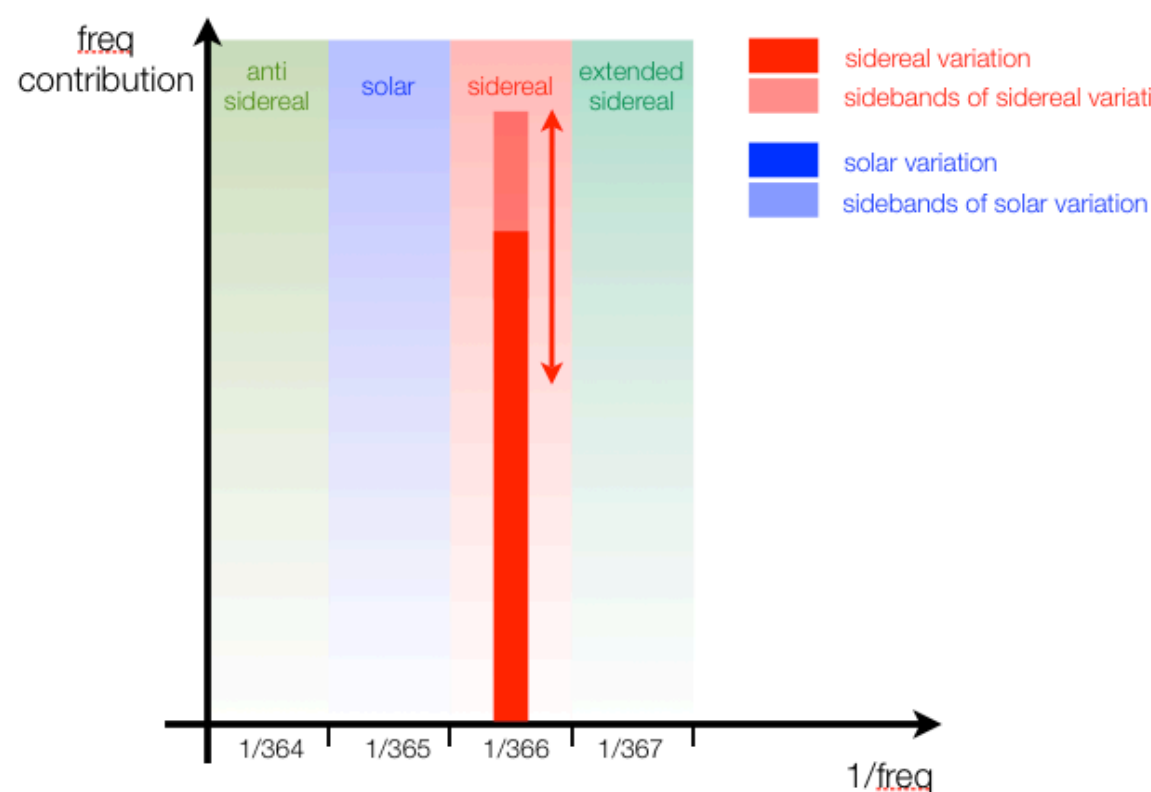
An annual modulation of the **solar** (sidereal) distribution does not compensate and produces distortions on the **sidereal** (solar) anisotropies



anti- / extended-sidereal reference frames

A static distribution in solar (**sidereal**) reference frame averages to zero in sidereal (solar) frame after one year

An annual modulation of the solar (**sidereal**) distribution does not compensate and produces distortions on the sidereal (**solar**) anisotropies



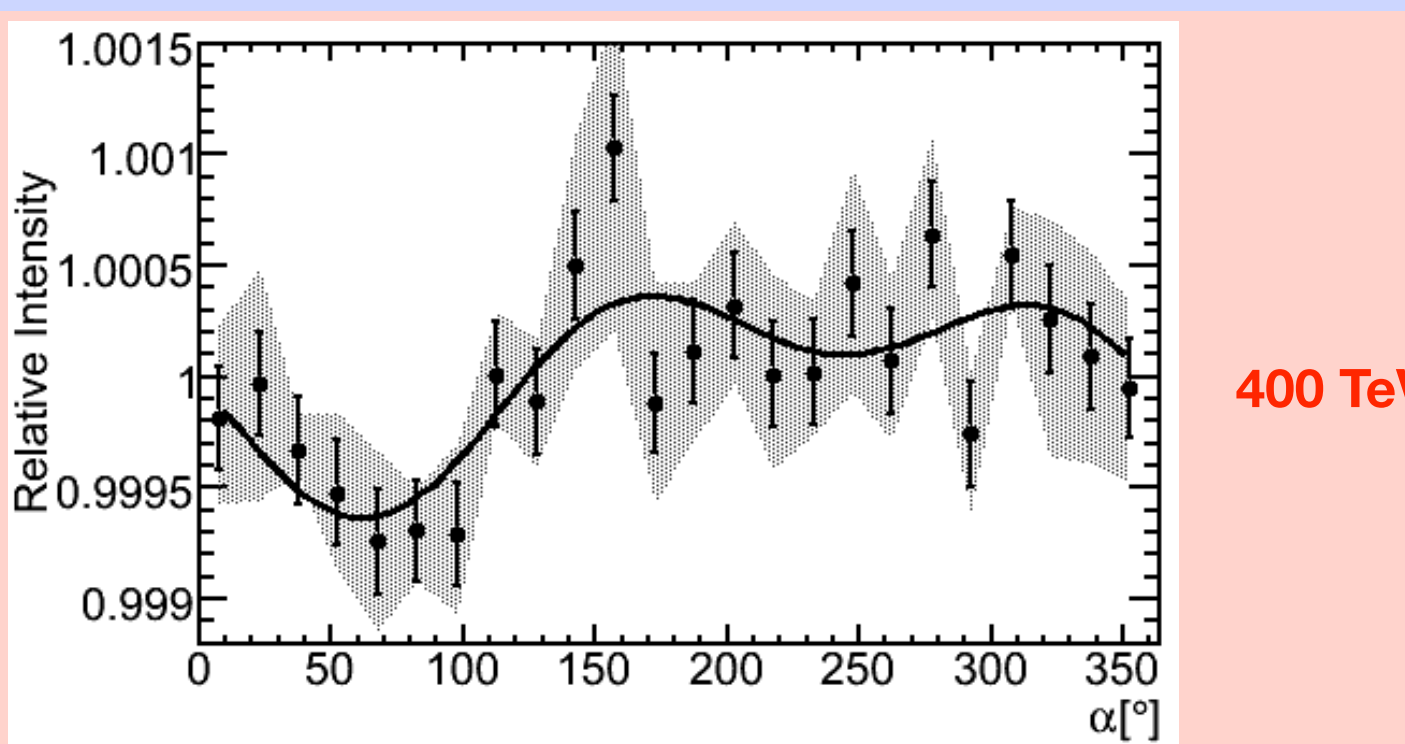
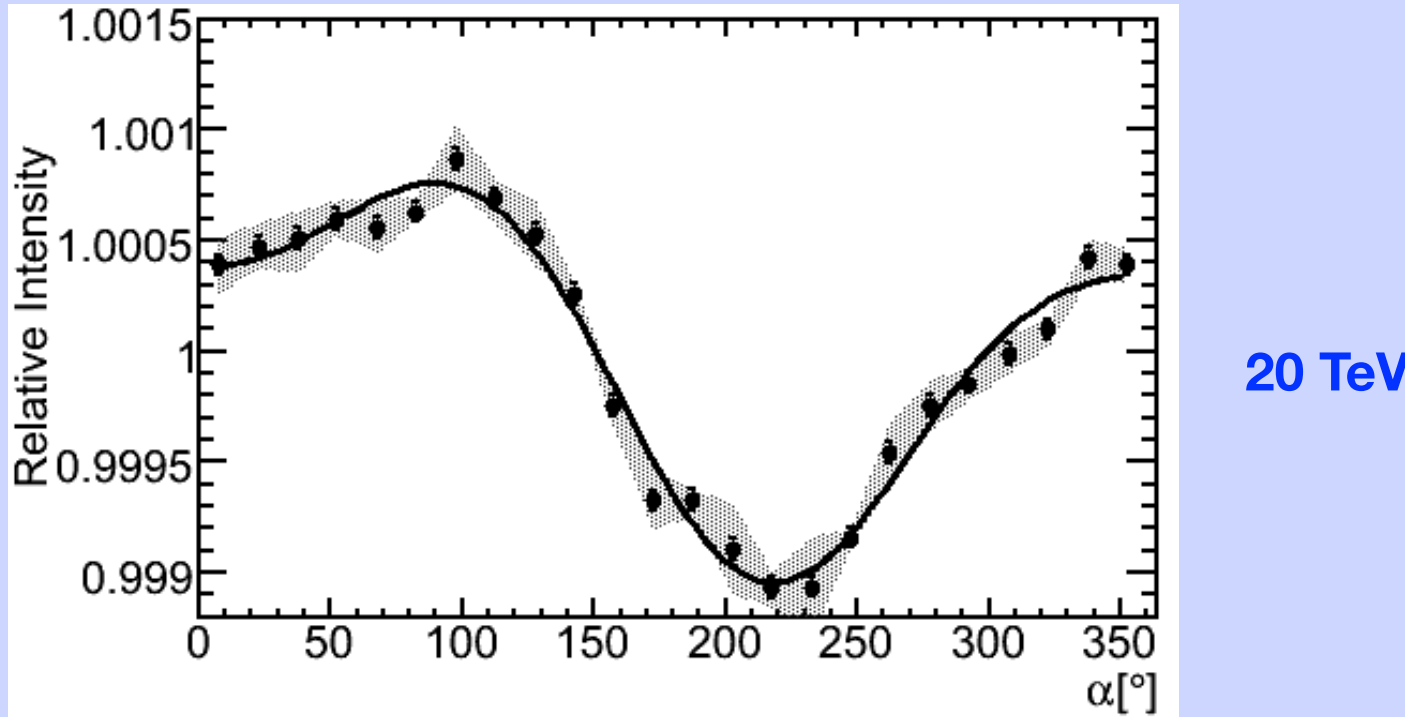
Summary of measurements for IC59

$$\sum_{j=1}^{n=2} A_j \cos[i(\alpha - \phi_j)] + B$$

	E_{primary} (TeV)	events (10^9)	A_1 (10^{-4})	φ_1 ($^\circ$)	A_2 (10^{-4})	φ_2 ($^\circ$)	χ^2/ndf
sidereal	20	17.9	$7.9 \pm 0.1 \pm 0.4$	$50^\circ.5 \pm 1^\circ.0 \pm 1^\circ.1$	$2.9 \pm 0.1 \pm 0.4$	$299^\circ.5 \pm 1^\circ.3 \pm 1^\circ.5$	95/19
	400	0.5	$3.7 \pm 0.7 \pm 0.7$	$239^\circ.2 \pm 10^\circ.6 \pm 10^\circ.8$	$2.7 \pm 0.7 \pm 0.6$	$152^\circ.7 \pm 7^\circ.0 \pm 4^\circ.2$	34.19
solar	20		$1.9 \pm 0.1 \pm 0.6$	$267^\circ.1 \pm 3^\circ.8 \pm 7^\circ.5$			
	400		$2.9 \pm 0.7 \pm 1.0$	$272^\circ.1 \pm 13^\circ.3 \pm 5^\circ.0$			
anti-sidereal	20		0.4 ± 0.1	$1^\circ.5 \pm 18^\circ.5$			
	400		0.5 ± 0.7	$324^\circ.6 \pm 75^\circ.4$			
extended-sidereal	20		0.7 ± 0.1	$165^\circ.7 \pm 10^\circ.3$			
	400		0.7 ± 0.7	$212^\circ.9 \pm 54^\circ.5$			

Systematic uncertainties IceCube-59

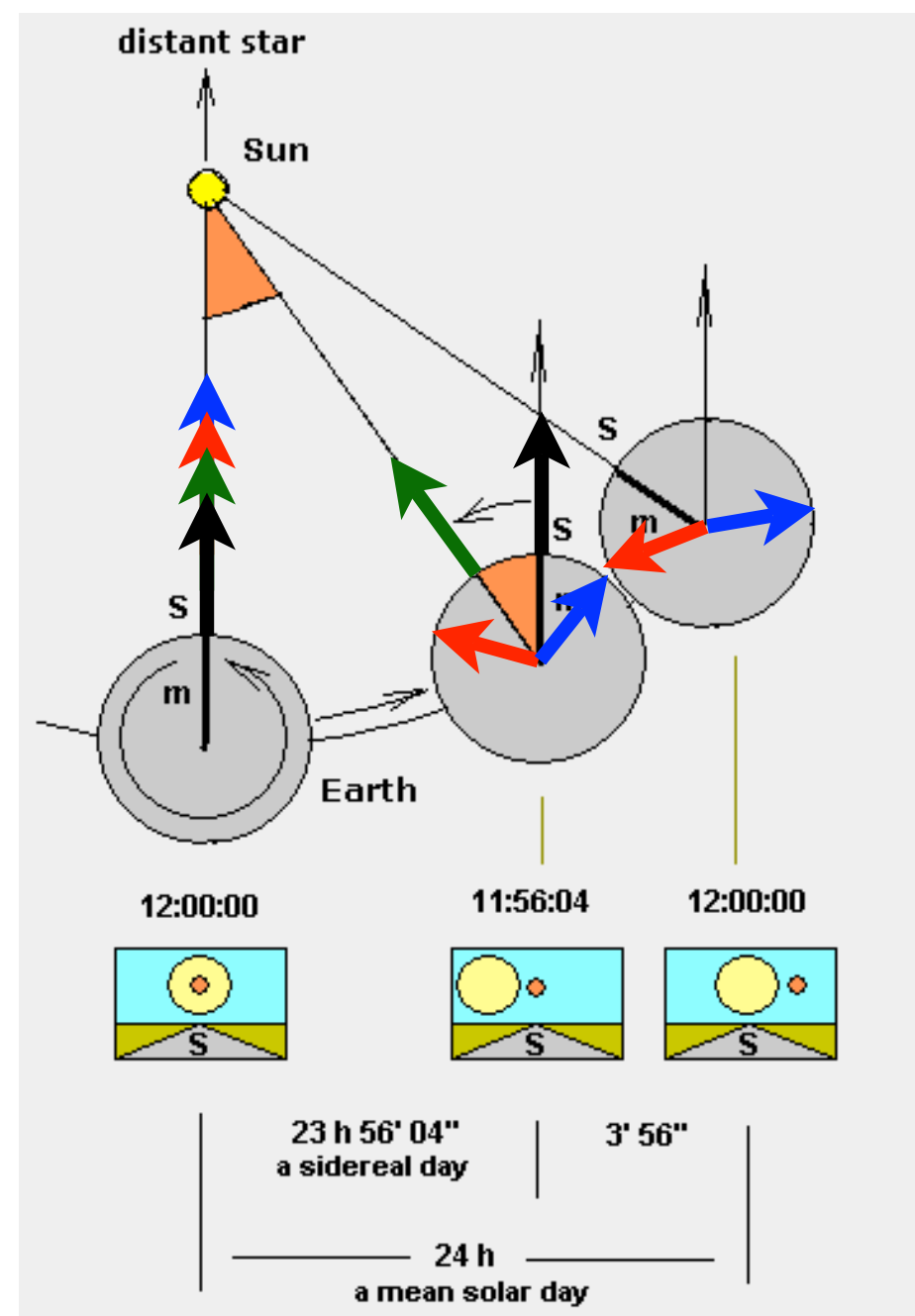
statistical stability tests + anti-sidereal effect



statistical stability tests:

- ▶ summer/winter season datasets
- ▶ rate \geq median daily rate
- ▶ even/odd sub-runs (2 mins data)
- ▶ random sub-run selection
- ▶ use ~ 20 hr full days (214/324 d)

anti- / extended-sidereal reference frames



The anti- / extended-sidereal reference frames are unphysical and no anisotropy is expected

An anisotropy in anti-sidereal (extended-sidereal) frame is to be associated to the corresponding distortion of the sidereal (solar) arrival distributions

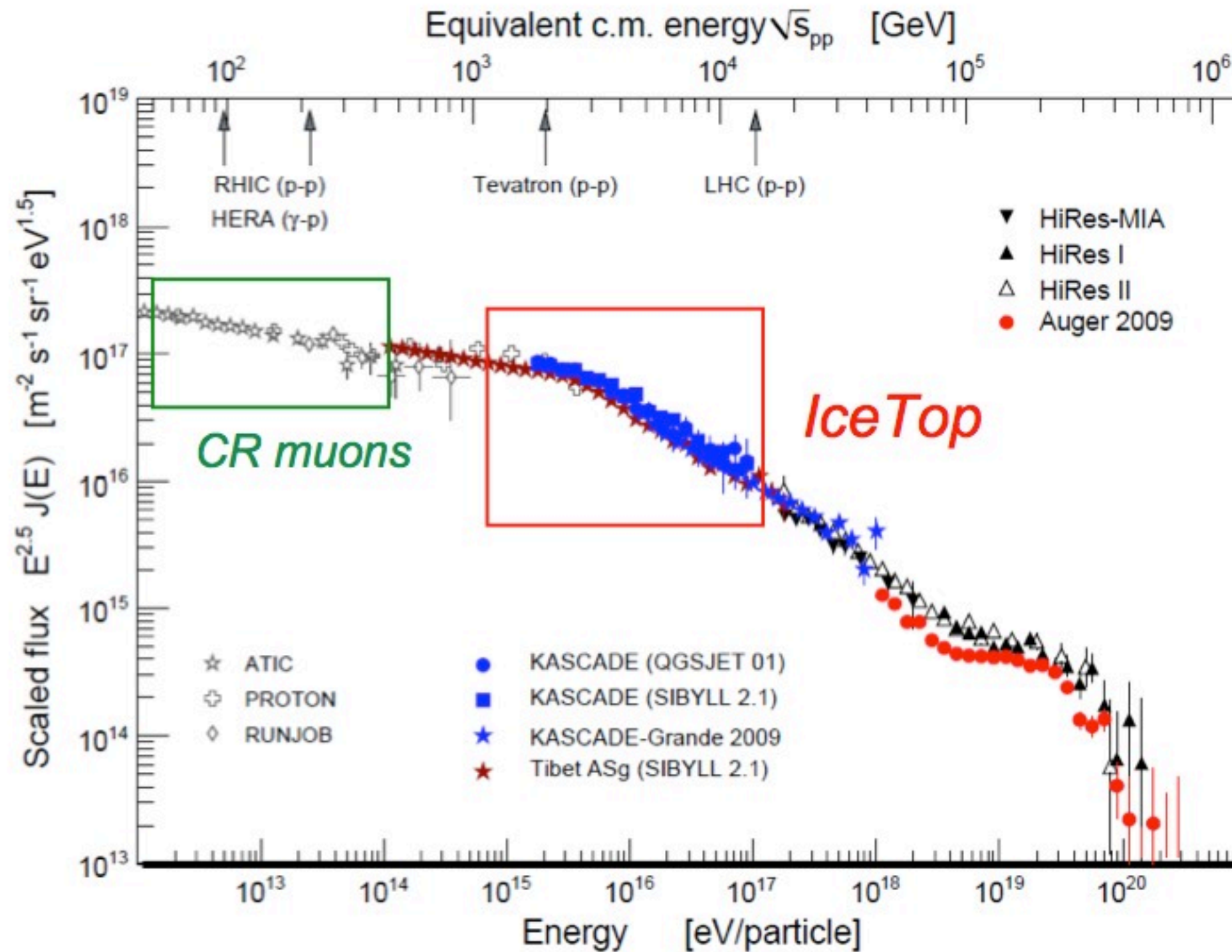
solar time

sidereal time

anti-sidereal time

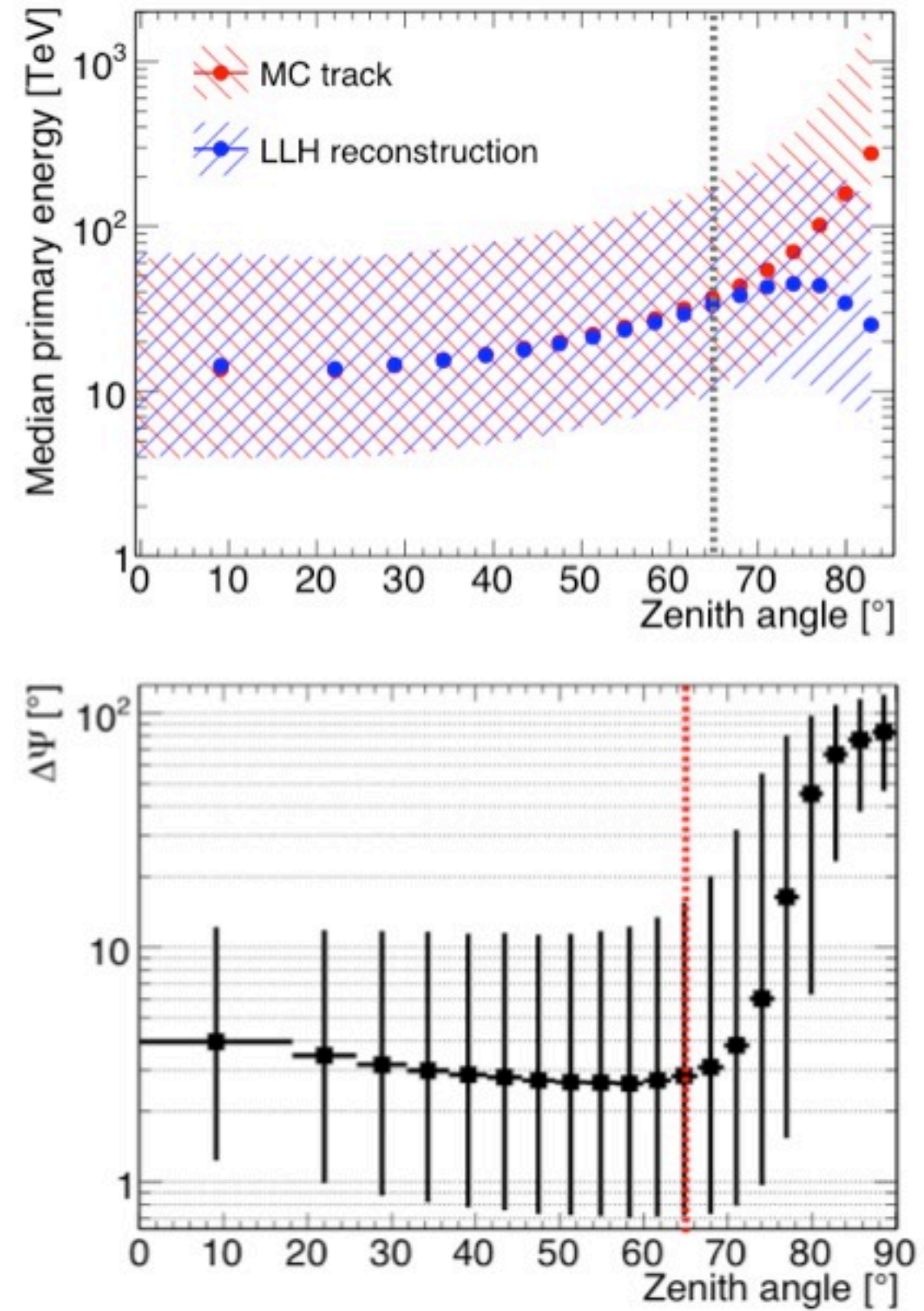
extended-sidereal time

Cosmic Ray Energy Spectrum



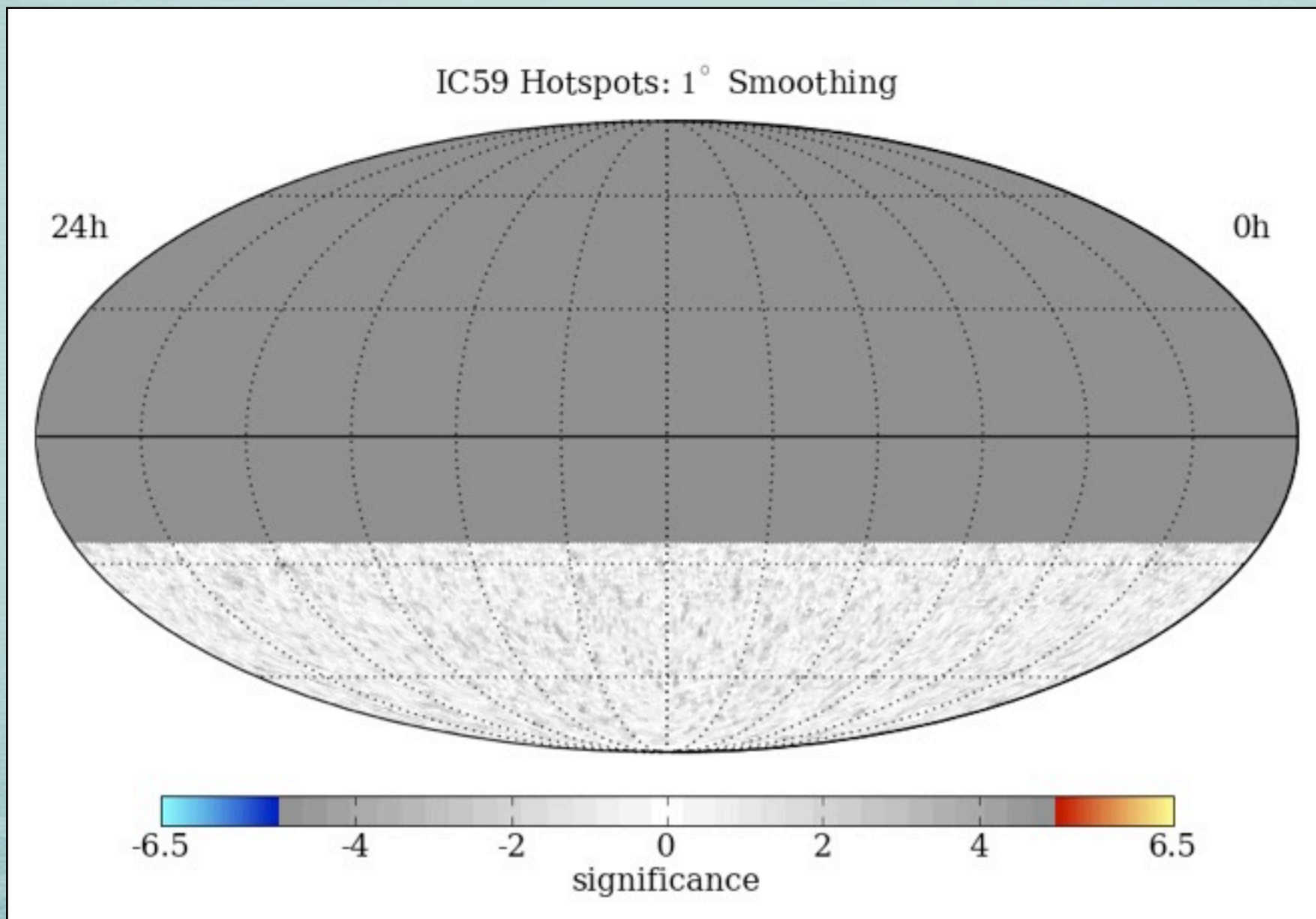
IceCube-59 DST data

- Data taken between May 20, 2009 and May 30, 2010. Integrated livetime 335.5 days.
- 3.4×10^{10} events stored in a special format suitable for high data rate.
- Simulations: median energy and angular resolution depend on zenith angle.
- Zenith angle cut: accept events $< 65^\circ$.



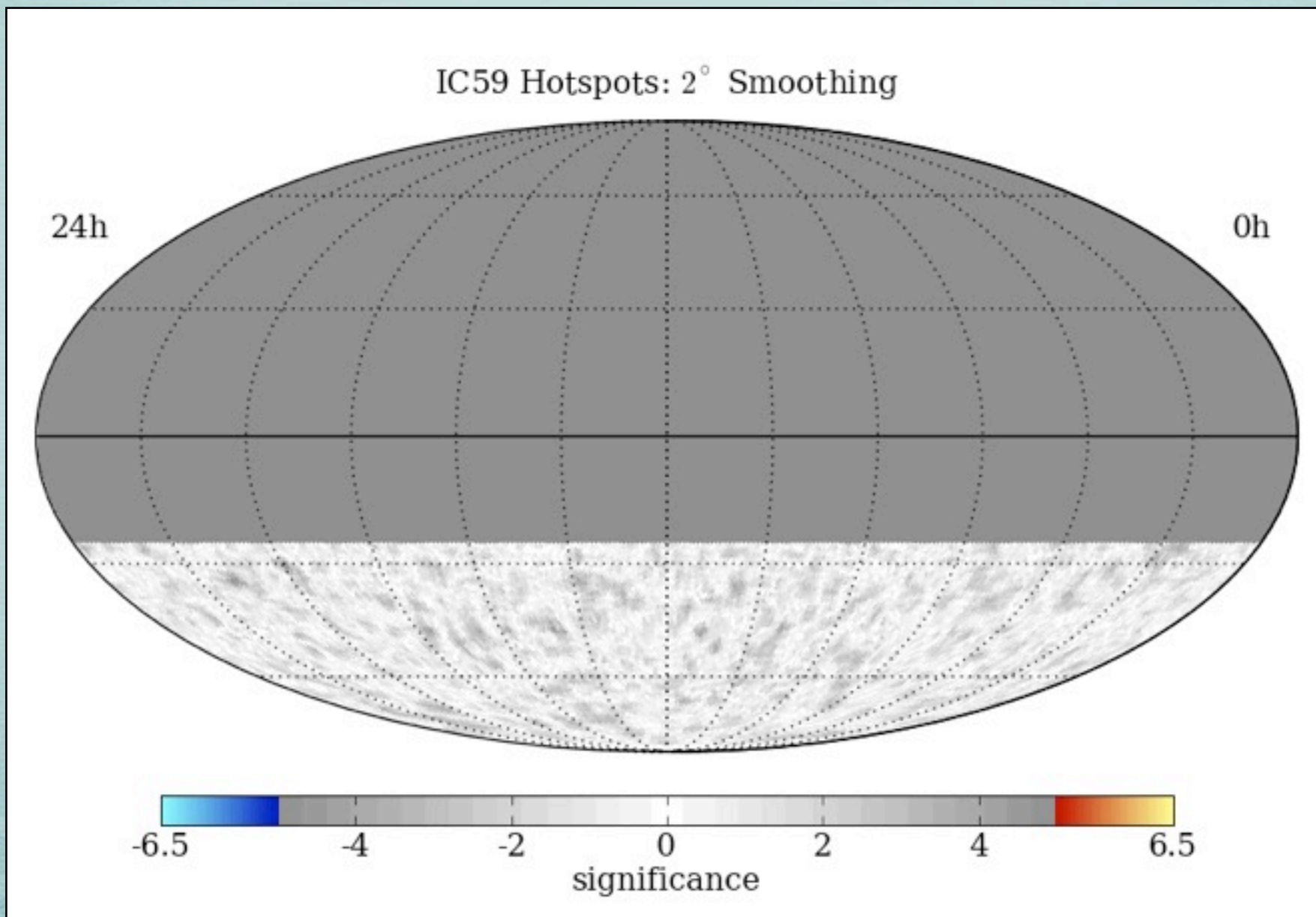
MAP SMOOTHING SCAN

Scan from 1 - 30° in smoothing
Different regions have different optimal angular smoothing
Significances are pre-trial



MAP SMOOTHING SCAN

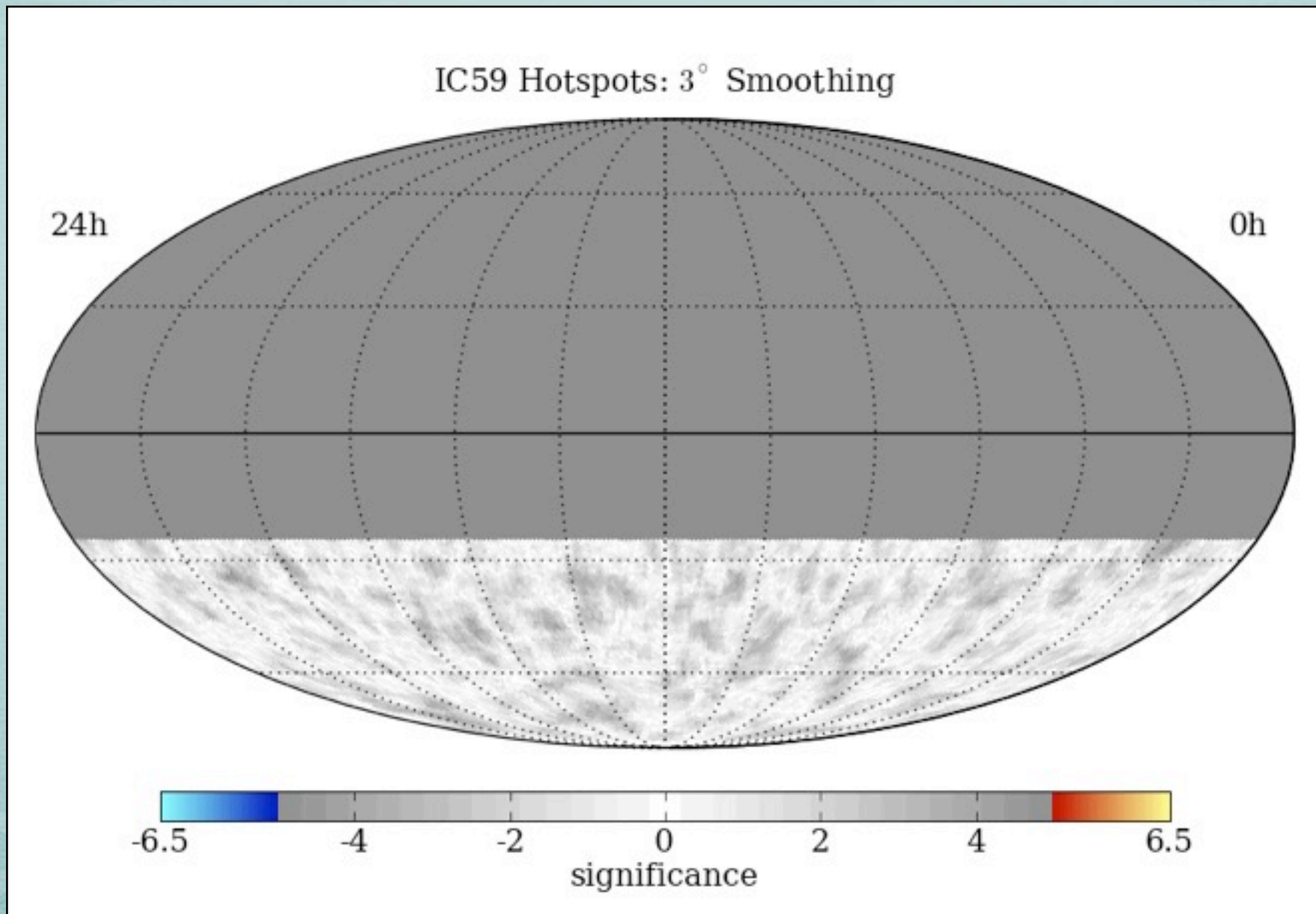
Scan from 1 - 30° in smoothing
Different regions have different optimal angular smoothing
Significances are pre-trial





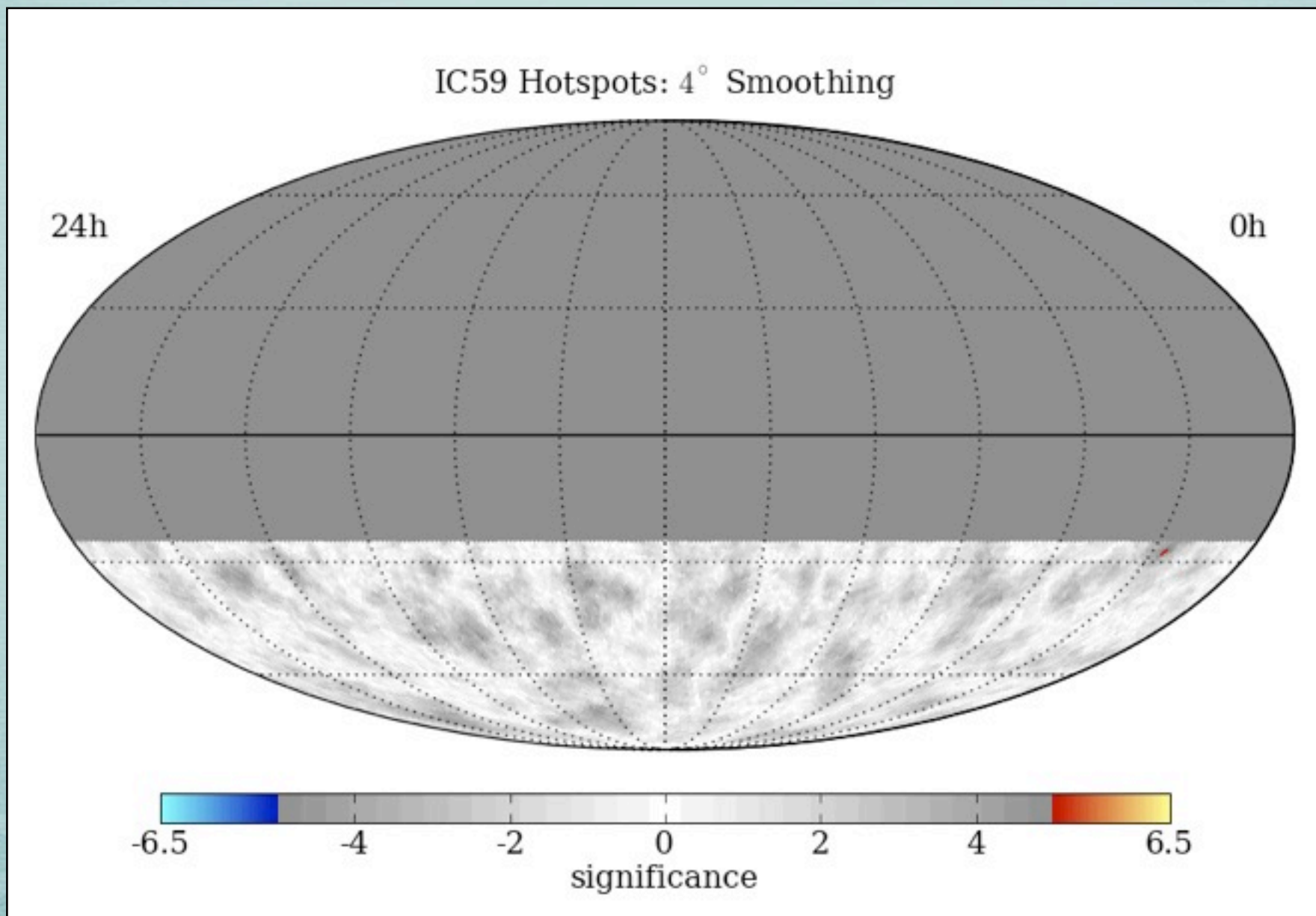
MAP SMOOTHING SCAN

Scan from 1 - 30° in smoothing
Different regions have different optimal angular smoothing
Significances are pre-trial



MAP SMOOTHING SCAN

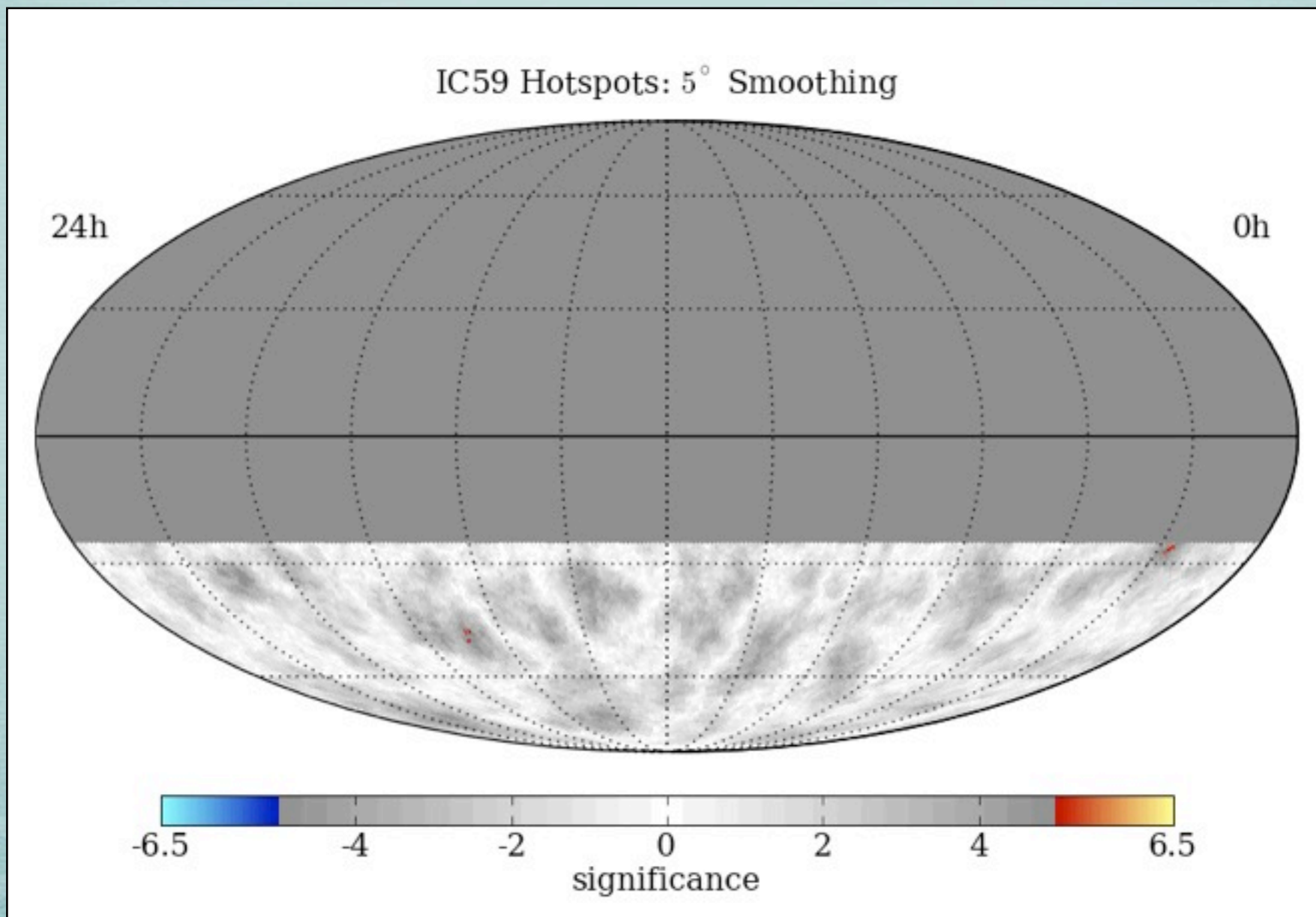
Scan from 1 - 30° in smoothing
Different regions have different optimal angular smoothing
Significances are pre-trial





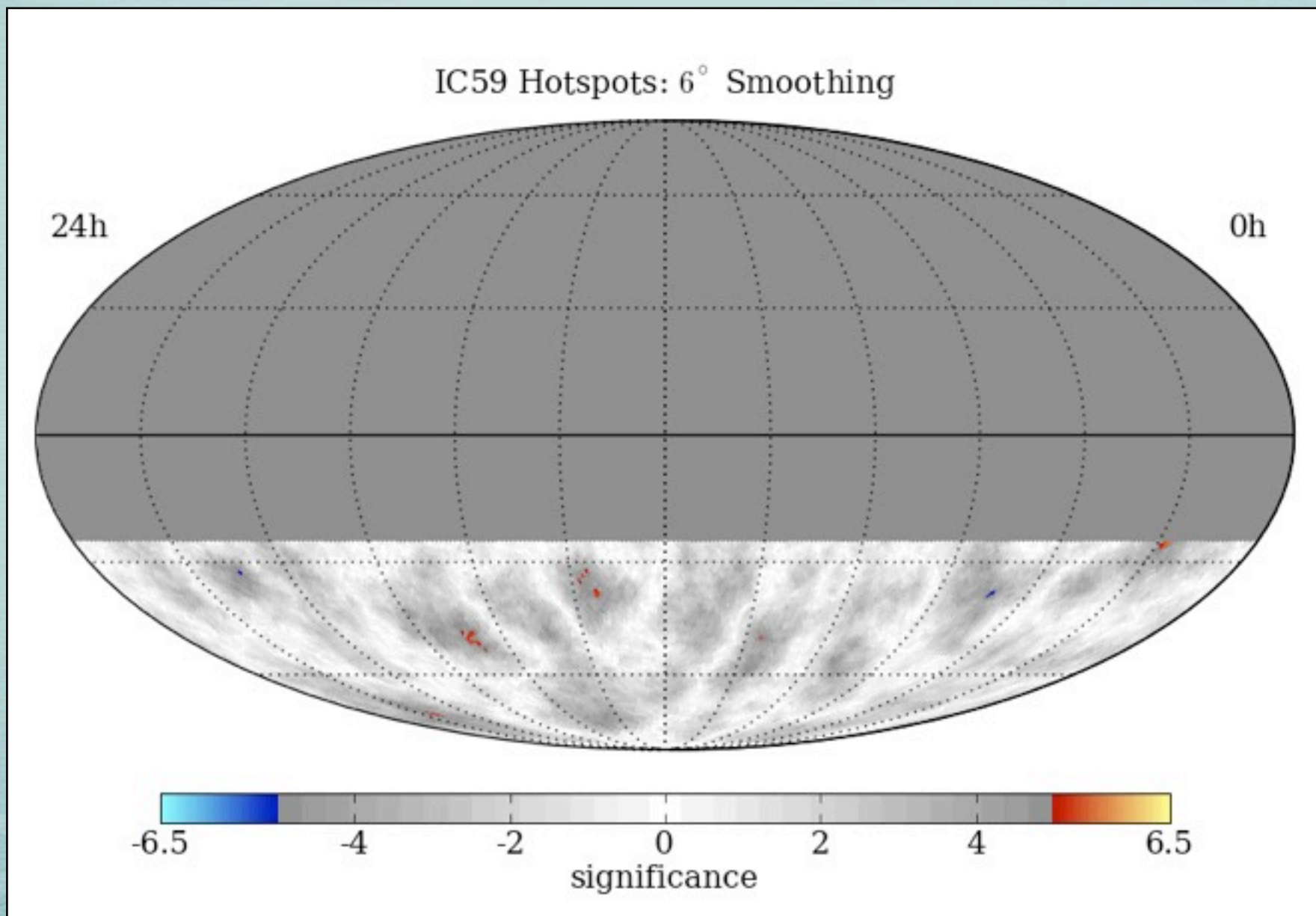
MAP SMOOTHING SCAN

Scan from 1 - 30° in smoothing
Different regions have different optimal angular smoothing
Significances are pre-trial



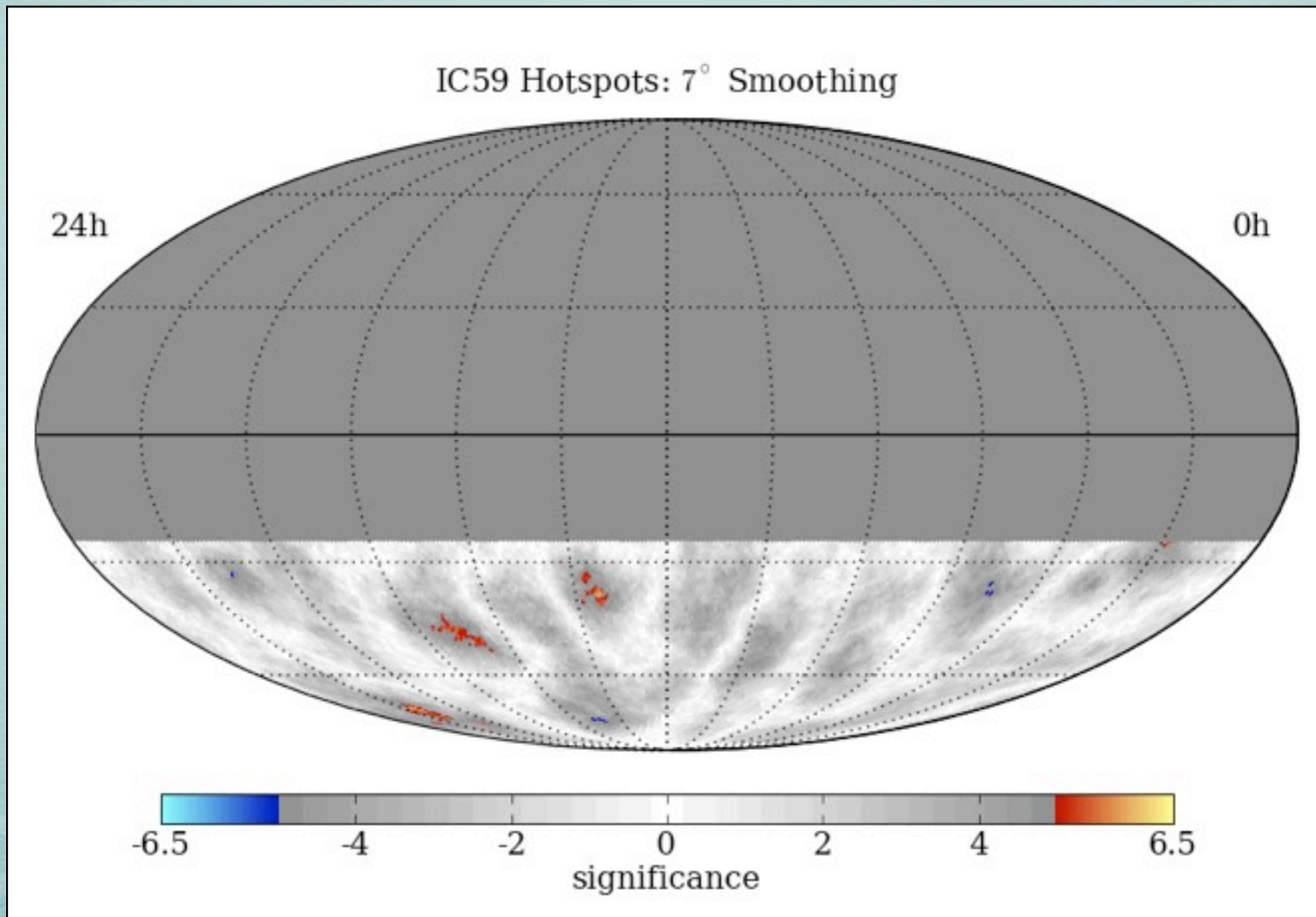
MAP SMOOTHING SCAN

Scan from 1 - 30° in smoothing
Different regions have different optimal angular smoothing
Significances are pre-trial



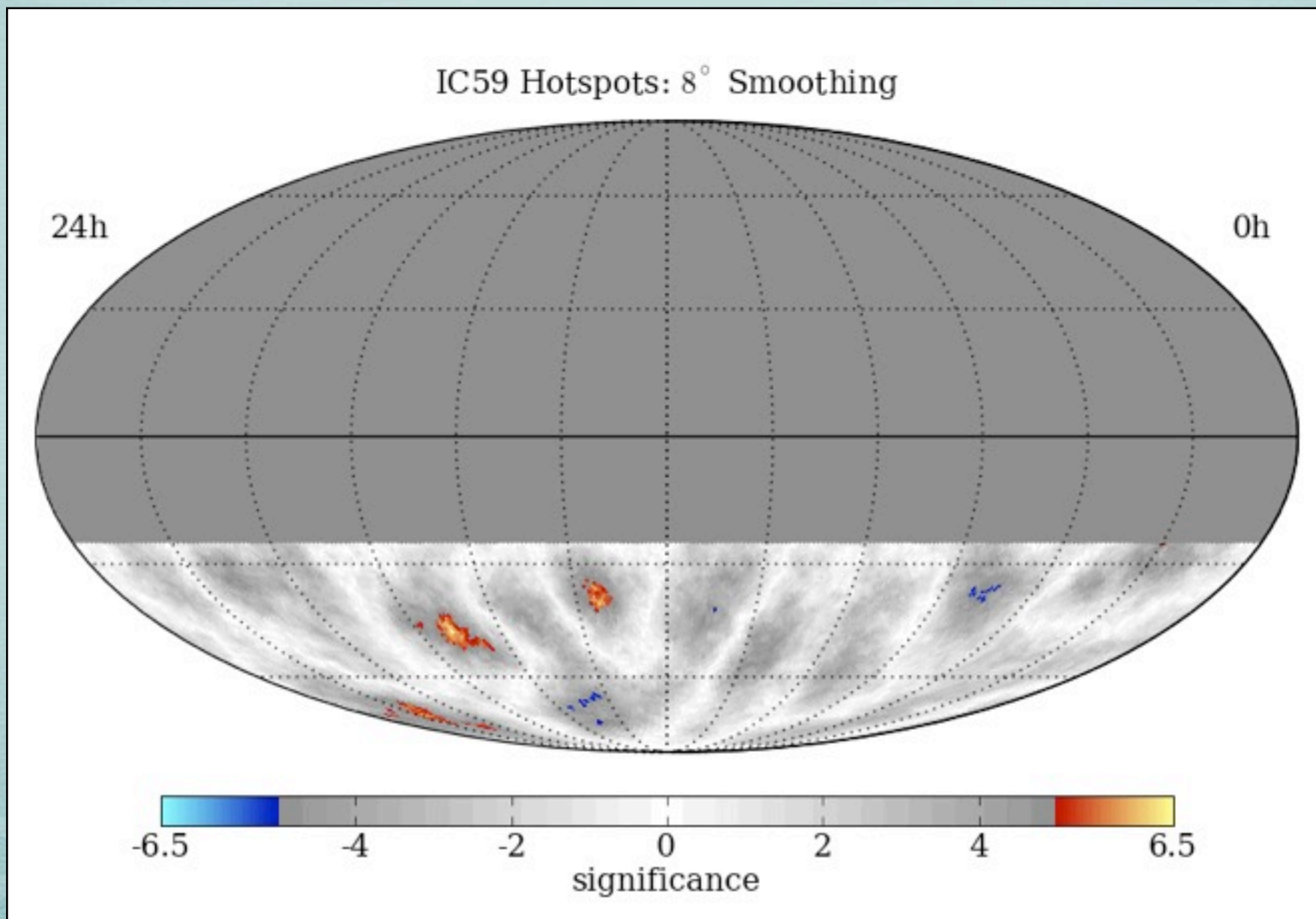
MAP SMOOTHING SCAN

Scan from 1 - 30° in smoothing
Different regions have different optimal angular smoothing
Significances are pre-trial



MAP SMOOTHING SCAN

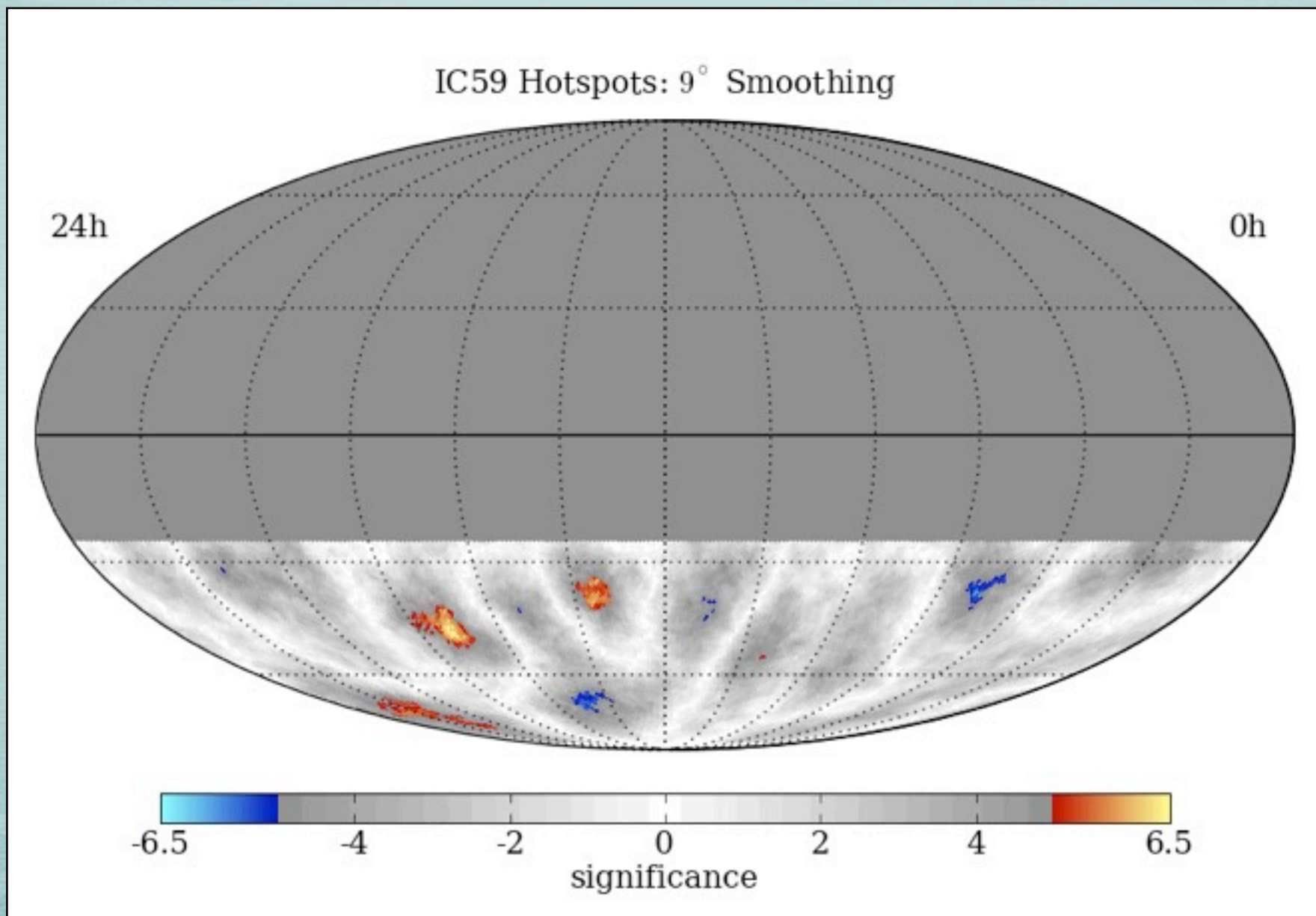
Scan from 1 - 30° in smoothing
Different regions have different optimal angular smoothing
Significances are pre-trial





MAP SMOOTHING SCAN

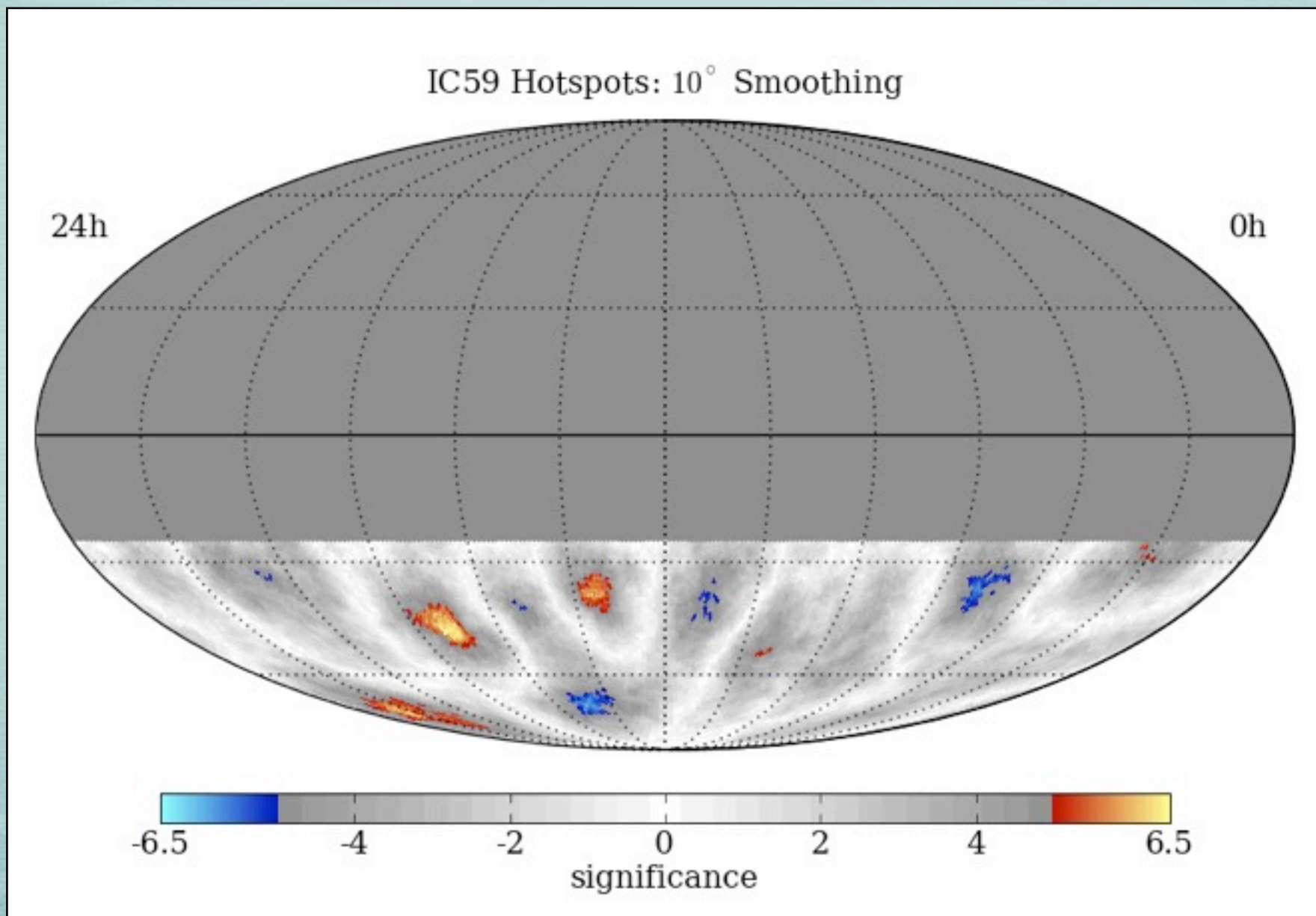
Scan from 1 - 30° in smoothing
Different regions have different optimal angular smoothing
Significances are pre-trial





MAP SMOOTHING SCAN

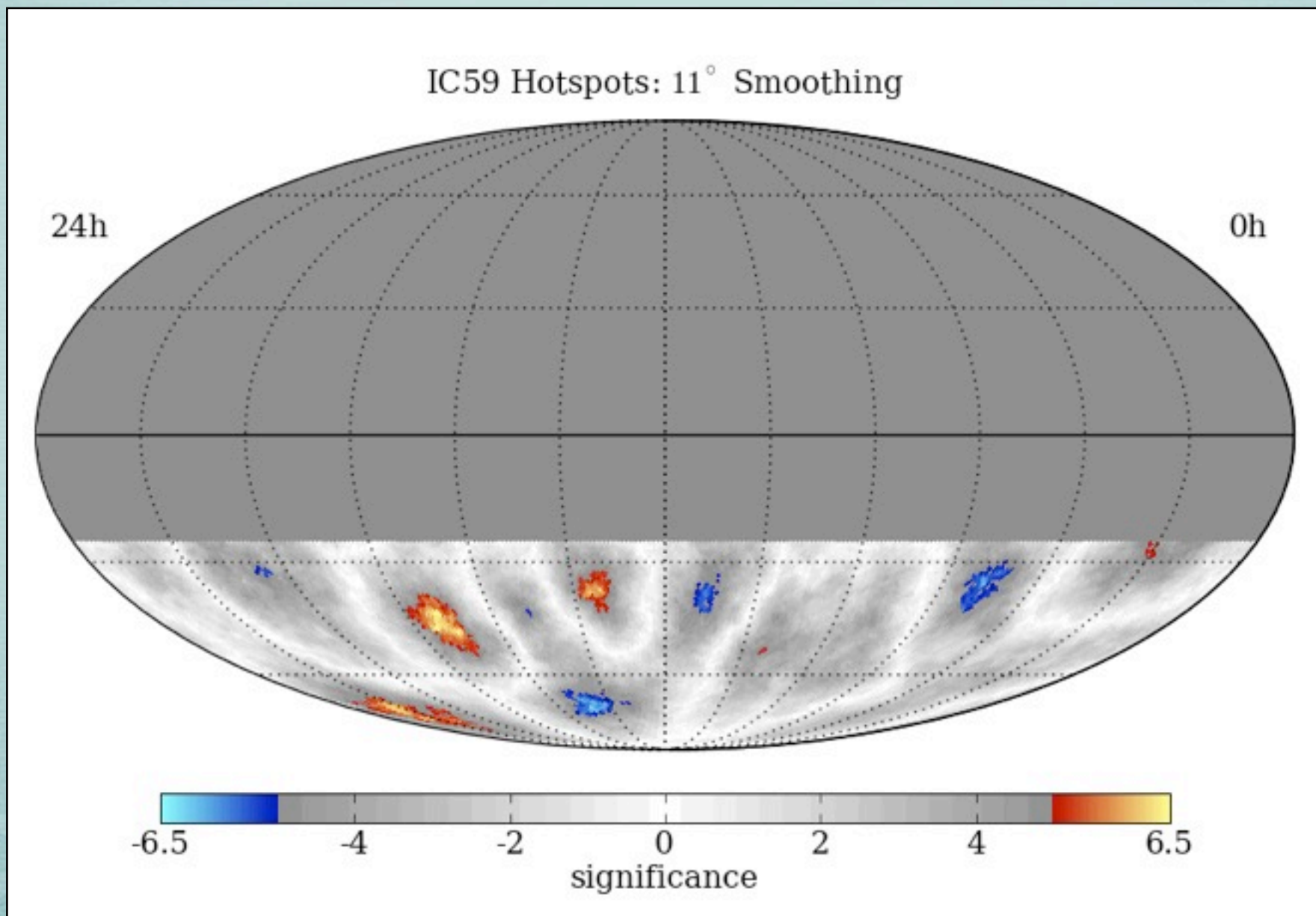
Scan from 1 - 30° in smoothing
Different regions have different optimal angular smoothing
Significances are pre-trial





MAP SMOOTHING SCAN

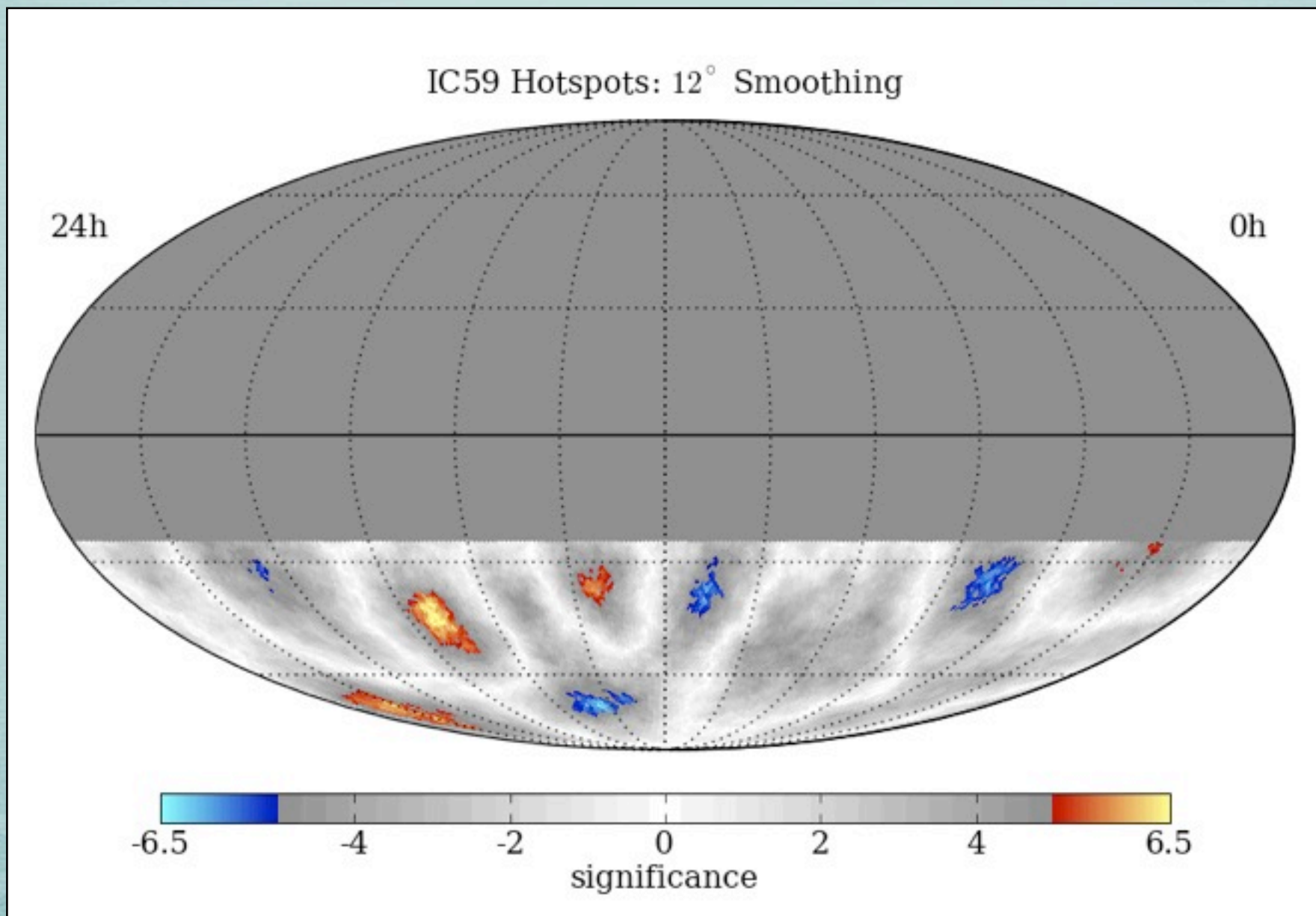
Scan from 1 - 30° in smoothing
Different regions have different optimal angular smoothing
Significances are pre-trial





MAP SMOOTHING SCAN

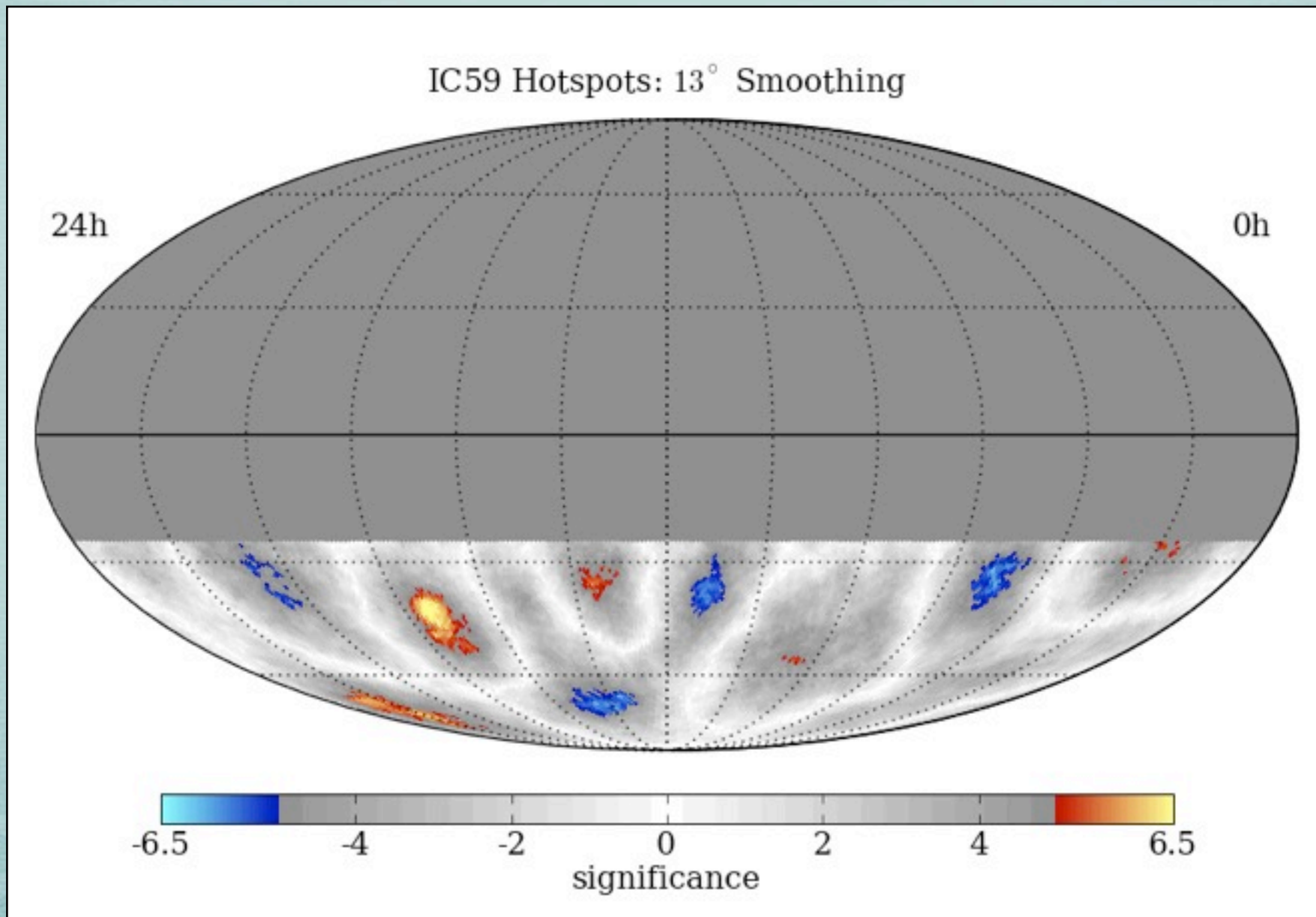
Scan from 1 - 30° in smoothing
Different regions have different optimal angular smoothing
Significances are pre-trial





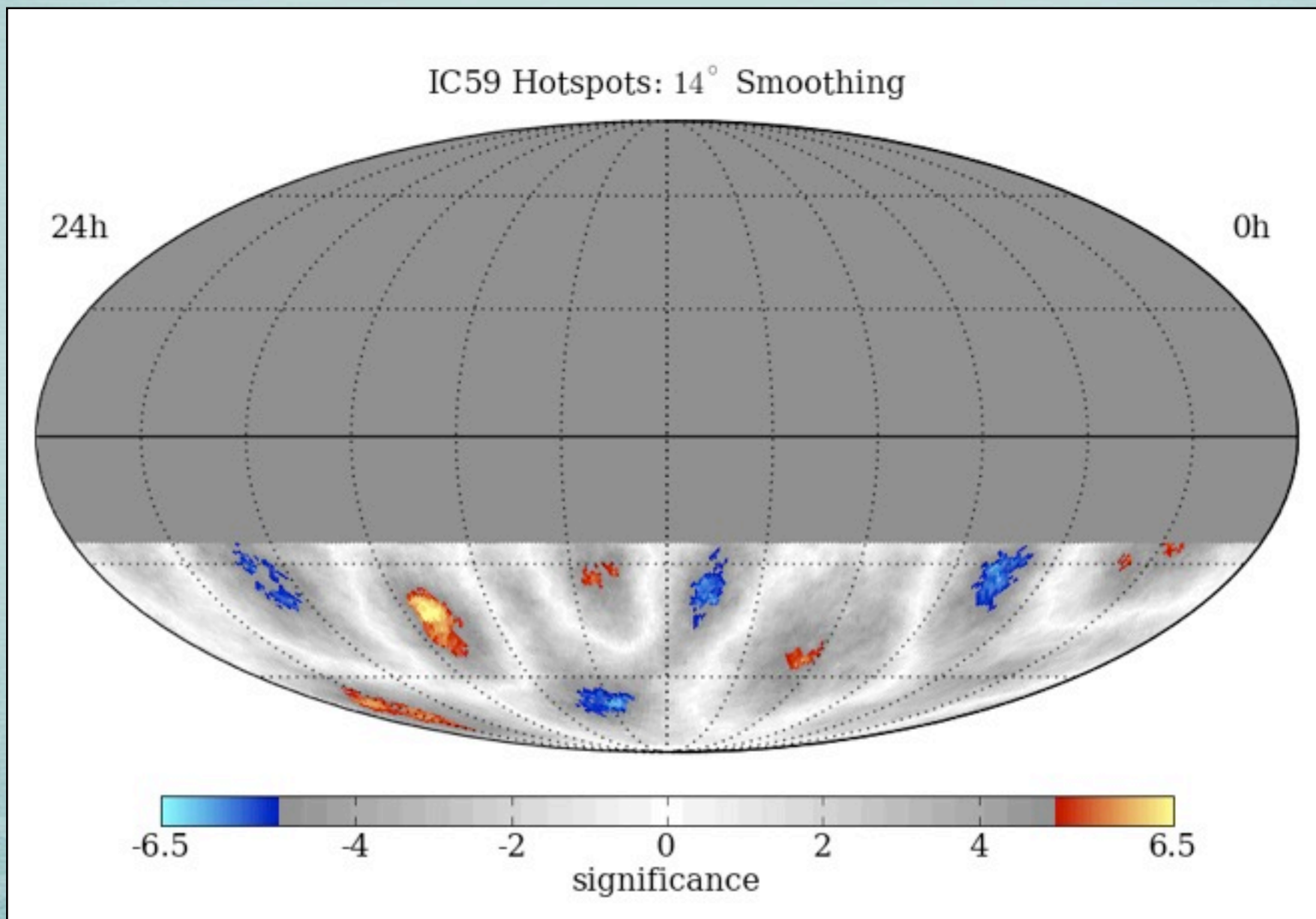
MAP SMOOTHING SCAN

Scan from 1 - 30° in smoothing
Different regions have different optimal angular smoothing
Significances are pre-trial



MAP SMOOTHING SCAN

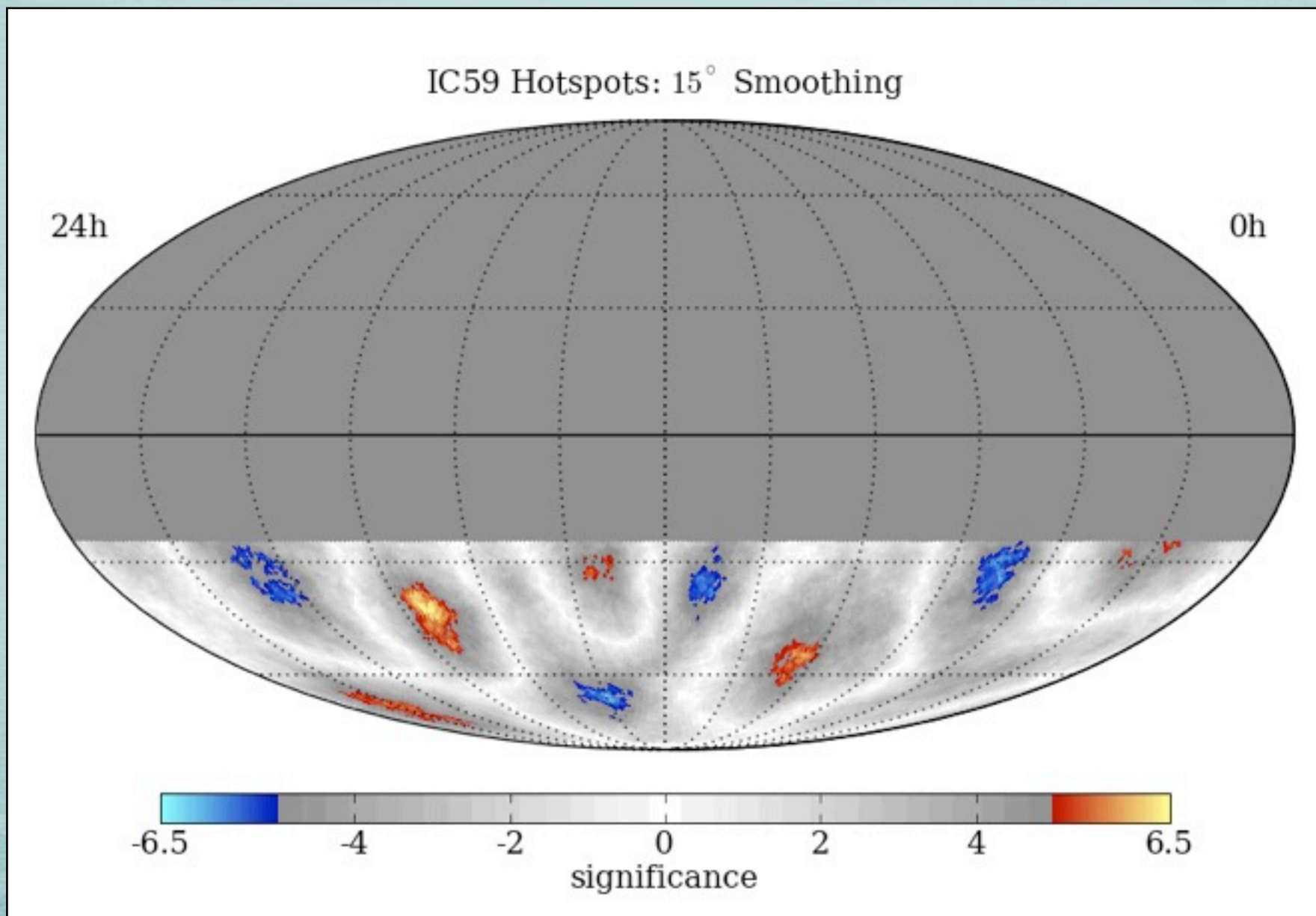
Scan from 1 - 30° in smoothing
Different regions have different optimal angular smoothing
Significances are pre-trial





MAP SMOOTHING SCAN

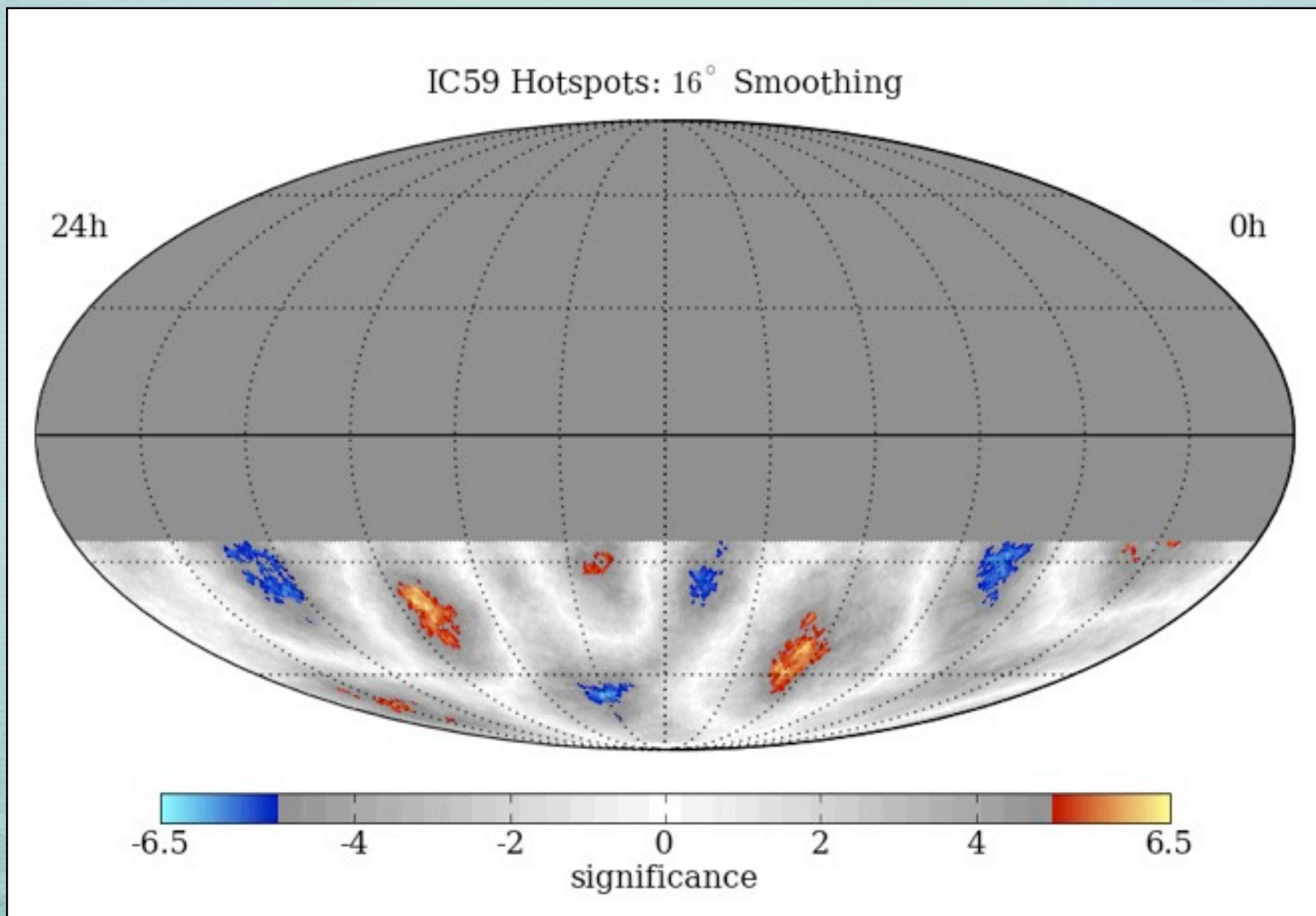
Scan from 1 - 30° in smoothing
Different regions have different optimal angular smoothing
Significances are pre-trial





MAP SMOOTHING SCAN

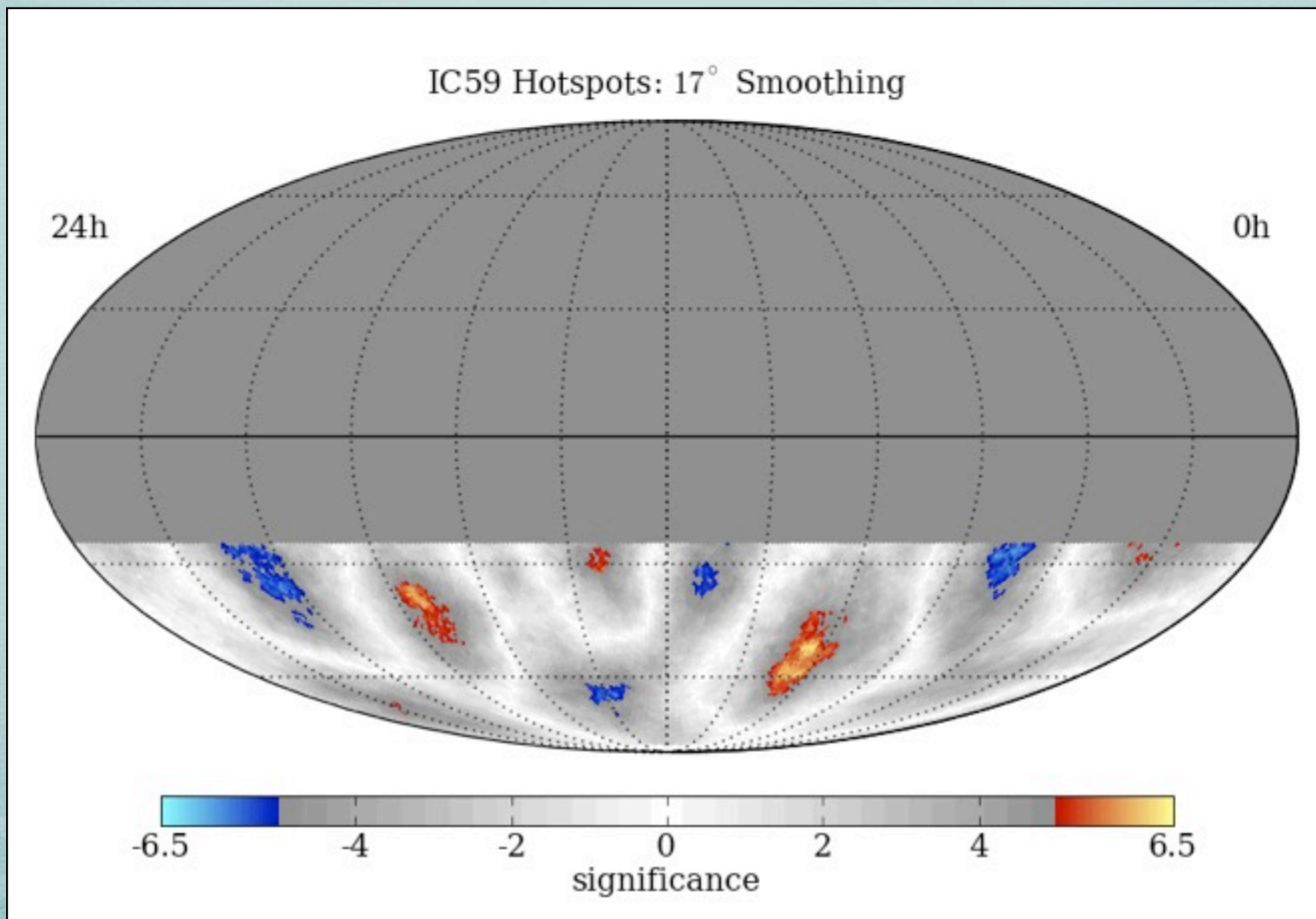
Scan from 1 - 30° in smoothing
Different regions have different optimal angular smoothing
Significances are pre-trial





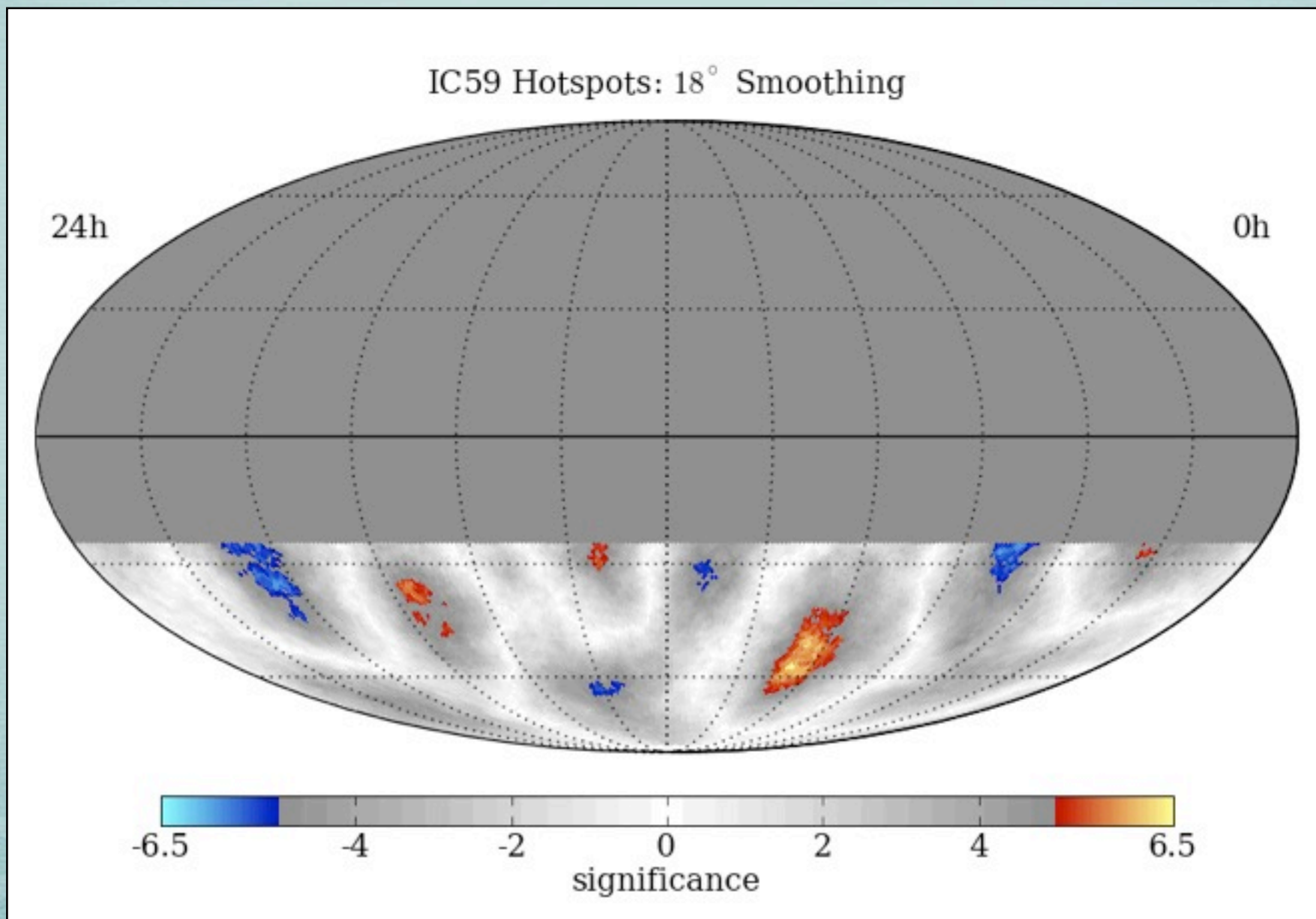
MAP SMOOTHING SCAN

Scan from 1 - 30° in smoothing
Different regions have different optimal angular smoothing
Significances are pre-trial



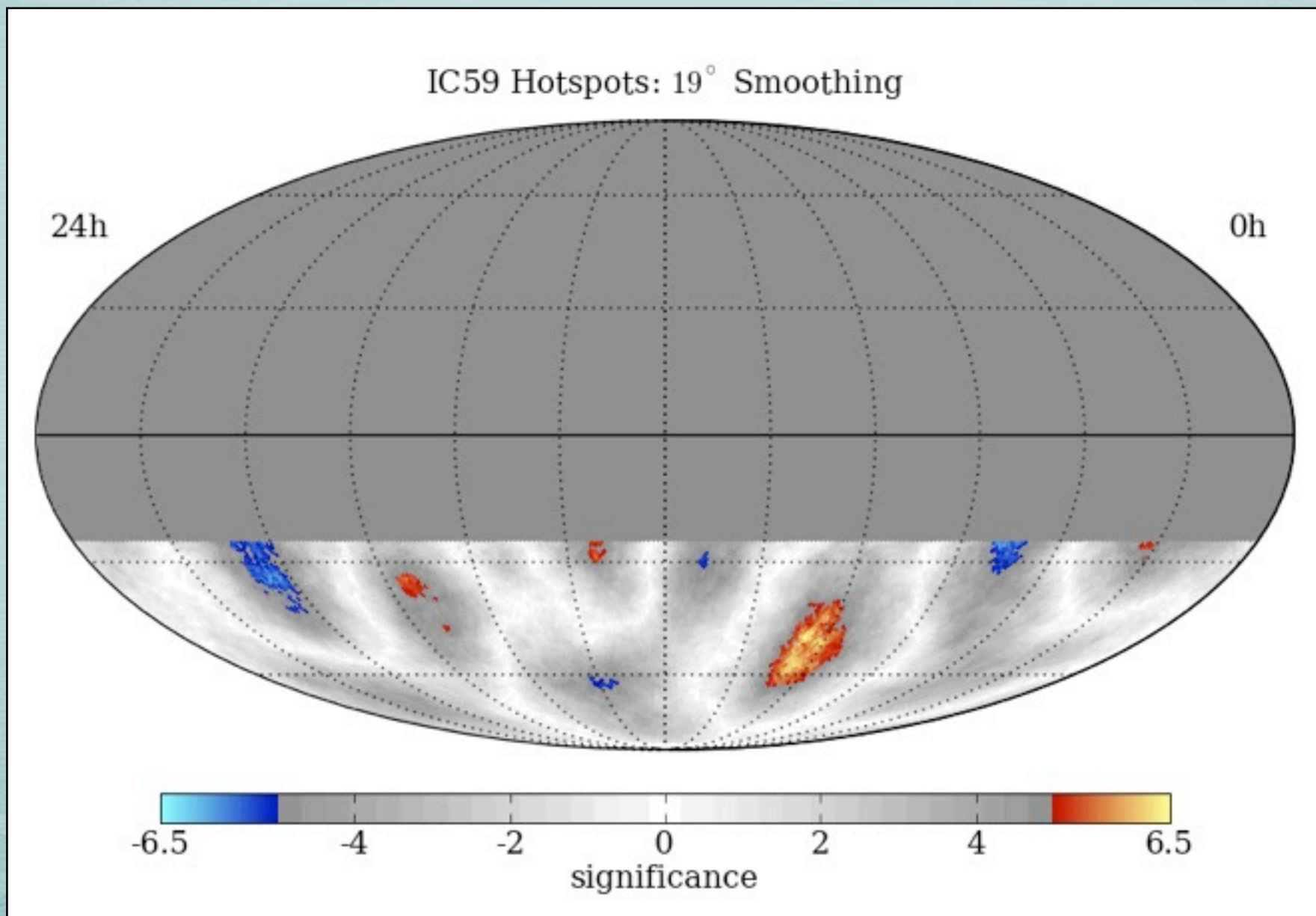
MAP SMOOTHING SCAN

Scan from 1 - 30° in smoothing
Different regions have different optimal angular smoothing
Significances are pre-trial



MAP SMOOTHING SCAN

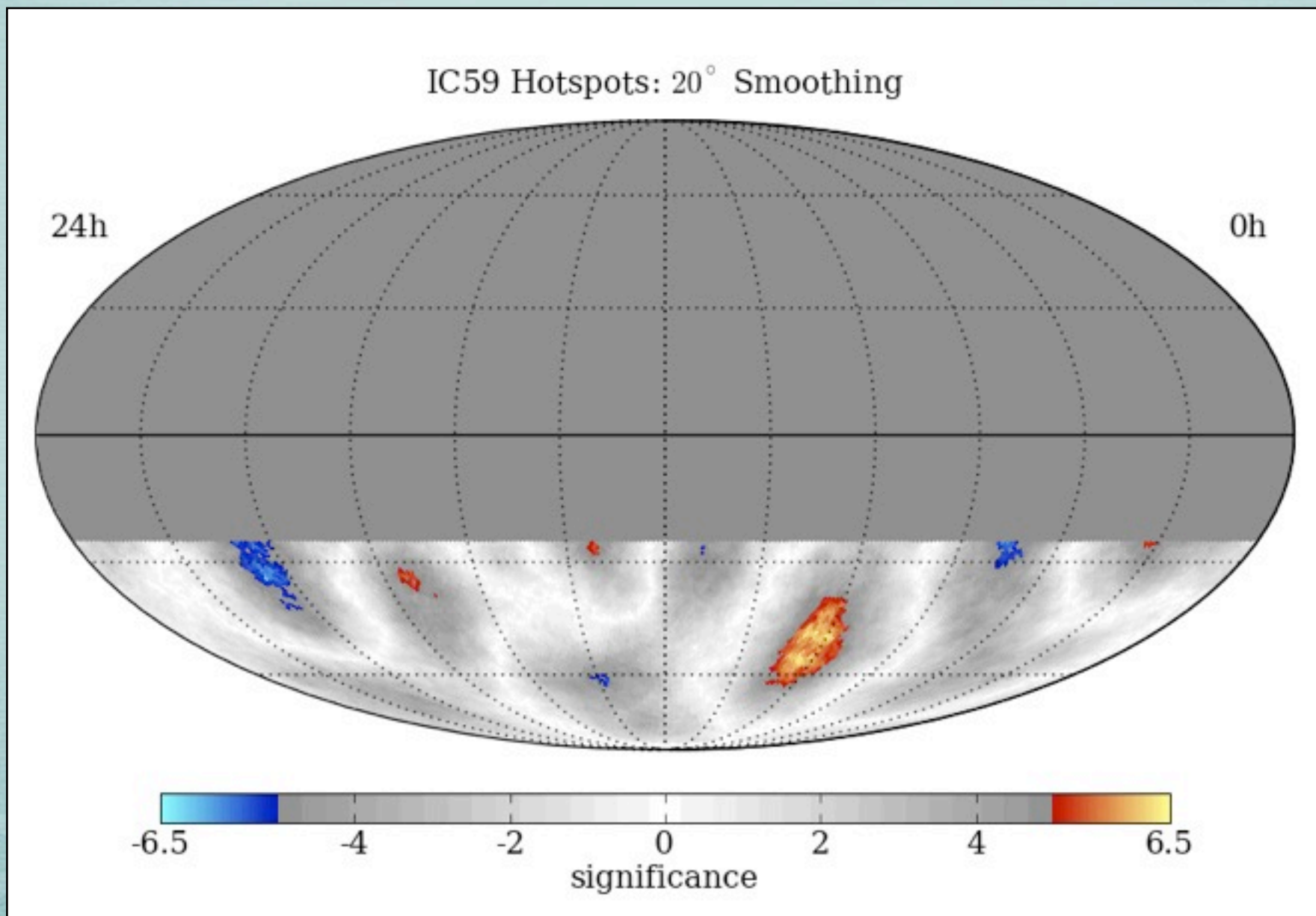
Scan from 1 - 30° in smoothing
Different regions have different optimal angular smoothing
Significances are pre-trial





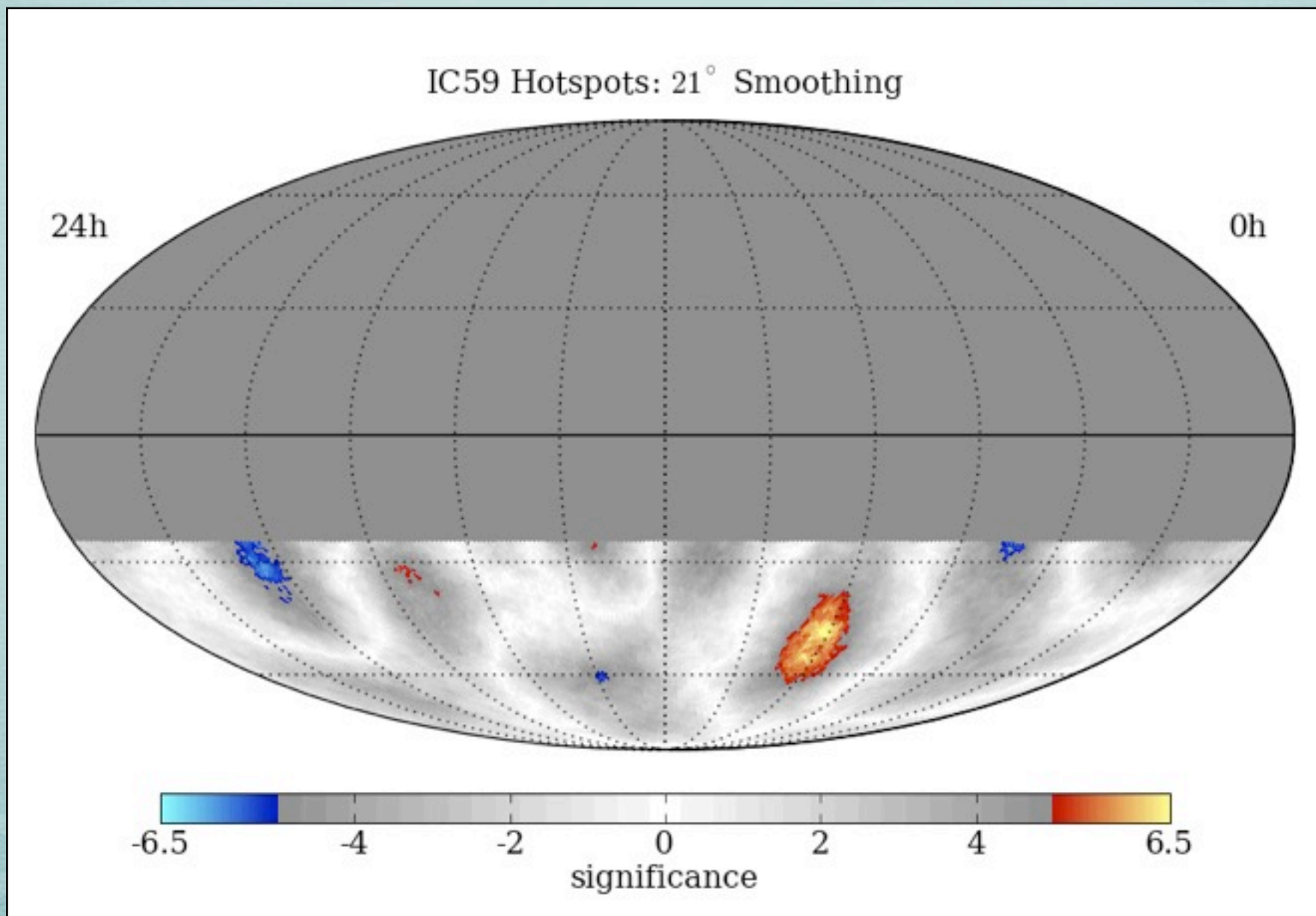
MAP SMOOTHING SCAN

Scan from 1 - 30° in smoothing
Different regions have different optimal angular smoothing
Significances are pre-trial



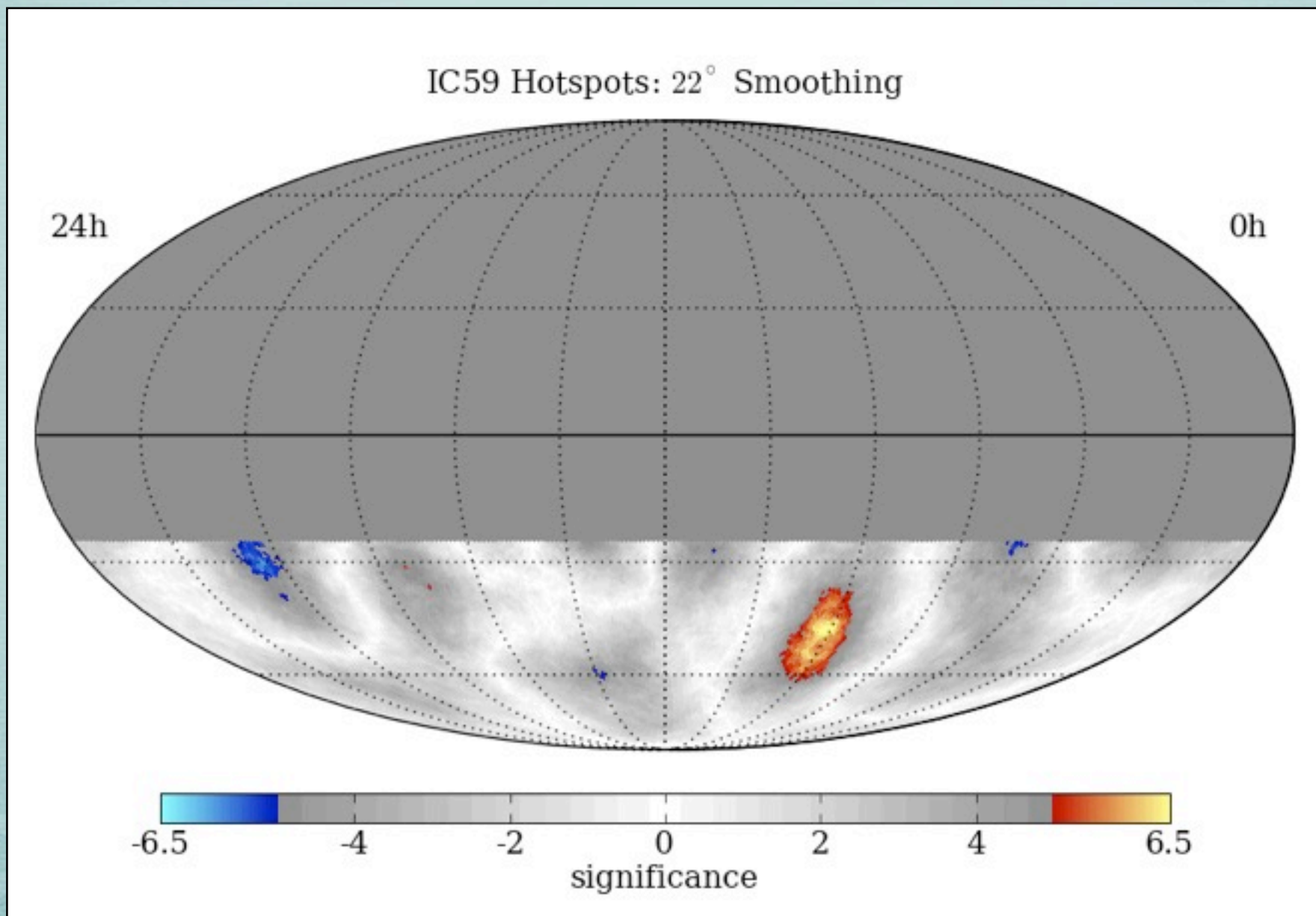
MAP SMOOTHING SCAN

Scan from 1 - 30° in smoothing
Different regions have different optimal angular smoothing
Significances are pre-trial



MAP SMOOTHING SCAN

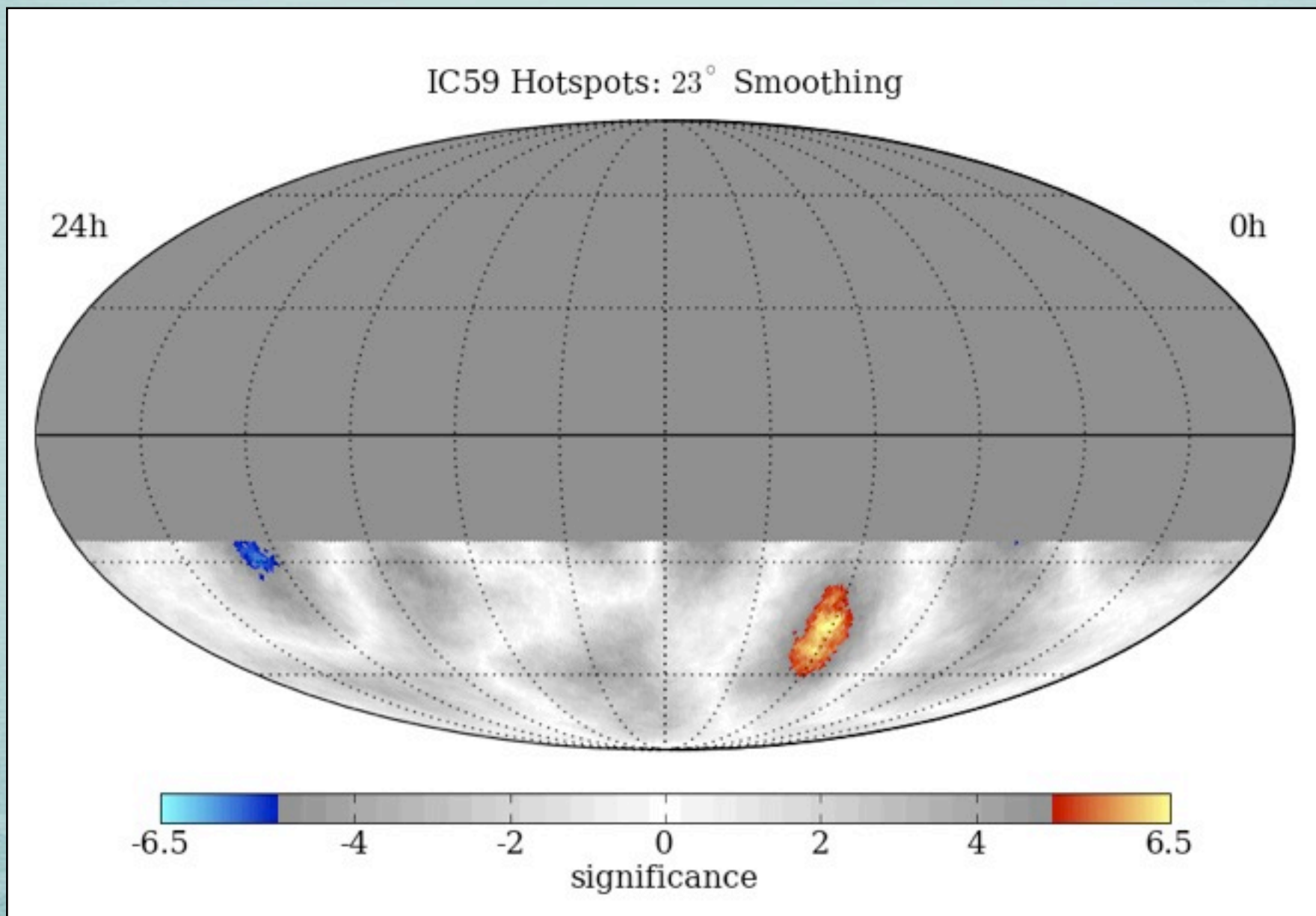
Scan from 1 - 30° in smoothing
Different regions have different optimal angular smoothing
Significances are pre-trial





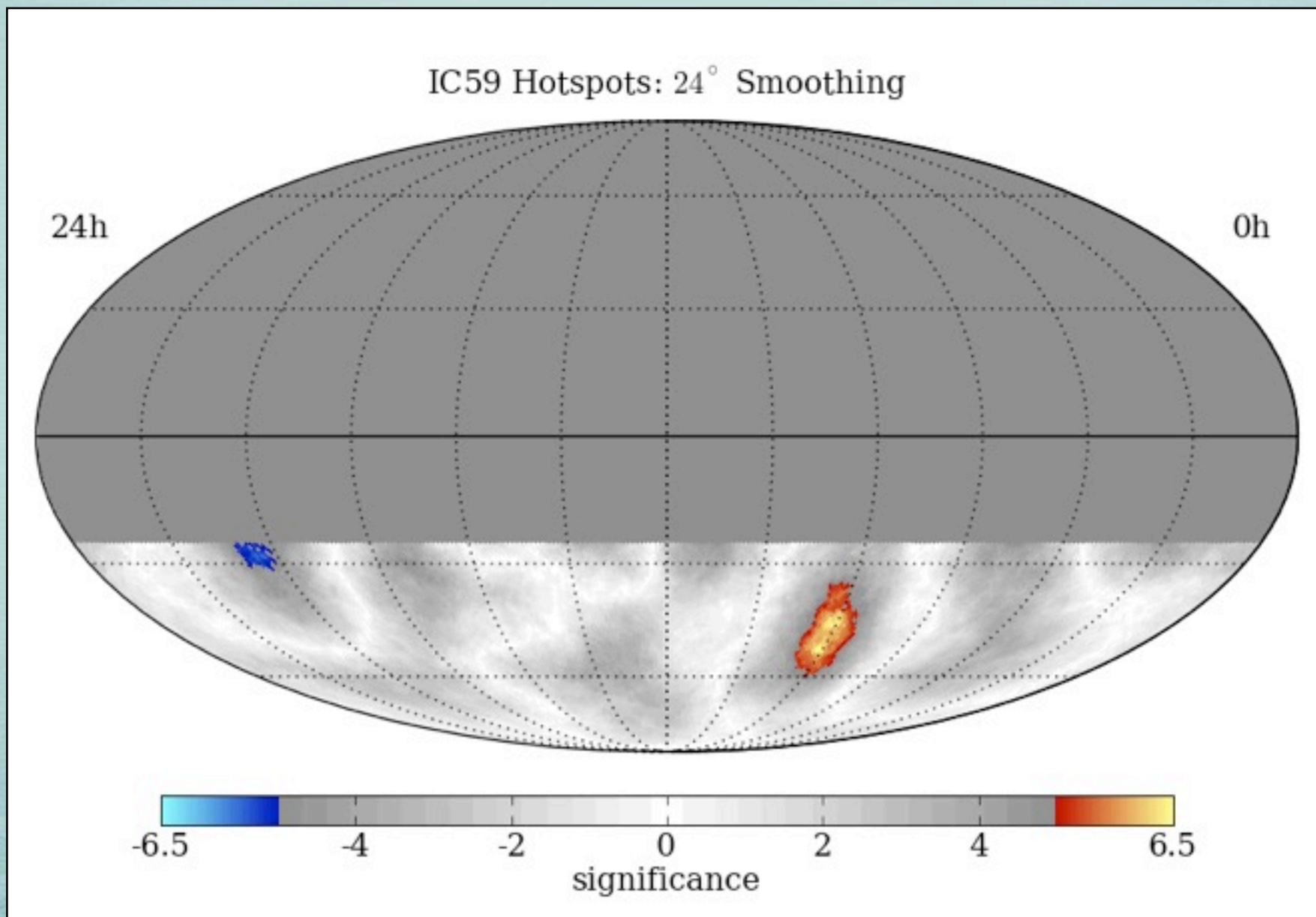
MAP SMOOTHING SCAN

Scan from 1 - 30° in smoothing
Different regions have different optimal angular smoothing
Significances are pre-trial



MAP SMOOTHING SCAN

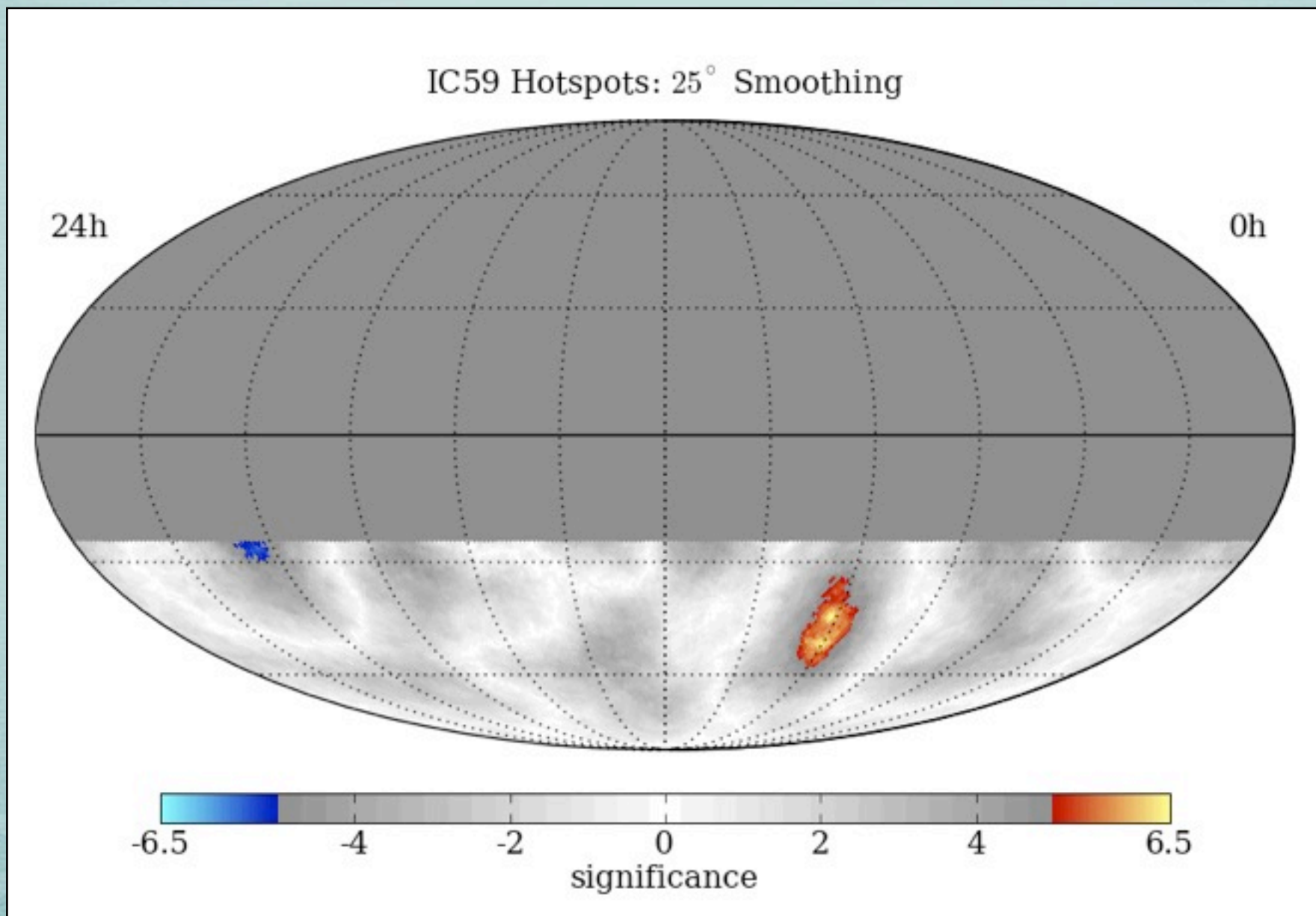
Scan from 1 - 30° in smoothing
Different regions have different optimal angular smoothing
Significances are pre-trial





MAP SMOOTHING SCAN

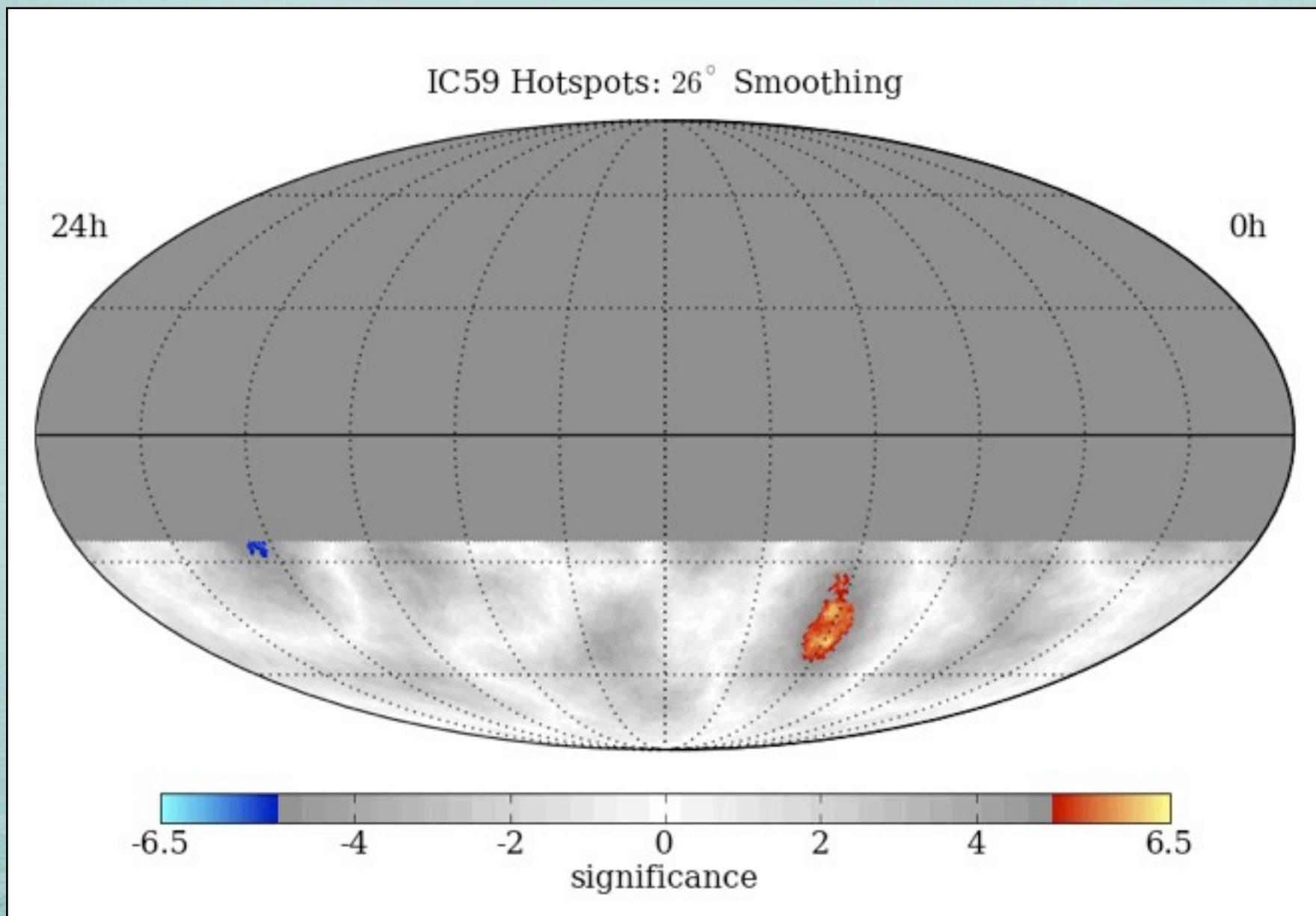
Scan from 1 - 30° in smoothing
Different regions have different optimal angular smoothing
Significances are pre-trial





MAP SMOOTHING SCAN

Scan from 1 - 30° in smoothing
Different regions have different optimal angular smoothing
Significances are pre-trial

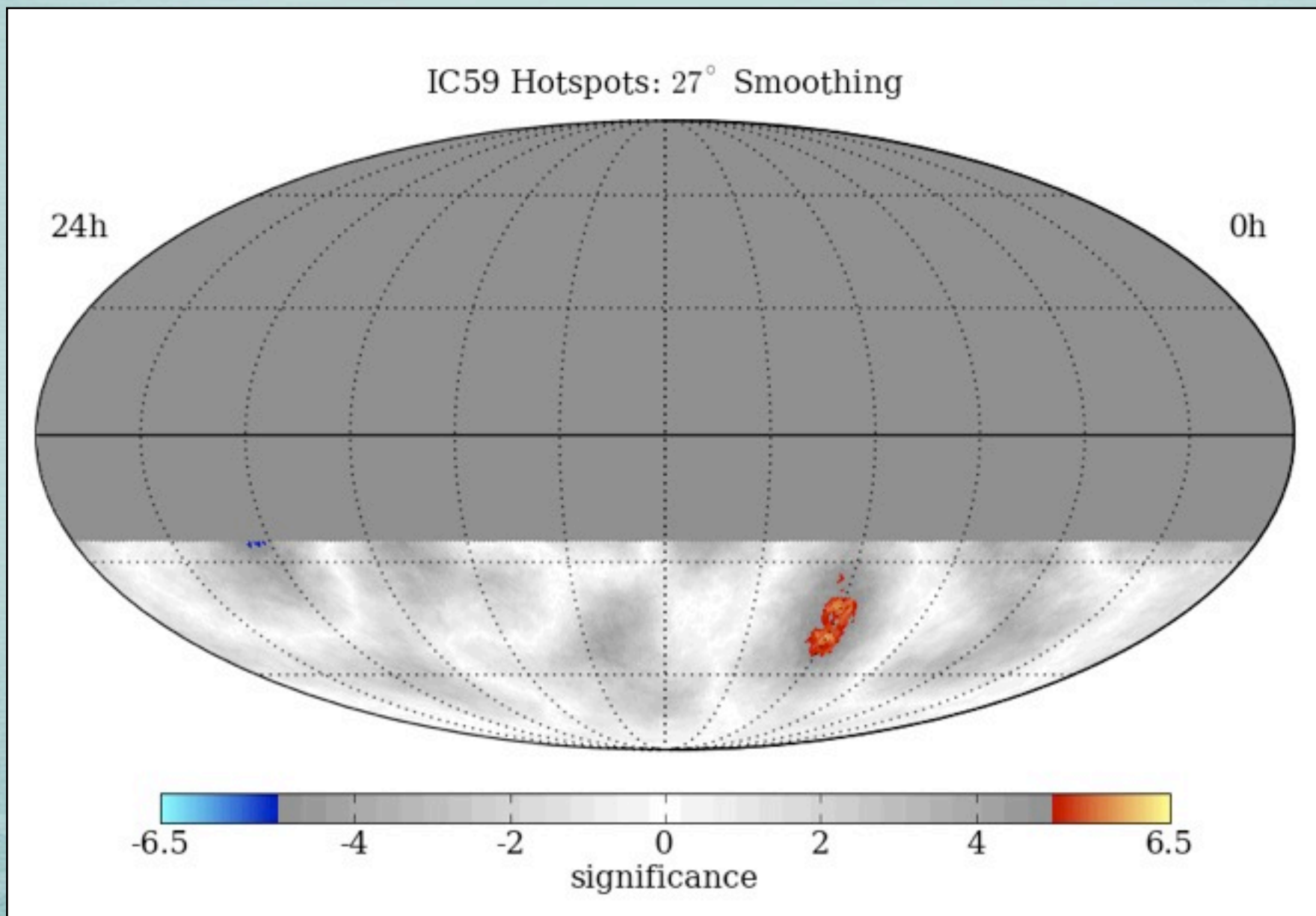


60



MAP SMOOTHING SCAN

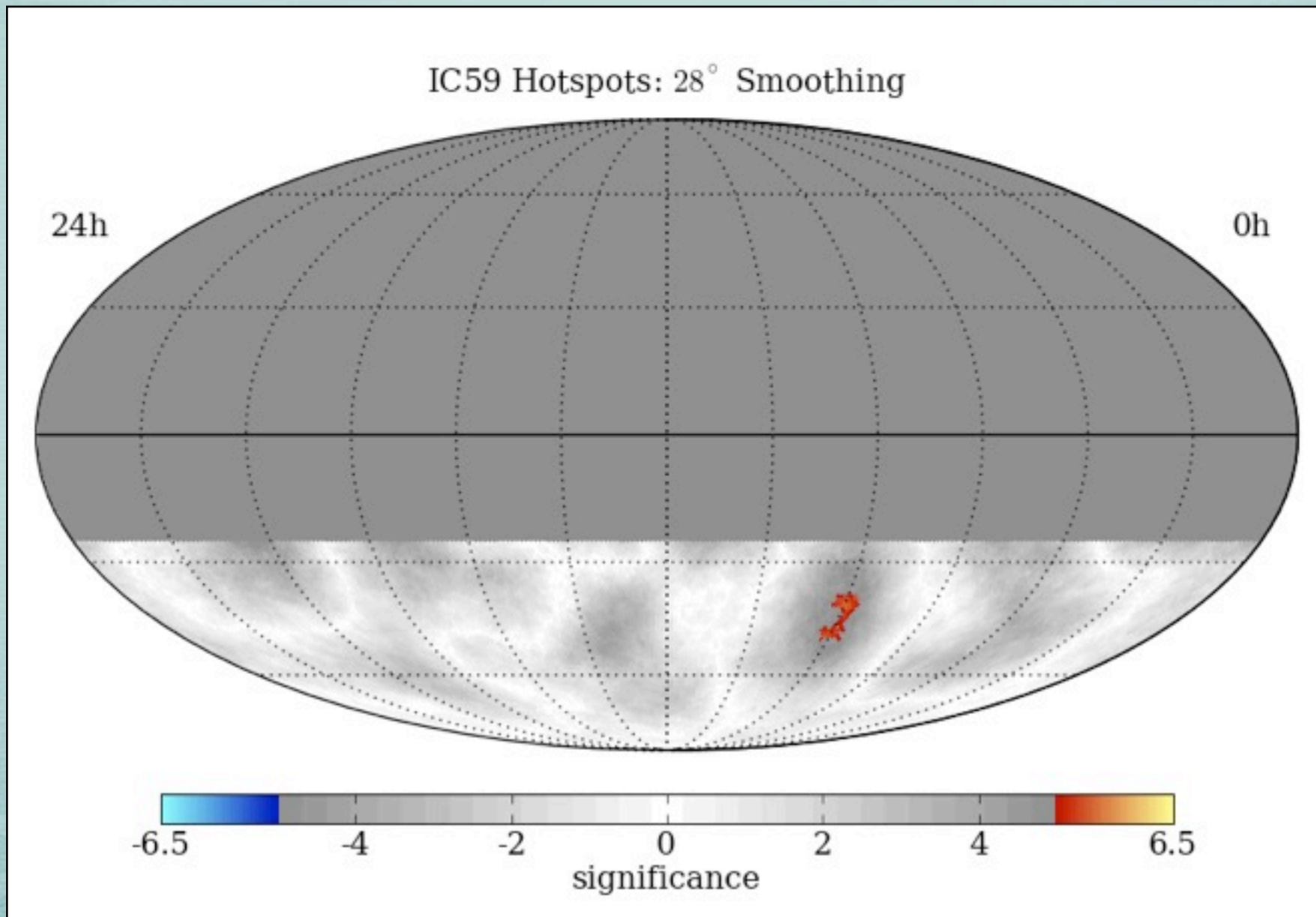
Scan from 1 - 30° in smoothing
Different regions have different optimal angular smoothing
Significances are pre-trial





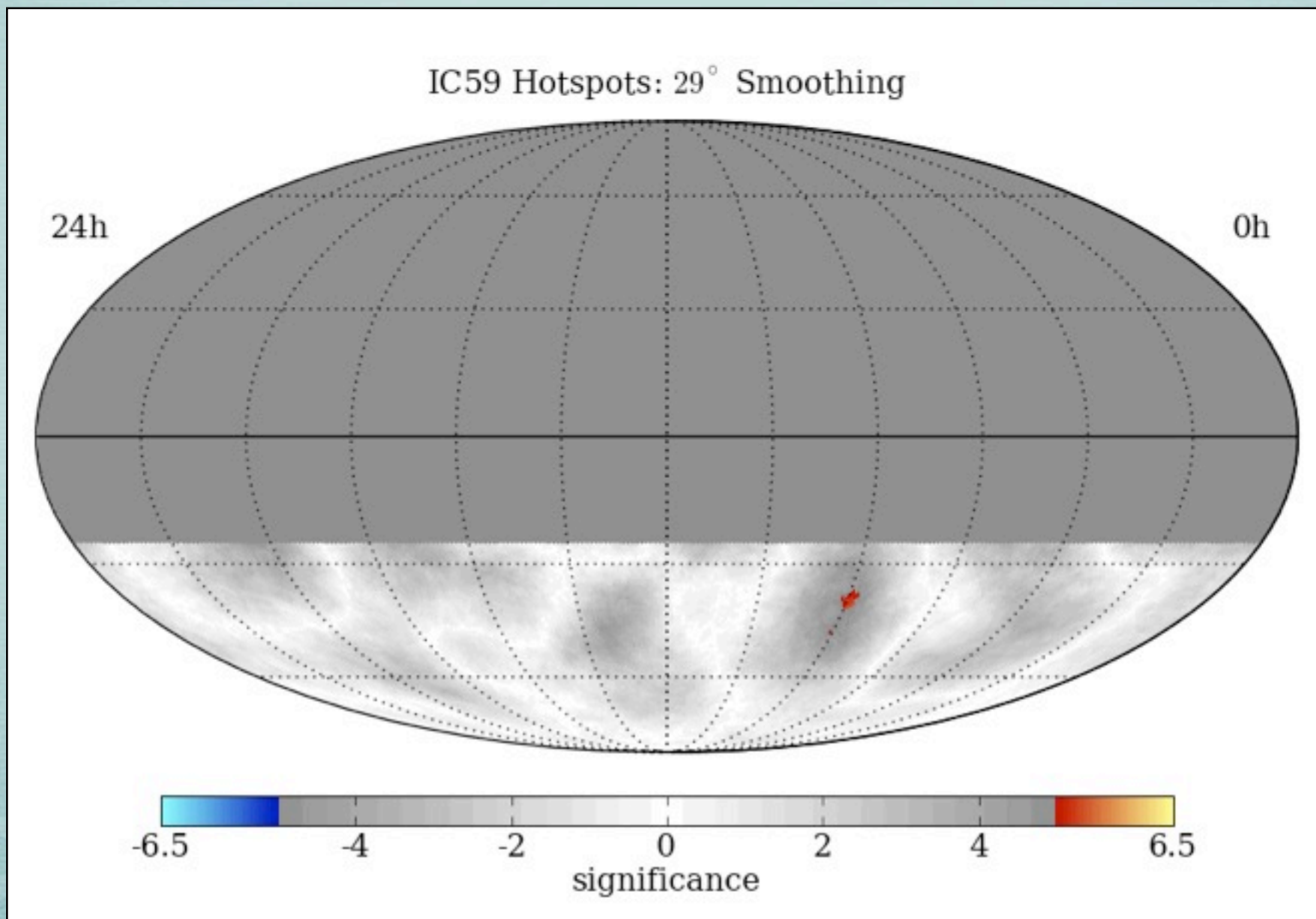
MAP SMOOTHING SCAN

Scan from 1 - 30° in smoothing
Different regions have different optimal angular smoothing
Significances are pre-trial



MAP SMOOTHING SCAN

Scan from 1 - 30° in smoothing
Different regions have different optimal angular smoothing
Significances are pre-trial





MAP SMOOTHING SCAN

Scan from 1 - 30° in smoothing
Different regions have different optimal angular smoothing
Significances are pre-trial

